DIAGNOZA - GENEZA - PROGNOZA => PODSTAWA KAŻDEJ DECYZJI

POLSKIE TOWARZYSTWO
DIAGNOSTYKI
TECHNICZNEJ

PTDT

afiliowane przy

Wydziale Nauk
Technicznych
Polskiej Akademii Nauk

DDiagnostyka

Józef Korbicz
Jan Maciej Kościelny
Editors

**Modeling,
Diagnostics
and Process
Control**

Implementation
in the DiaSter System

Springer

Nr 3(55)/2010

Spis treści / Contents

DATA SOURCES DIVERSITY IN TECHNICAL OBJECTS STATE ASSESSMENT WITH INFORMATION FUSION TECHNIQUES

Wojciech JAMROZIK

Silesian University of Technology, Department of Fundamentals of Machinery Design
44-100 Gliwice ul. Konarskiego 18a, tel (032) 237 10 63, fax (032) 237 13 60, wojciech.jamrozik@polsl.pl

Summary

The paper deals with a relationship between diversity of diagnostic signals sources and efficiency of technical objects states assessment with use of classifier fusion techniques. There is often stated that there should be some differences in sources of signals that are classified and fused. The intuition tells that none or minimal improvement of classification rate is gained when the diversity within the fused classifier set is low. To prove this thesis an active diagnostic experiment was carried out. Diagnostic signals were generated on basis of the thermogram sequences acquired during rotating machinery operation by two IR-cameras. Because in both sequences regions of interests representing the same assemblies of the machine are present, it can be assumed that there is hardware redundancy applied. With use of k-NN classifiers and fuzzy integral and proportional conflict redistribution aggregation rules, the state of the machine is possible to be assessed. The analysis of obtained results showed that there was no strong relationship between the diversity of classifiers and the efficiency of state classification.

Keywords: machine diagnostics, termovision, classifier fusion.

RÓŻNORODNOŚĆ ŹRÓDEŁ DANYCH W OKREŚLANIU STANU OBIEKTÓW TECHNICZNYCH Z ZASTOSOWANIEM TECHNIK FUZJI INFORMACJI

Streszczenie

W artykule omówiono związek pomiędzy różnorodnością źródeł sygnałów diagnostycznych a efektywnością oceny stanu technicznego maszyny z wykorzystaniem technik fuzji klasyfikatorów. Często zasadne jest twierdzenie, że sygnały diagnostyczne powinny być pozyskiwane z różnorodnych źródeł. Intuicyjnie można przyjąć, że w przypadku wykorzystania w procesie fuzji zbliżonych klasyfikatorów, zwiększenie sprawności klasyfikacji będzie bliskie zeru. W celu udowodnienia tej tezy przeprowadzono aktywny eksperyment diagnostyczny. Sygnały diagnostyczne zostały pozyskane z sekwencji termogramów przedstawiających pracującą maszynę wirnikową. Sygnały zarejestrowano z wykorzystaniem dwóch kamer termowizyjnych. Klasyfikacji stanu maszyny dokonano przy użyciu klasyfikatora k najbliższych sąsiadów, a w procesie fuzji klasyfikatorów wykorzystano całkę rozmytą oraz regułę proporcjonalnej redystrybucji konfliktów jako operatory agregacji. Analiza otrzymanych wyników pokazała, że nie występuje silna relacja pomiędzy różnorodnością klasyfikatorów, a efektywnością oceny stanu technicznego.

Słowa kluczowe: diagnostyka maszyn, termowizja, fuzji informacji.

1. INTRODUCTION

In a process of technical object diagnosing three main stages can be distinguished: fault detection, localization and identification [2]. Nowadays, in diagnostic systems, tasks mentioned above are realized with use of various methods. In the case of objects with an uncomplicated structure the application of input-output models or the diagnostic signals observation with use of limitation control (eg. control of signals credibility, alarm bounds, signals change rate and verification of binary values) would be sufficient. For a group of more complex objects, with strong interactions between diagnostic signals, simple methods listed above are ineffective. For this reason methods that assure proper decision rate in diagnostic systems are still examined.

Among many elaborated methods, there are two widely used that could lead to increase of diagnostic signal reliability. In the classifier fusion techniques signals obtained with use of hardware or software redundancy are often applied. Having multiple diagnostic signals we can build many classifiers and then combine them in order to increase classification accuracy. The use of redundancy influence the diversity of a single classifiers. The classifiers build on a partially (or full) redundant data should result in a low increase of the fused classifier accuracy in

comparison to each member classifier accuracy. This theoretical assumption is very intuitive. A dependent set of classifiers may be either better than the independent set or worse than the single worst member of the classifier group. The diversity can be both: harmful or beneficial [8].

In this study the influence of partially redundant and depending diagnostic signals used in classification on the machine technical state assessment was investigated. First two aggregation operators used in classifier fusion were introduced and the diagnostic experiment is described. Than the experimental result were studied. In the final part of the paper conclusions were presented.

2. CLASSIFIER FUSION

To combine (fuse) several individual classifiers two main stages must take place:
- Classifier outputs should be adjusted,
- Adjusted outputs are aggregated with use of the aggregation operator.

The adjustment is often performed on the stage of calculation of degrees of a support, evidences or other quantities that are used later in the aggregation process. In the study two aggregation operators were used. The first was based on the fuzzy integral calculation. The second one incorporates the proportional conflict redistribution (PCR) rules in the frame of Dezert-Smarandache theory of plausible and paradoxical reasoning.

2.1. Fuzzy integral
The classifier outputs can be organised in a decision profile as the following matrix [9]:

$$DP(x) = \begin{bmatrix} d_{1,1}(x) & \dots & d_{1,j}(x) & \dots & d_{1,c}(x) \\ \dots & & & & \\ d_{i,1}(x) & \dots & d_{i,j}(x) & \dots & d_{i,c}(x) \\ \dots & & & & \\ d_{L,1}(x) & \dots & d_{L,j}(x) & \dots & d_{L,c}(x) \end{bmatrix}$$
$$(1)$$

The use of a fuzzy integral (FI) aggregation operator measure allows measurement of the "strength" not only for individual classifiers but also for all subsets of classifiers that express how good is the experts ensemble for given input x. The process of combination is shown in fig. 1, and can be described as follows:
- For a input x the sorting of k-th column of DP(x) is performed, in order to obtain the vector $[d_{i1,k}(x), d_{i1,k}(x), \dots, d_{iL,k}(x)]^T$, where $d_{i1,k}(x)$ is the highest degree of support and $d_{iL,k}(x)$ is the lowest.

- Fuzzy densities, $g^{i1}, \dots, g^{iL}$, are arranged correspondingly to the degree of the support vector.
- The first element in the fuzzy measure vector, $g(1)$, is set to g^{i1}.
- $g(t)$ is calculated recursively, for $t = 1, \dots, L$ using following equation:

$$g(t) = g^{it} + g(t-1) + \lambda g^{it} g(t-1) \qquad (2)$$

where λ is the unique real root (> -1) of the polynomial:

$$\lambda + 1 = \prod_{i=1}^{L} (1 + \lambda g^i), \qquad \lambda \neq 0 \qquad (3)$$

- The final degree of support, for the class ω_k is calculated with the following formula:
-

$$\mu_k(x) = \max_{i=1}^{L} \{\min\{d_{it,k}(x), g(t)\}\} \qquad (4)$$

which is called *Sugeno fuzzy integral*.
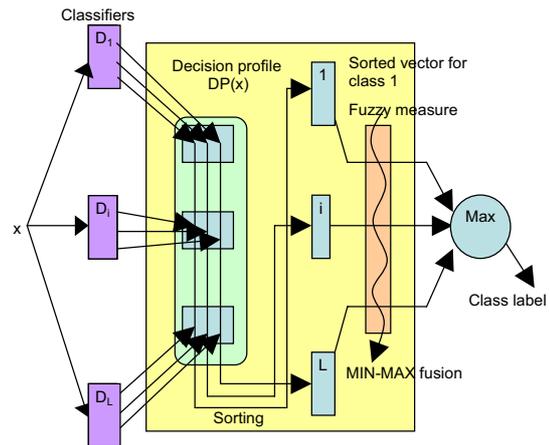
Fig. 1. Fusion scheme with use of the fuzzy integral [14]

2.2. Proportional Conflict Redistribution

Proportional conflict redistribution takes place in the framework of Dezert-Smarandache theory (DSmT) of plausible and paradoxical reasoning [4]. The DSmT has been developed to overcome several limitations of Dempster-Shafer (DST) evidence theory [12], and can be regarded as its generalization. In the DSmT possible propositions of the same event are stored in the frame of discernment Θ. The general basic belief assignment (gbba) is a primitive of DSmT theory. Each of evidence defines a mass function m, mapping the power set Θ to the interval between 0 and 1. Properties of mass assignment are as follows:

$$m(\varnothing) = 0$$
$$\sum_{A \in 2^{\Theta}} m(A) = 1 \qquad (5)$$

where 2^{Θ} is the power set on which the gbba is defined. The 2^{Θ} is the set of all subsets generated from Θ with union operator only. A subset with none-zero mass is called a focal element, and the value of *m(A)* represents the degree of evidential support of exact set *A*. The final aggregation of two or more belief assignments can be realized with one of proportional conflict redistribution rules. The probably most sophisticated rule is PCR6, defined by eq. (6) [5]:

$$m_{PCR6}(X) = m_c(X) +$$
$$\sum_{i=1}^{M} m_i(X)^2 \sum_{\substack{\bigcap_{k=1}^{M-1} Y_{\sigma_i(k)} \cap X \equiv \varnothing \\ (Y_{\sigma_i(1)},\dots,Y_{\sigma_i(M-1)}) \in (2^{\Theta})^{M-1}}} \left(\frac{\prod_{j=1}^{M-1} m_{\sigma_i(j)}(Y_{\sigma_i(j)})}{m_i(X) + \sum_{j=1}^{M-1} m_{\sigma_i(j)}(Y_{\sigma_i(j)})} \right)$$

$$(6)$$

where m_c is the conjunction rule defined as follows:

$$m_c(X) = \sum_{Y_1 \cap \dots \cap Y_M = X} \prod_{j=1}^{M} m_j(Y_j) \qquad (7)$$

The factor σ_i is a counter ($\sigma_i = 1,\dots,M$) used to avoid situation when $j = i$:

$$\begin{cases} \sigma_i(j) = j & \text{if } j < i \\ \sigma_i(j) = j+1 & \text{if } j \geq i \end{cases} \qquad (8)$$

The process of combination with use of PCR6 rule is shown in fig. 2.
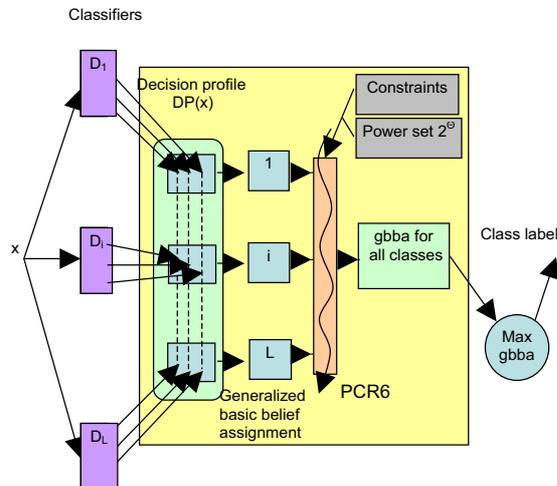
Fig. 2. Fusion scheme with use of the PCR6

2.3. Support and mass function calculation

A simple method for support/evidence calculation on the basis of k-Nearest Neighbours classifier has been introduced in [10]. Each classifier gives output in the form of a class label (on the abstract level). To obtain a class distribution a distance measure is used. The distance is calculated from given sample x, to number of known samples. Identification of k nearest neighbours of the sample x is made irrespective to the class label. From chosen k samples a vector k_i with samples belonging to the class C_i, $i = 1\dots M$ (*M* is the number of classes) can be obtained. According to that the degree of support and/or the mass function is calculated [10]:

$$m(\{C_i\}) = \frac{k_i}{\sum_{j=1}^{M} k_j} \qquad (9)$$

For each class the classification result and the class distribution is obtained.

3. DIAGNOSTIC EXPERIMENT

Fusion of classifiers required needed to investigate the influence of the signal sources diversity on the final decision about the machine technical state, demands several preliminary operations consisted of:
- Gathering thermovision images.
- Processing images and estimation of diagnostic signals.
- Classifying the machine technical state.
- Building a decision profile.
- Fusing obtained classifier outputs with use of chosen methods.

3.1. Diagnostic signals evaluation

In order to classify a machine technical state an active diagnostic experiment was performed. The laboratory stand consists of a model of rotating machinery and (fig. 3) thermovision acquisition system. Acquisition of thermograms was performed with two IR cameras that differed in matrix resolution (640x480 and 320x240). Cameras optical axes were placed perpendicularly and parallel (with small deviation) to the shaft. Thermograms were recorded every 15 seconds by both cameras and exemplary ones were presented in fig. 4 and fig. 5. In each thermogram 3 Regions of Interest (ROIs) were defined, representing bearing housings and belt pulleys.
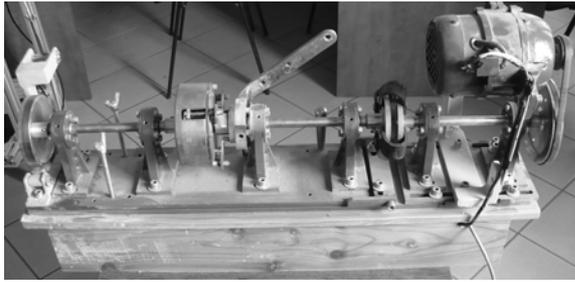
Fig. 3. View of the laboratory stand

The following technical states were simulated:
S1 – machine without faults (no load);
S2 – 30% load on the brake;
S3 – 50% load on the brake;
S4 – 70% load on the brake.

It is necessary to point that technical states that differs only in the load value are very similar and it is difficult to identify the weak change on the basis of diagnostic signals obtained by estimation of thermogram sequences [11].

Diversity of signal sources was limited, because data for diagnostic signals were acquired with devices using the same physical laws to measure spatial temperature distribution. Regions R3 and R6 represented the same bearing housing, thus some partial redundancy was introduced into the acquired data set.
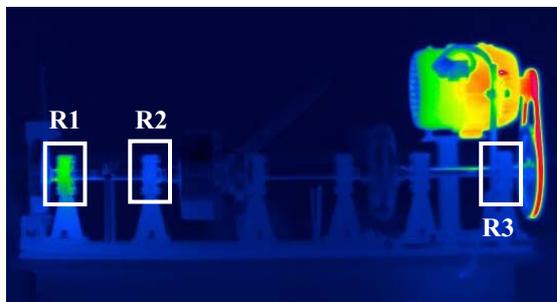
Fig. 4. Thermogram acquired by IR camera 1, with marked ROIs
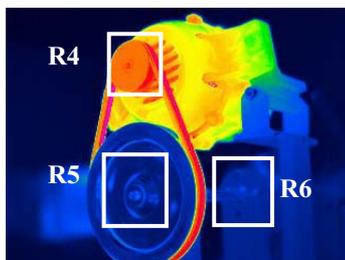
Fig. 5. Thermogram acquired by IR camera 2, with marked ROIs

Diagnostic signals must be determined through estimation of acquired thermovision images [3]. Sequences represented by six selected ROIs were transformed into frequency domain with use of 2D Fourier transform. For each considered thermogram two Fourier images (F-images) of magnitude and phase were calculated. In further studies only magnitude F-images were taken into consideration. Obtained F-images (fig. 6) were estimated with use of Circular Fourier Power (*CFP*) estimator, defined as follows [13]:

$$CFP = \sum_{r=\frac{X+D}{2}}^{r=\frac{X+D}{2}} \sum_{1 \le x^2 + y^2 \le r} F(x, y) \qquad (10)$$

where: *X*, *Y* are F-image width and height in pixels, *D* – diameter of the considered centralized circle of the F-image in pixels, *x*=1,2,…,*X*, *y*=1,2,…,*Y* – pixel indexes of image width and height respectively. In the research the CFP feature was calculated only for the F-images of amplitude. Parameter *D* was determined experimentally during the previous research and was fitted to obtain maximum classification efficiency [1].
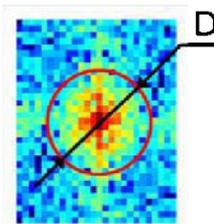
Fig. 6. F-image and CFP diameter

3.2. Classification

For the research purpose k-NN classifiers were used. The neighbours number was set on 10 on the basis of preliminary studies [1]. The classification performances were computed using the leave-one-out classifier error estimation method. In this method the whole training set containing *N* elements was divided into two subsets. First containing only one element is the testing subset. The training subset incorporated *N*-1 elements. The training and testing process was performed *N*-times. The classifier performance measure was the relative number of misclassifications, which was calculating using the following formula:

$$err = \frac{N_e}{N} \qquad (11)$$

where: *N* is the number of considered samples and N_e is the number of misclassified samples. On the basis of an error measure the classifier efficiency was determined as:

$$eff = (1 - err) \cdot 100\% \qquad (12)$$
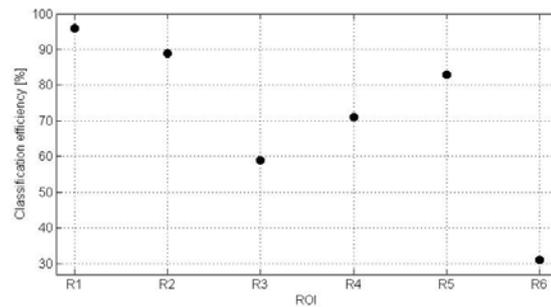
Fig. 7. Classification efficiency obtained for signals estimated for single ROI
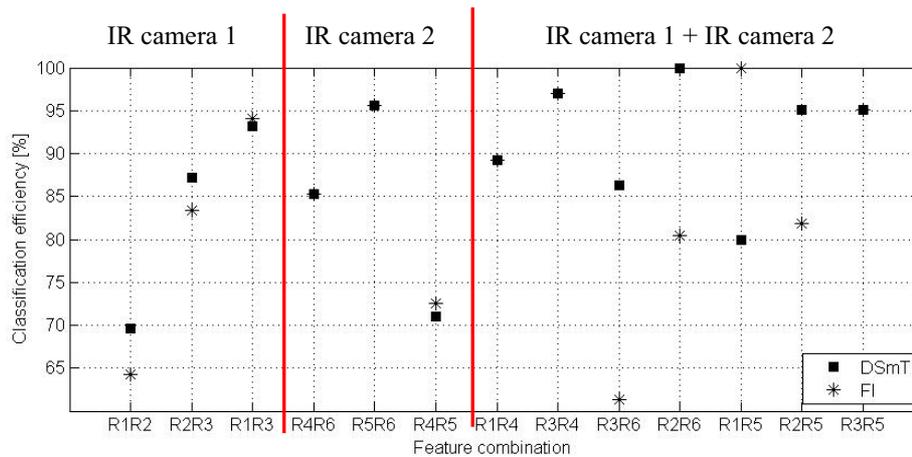
Fig. 8. Classification efficiency for various combinations of signals obtained for different ROIs

4. RESULTS

Basing on the classification scheme described in the previous section the technical state classification was performed. The first classification was made for features obtained from individual ROIs. In fig. 7 obtained results were presented graphically. It can be seen that for ROI marked as R1 maximal classification rate, equal to 96% were procured. For remaining ROIs the efficiency varieed from 34% for R6 to 89% for R2. Generally results given by classifiers trained with the data acquired by IR camera 1 observing parallel the shaft (R1, R2 and R3) were better than when dealing with data acquired by the IR camera 2.

Results of state recognition obtained after the classifier fusion with means of FI and DSmT were gathered and presented in fig. 8. In all cases the fusion of two classifiers was considered. Used features were strong bounded with the selected ROI, it can be revealed that when fused classifiers were trained on features calculated for ROIs only slight increase of recognition rate could be observed for just one case (R5R6, *eff* = 96,5%) in comparison to the best efficiency for an individual classifier. When the fused classifiers were trained, on signals estimated from ROIs selected from thermograms acquired by different cameras, considerable increase of classification efficiency can be observed.

Combinations of R2R6 and R1R5 led to the accuracy rate of 100%. It also must be noticed that overall classification efficiency was better as in the case of fusing signals generated from ROIs placed within one thermogram.

When analyzing results the special attention must be drown to the case when features were calculated for thermogarms acquired by various cameras but representing the same bearing housing. For the single classifier efficiencies obtained for features calculated for ROIs R3 and R6 were equal 59% and 31% respectively. The aggregated efficiency of features from both ROIs was higher as those for single ones and is as high as 62% when the final decision about the machine technical state was made with use of the fuzzy integral aggregation operator, and 87% in the case of PCR6 aggregation rule. These values indicate that the fact that partial hardware redundancy can lead to very good results, even when single classifiers have fairly strong support for misclassifications. Thus the diversity of signal sources was not indispensible for proper machine technical state assessment with use of the classifier fusion techniques.

Another interesting matter is the influence of weakest individual classifier on the result of classifier fusion. The lowest classification accuracy for single classifiers was 34% for R6. When signal obtained for R6 was classified and then combined

with output from other classifier trained by signal calculated for ROI placed in thermogram acquired by the second IR camera lowest accuracy was almost twice as high as for the single R6 classifier.

Summarizing it can be stated that among tested fusion methods the best results can be obtained with use of the proportional conflict redistribution rules. However, differences between methods can often be omitted.

5. CONCLUSIONS

In the paper the fusion of classifier trained on features calculated for thermograms acquired by two IR cameras in order to assess observed machine technical state was presented. After performing a number of experiments it can be stated that dependency between data sources diversity and the classification efficiency is not clear. The diversity is not indispensible to observe increase of classification accuracy rates, when individuals classifiers are fused in order to made the decision about the machine technical state.

Further investigations will survey the fusion of classifiers trained on diverse data, e.g. thermograms and vibration signals. Also analytical redundance will be taken into consideration, e.g. calculating multiple features from one thermogram, as the training data for classifiers used in the fusion process.

REFERENCES

[1] Fidali M., Jamrozik W.: *Search for optimal estimators of thermogram Fourier images.* Burczyński T. Cholewa W., Moczulski W., eds. Recent developments in artificial intelligence methods, AI-Meth Series, Gliwice, 2009.

[2] J. Korbicz, J. Kościelny, Z. Kowalczuk, and W. Cholewa, eds.: *Fault Diagnosis. Models, Artificial Intelligence.* Applications. Berlin, Heidelberg, New York, Hong Kong, London, Milan, Paris, Tokyo, Springer, 2004.

[3] Fidali M.: *An idea of continuous thermographic monitoring of machinery.* in QIRT 2008 Proceedings, 9th International Conference on Qualitative InfraRed Thermography, July 2-5, Kraków, Poland, 2008.

[4] J. Dezert and F. Smarandache, DSmT: *A new paradigm shift for information fusion.* CoRR, vol. abs/cs/0610175, 2006.

[5] A. Martin and C. Osswald: *A new generalization of the proportional conflict redistribution rule stable in terms of decision.* CoRR, vol. abs/0806.1797, 2008.

[6] L. I. Kuncheva: *"Fuzzy" vs "non-fuzzy" in combining classifiers designed by boosting.* IEEE Transactions on Fuzzy Systems 11: 729–741, 2003.

[7] A. Verikas, A. Lipnickas, K.Malmqvist, M. Bacauskiene, A. Gelzinis: *Soft combination of neural classifiers: A comparative study.* Pattern Recognition Letters, 20: 429–444, 1999.

[8] S. Hashem: *Treating harmful collinearity in neural network ensembles. In A. J. C. Sharkey, editor.* Combining Artificial Neural Nets. Springer-Verlag, London, 1999, pp. 101–125.

[9] C. A. Shipp , L. I. Kuncheva: *Relationships between combination methods and measures of diversity in combining classifiers.* Information Fusion, 3(2): 135–148, 2002.

[10] D. Han, C. Han, and Y. Yang, *Multiple k-nn classifiers fusion based on evidence theory, in Automation and Logistics,* 2007 IEEE International Conference on, pp. 2155–2159, Aug. 2007.

[11] Jamrozik W., Fidali M.: *Classifier fusion using the PCR6 rule for assessment of machine technical state.* Burczyński T. Cholewa W., Moczulski W., eds. Recent developments in artificial intelligence methods, AI-Meth Series, Gliwice, 2009.

[12] G. Shafer: *A mathematical theory of evidence.* Princeton university press, 1976.

[13] Fukushima M., Ogawa K., Kubota T., and Hisa N.: *Quantitative tissue characterization of diffuse liver diseases from ultrasound images by neural network. IEEE Proc. Nucl. Symp.* 2:1233-1236, 1997.

[14] Kuncheva L. I.: *Combining pattern classifier.* Wiley, USA, 2004.

Wojciech JAMROZIK is, since 2007, PhD student in the Department of Fundamentals of Machinery Design at Silesian University of Technology at Gliwice. The main areas of his interest are applications of vision system in diagnostic systems, image processing, analysis and recognition. He deals also with the fusion of images and information.

OPTIMUM CHOICE OF SIGNALS' FEATURES USED IN TOOTHED GEARS' DIAGNOSIS

Łukasz JEDLIŃSKI, Józef JONAK

Lublin University of Technology, Mechanical Faculty, Department of Machine Design
36 Nadbystrzycka Street, 20-618 Lublin, Poland
tel. +4881 53-84-499, email: l.jedlinski@pollub.pl, jonak@pollub.pl

Summary

The article proposes an algorithm to choose optimum diagnostic features used in toothed gears' diagnosis. The test object is a single-bevel gear in the research area. From the gear in two technical states there were collected vibration signals and eight features were calculated. Feature and machine state correlation degree depends on the type of damage and analyzed object properties. Some features are insensitive to particular damage or may transmit the same information. Signal features choice is a crucial step which influences the final technical condition evaluation. With the algorithm that automatically verifies features' usability there were chosen four best correlated with the technical condition of the object. Gear state classifiers were two neural networks, one formed of four features and the other of all eight. The other one was set to check features' choice accuracy.

Keywords: bevel gear, feature selection, artificial neural network.

OPTYMALNY WYBÓR CECH SYGNAŁÓW WYKORZYSTYWANYCH W DIAGNOZOWANIU PRZEKŁADNI ZĘBATYCH

Streszczenie

W artykule przedstawiono algorytm doboru optymalnych cech diagnostycznych używanych w diagnozowaniu przekładni zębatych. Obiektem badań była przekładnia jednostopniowa stożkowa badana na stanowisku badawczym. Z przekładni w dwóch stanach technicznych zarejestrowano sygnały drgań i obliczono osiem cech. Stopień korelacji cechy ze stanem maszyny zależy od rodzaju uszkodzenia i właściwości analizowanego obiektu. Niektóre cechy nie są czułe na dane uszkodzenie, lub mogą przekazywać tę samą informację. Wybór cech sygnału jest krytycznym krokiem, który ma wpływ na ostateczny wynik oceny stanu technicznego Za pomocą algorytmu, który w sposób automatyczny weryfikuje przydatność cech wybrano cztery najbardziej skorelowane ze stanem technicznym obiektu. Klasyfikatorem stanu przekładni były dwie sieci neuronowe, pierwsza utworzona dla czterech cech a druga dla wszystkich ośmiu. Druga sieć miała na celu sprawdzenie poprawności wyboru cech.

Słowa kluczowe: przekładnia stożkowa, selekcja cech, sztuczne sieci neuronowe.

1. INTRODUCTION

Technical condition deduction especially in an early stadium of damage development and noisy vibroacoustic signals needs signal processing. There are many methods used successfully. Among them there are statistical methods, time and frequency analyses such as Wigner-Ville distribution and short time Fourier transformation, wavelet analysis, bispectrum analysis, cepstrum. Statistical methods are quite easy but effective method in machines' technical condition evaluation. Many researchers confirmed its effectiveness in toothed gears' diagnosis [4, 8]. Most frequently used are time features such as RMS, kurtosis, crest factor, frequency features and features specially created for toothed gears testing FM0, NA4, NB4 [6]. Numerous features (mentioned in literature there are

more than twenty [3, 10]) cause the diagnosing person problems with tracing them and their interpretation, especially when features' trends are inconsistent. Feature and machine state correlation degree depends on the type of damage and analyzed object properties. Some features are insensitive to particular damage or may transmit the same information. Signal features choice is a crucial step which influences the final technical condition evaluation [9].

Features selection may be done automatically. Using different methods it is possible to get optimal data fast and objectively. Combining statistical methods with artificial intelligence we get a credible and efficient tool to detect tooth gears' damages. In [1] using the time and frequency features there was multi-bevel gears' state diagnosed – the gears are used in transportation in coal mine. Using the main

PCA components analyze big redundancy of data was confirmed and their size was reduced what built up their usability in further technical condition analyze. Yang [9] used time and frequency measures which were used as an input data for the neural network to evaluate the reliability of induction motor. Reduction of the data size from thirteen to three was obtained by using the features' extraction method [10]. Similar algorithm was used by Lei [3] to choose more features sensitive to damages in electric motor bearings. Artificial neural networks and SVM (Support Vector Machine) method were used do detect pitting by Samanta [5]. As an input vibration signal features optimized with genetic algorithms were used. In the problem of class differentiation, where genetic algorithms were classifiers, Zhu [11] used RIF (Relative Importance Factor) method to detect less important to classification process features. Removal of these improved class identification.

To evaluate technical condition of the toothed gear signal features which were the input data for the neural network there were used in this work. There were used time and frequency features together with specially designed for gears' diagnosis FM0, NB4, frequently mentioned in NASA technical reports [2]. Neural network classified the gear state as „good" or „bad". Large number of features on input implicates longer teaching and calculation time and bigger number of cases. In addition to this, if the data is not linked to the technical condition, state classification error may rise. In consequence, to choose only highly correlated with the gear technical condition features the algorithm described in [3, 9] was used.

2. VIBRATIONS MEASUREMENT AND THE TEST OBJECT

Test station was formed with two toothed gears, electric motor, water brake and control measurement instruments. Electric motor rotary speed was set using the control unit which enables research with different rotary speed. Additionally, the rotary speed was raised using cylindrical wheel multiplier mounted between the motor and the tested gear. Brake load was changed in several ranges. Moment transferred by shafts and clutches. The test object was a single-bevel gear. The driving wheel had 19 teeth, and driven 42 teeth. Both input and output shafts were propped by two rolling bearings.

Kinematical scheme of the gear is shown in Fig. 1. The test object was New. In the test two pairs of toothed wheels were tested, first pair had side teeth surfaces damaged after trowelling, second pair was undamaged.
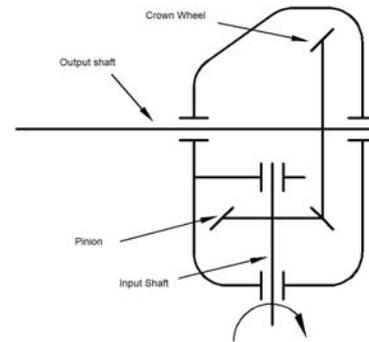
Fig. 1. Kinematical scheme of the tested gear

The measurement system was forded from a controller, National Instruments measurement cards and two triaxal Bruel&Kjaer sensors. Sensors location on the gear is show in Fig. 2. Sampling frequency was 40 kHz. Presented figures are for the maximum rotary speed of the input shaft equal 6196 rpm and load equal 34 % maximum load.
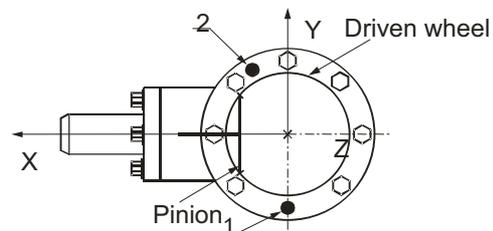
Fig. 2. Sensors 1 and 2 location on the gear

3. FEATURES SELECTION ALGORITM

Eight features were calculated for presented signals – three in time domain and five specially created for gears' diagnosis. Formulas for three first features (kurtosis k, crest factor C and impulse factor I) may be found in literature [2] and the other measures in [2, 4, and 6].

Since many measures lengthens calculation time and may cause limitations to neural network's ability to generalize algorithm presented in [3, 10] was used to choose optimum features. The input data is three-dimensional array M_c x C x J, where: J is a number of signal features, M_c number of values for each of the features and C number of object states. $p_{m,c,j}$ is read as m value of j measure for c state of the object, where: $m=1,2,...,M_c$; $c=1,2,...,C$; $j=1,2,...,J$. In this work two states of the object are concerned ($C=2$) for which eight features were calculated ($J=8$) with two hundred twenty-nine values ($M_c = 229$). Calculation method consists of following steps [3, 9]:

Step (1)

Calculate average distance between particular values of measures in the same state

$$D_{c,j} = \sqrt{\frac{1}{M_c \times (M_c - 1)} \sum_{l,m=1}^{M_c} (p_{m,c,j} - p_{l,c,j})^2} \, , l,m = 1,2,...,M_c$$

Next, calculate average distance for C states of the object

$$D_j^{(w)} = \frac{1}{C}\sum_{c=1}^{C} D_{c,j}$$

Step (2)

Calculate $V_j^{(w)}$ according to the formula:

$$V_j^{(w)} = \frac{\max(D_{c,j})}{\min(D_{c,j})}$$

Step (3)

Calculate average distance for all values of measures for the same state

$$a_{c,j} = \frac{1}{M_c}\sum_{m=1}^{M_c} p_{m,c,j}$$

Next, get the average distance between the values for different states

$$D_j^{(b)} = \sqrt{\frac{1}{C\times(C-1)}\sum_{c,e=1}^{C}(a_{e,j}-a_{c,j})^2}, c,e=1,2,...,C$$

Step (4)

Calculate $V_j^{(b)}$ for the object in a different state

$$V_j^{(b)} = \frac{\max(|a_{e,j}-a_{c,j}|)}{\min(|a_{e,j}-a_{c,j}|)}, c,e=1,2,...,C$$

Step (5)

Calculate λ_j as below:

$$\lambda_j = \left(\frac{V_j^{(w)}}{\max(V_j^{(w)})}+\frac{V_j^{(b)}}{\max(V_j^{(b)})}\right)^{-1}$$

Step (6)

Calculate the $D_j^{(b)}$ and $D_j^{(w)}$ ratio and E_j

$$E_j = \lambda_j \frac{D_j^{(b)}}{D_j^{(w)}}$$

Next normalize E_j by maximum value and get the evaluation criteria

$$\overline{E}_j = \frac{E_j}{\max(E_j)}$$

Dividing E_j by the maximum value causes the figures range 0 to 1. The closer to 1, the better this feature reflects the object state. Choice can be made using the criteria $\overline{E}_j \geq P$, where P is a chosen threshold value for the features.

4. METHOD AND RESEARCH RESULTS

4.1. Features choice

Figure 3 shows results of features' sensitivity evaluation according to the algorithm described above. Assuming threshold equals 0.5 four features were chosen: kurtosis, crest factor, impulse facto rand NB4.

To verify features choice neural networks were built for four chosen measures and all eight measures.
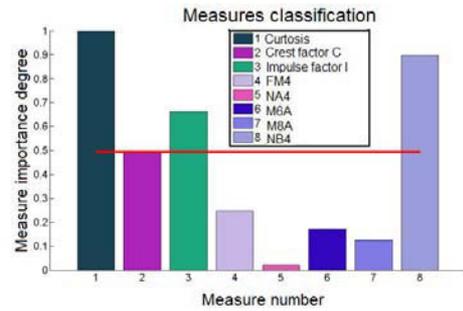
Fig. 3. Measures' sensitivity to damage evaluation

4.2. Neural networks

To create neural networks Statistica packet was used. Optimal networks were sought by Automatic Network Seek. Two types of networks were taken into consideration MLP and RBF. Different variants of networks: formed by different neuron numbers in the hidden layer, five hidden neuron activation and output functions (linear, logistic, tanh, expotential, and sinus). Best results for four features were received for MLP network with one hidden layer with nine neurons. Hidden neuron activation function was linear and output softmax. For eight features optima network is a MLP network with one hidden layer with four neurons, linear activation function and output logistic.

In version 8 of Statistica quality criteria implicates neural usability. Quality is calculated for teaching data, testing data and if there is such a set validation data. For classification problem quality is a relative number of cases successfully classified (referred to the total number of cases) presented in percentage terms [8].

5. RESULTS ANALYZE

Neural network was used to assign the gear state to one of two classes. In table 1 there are results for the data from the sensor 1, which was used in teaching process, testing and network validation. Testing data is used in the teaching process until the teaching is finished so that the network does not lose the ability to generalize when over taught. To check network's accuracy frequently third set of validation data is used - not used before in the teaching process so the validation quality is used to evaluate neural network. In case of the network formed for four features validation quality was 98.5 % and for eight variables on the input 89.7 %. Limiting features number by half caused nearly 9 % rise in gear state classification accuracy.

Table 1. Research results for data from sensor 1

No.	Number of features	Network type	Teaching quality [%]	Testing quality [%]	Validation quality [%]
1	4	MLP 4-9-2	96,27	97,06	98,53
2	8	MLP 8-4-2	81,99	94,12	89,70

Networks were checked also for the data from the other vibration sensor. In the network implementation mode after the addition of output variable there is only available quality testing (different meaning than when network teaching). For networks with four variables on the input testing quality was 100 %, when for eight variables 44.3 % (table 2).

Table 2. Research results for data from sensor 2

No.	Number of features	Network type	Testing quality [%]
1	4	MLP 4-9-2	100,00
2	8	MLP 8-4-2	44,32

6. SUMMARY

Using statistical methods in machines' diagnosis problem of too many signal features may arise. It may cause limited accuracy in state evaluation and lengthen the calculation time. Automatic choice of adequate features accelerates the process of creating a diagnostic system and for a researcher with little experience is a great help.

One of the basic applications of neural networks is classification. Crucial stage deciding on the correct network operation is relevant data choice (variables) reflecting appropriate classes. Frequently the quantity of data is not too big and the more variables are used in the teaching process the more cases are needed.

To detect the toothed wheel damages statistical methods were used in connection with neural networks. To improve the evaluation accuracy only features well correlated with the device chosen by the features' selection algorithm were used. Limiting the number of features from eight to four improved the classification accuracy by almost 9% to equal 98.5%. However, in both cases the results were satisfying. In contrast to this were the results for the data from sensor 2. The neural network in implementation mode for four features 100 % distinguished the gears' states when for eight features quality was 44, 3 % which is not a satisfying result.

7. LITERATURE

[1] Bartelmus W., Zimroz R.: *Identyfikacja optymalnych cech diagnostycznych wielostopniowych przekładni zębatych.* Prace Naukowe Instytutu Górnictwa Politechniki Wrocławskiej nr 113, Studia i materiały nr 31/2005 (str. 11-22).
[2] Decker H.: *Crack detection for aerospace quality spur gears.* NASA/TM-2002-211492.
[3] Lei Y., He Z., Zi Y., Hu Q.: *Fault diagnosis of rotating machinery based on multiple ANFIS combination with GAs.* Mechanical Systems and Signal Processing 21/2007 (str. 2280–2294).
[4] Madej H., Czech P., Konieczny Ł.: *Wykorzystanie dyskryminant bezwymiaro-wych w diagnozowaniu przekładni zębatych.* Diagnostyka 28/2003 (str. 17-22).
[5] Samanta B.: *Gear fault detection using artificial neural networks and support vector machines with genetic algorithms.* Mechanical Systems and Signal Processing 18/2004 (str. 625–644).
[6] Samuel P., Pines D.: *A review of vibration-based techniques for helicopter transmission diagnostics.* Journal of Sound and Vibration 282/2005 (str. 475-508).
[7] StatSoft, Inc. (2008). *STATISTICA (data analysis software system)*, version 8.0. www.statsoft.com.
[8] Wilk A., Łazarz B., Madej H.: *Diagnostyka wibroakustyczna przekładni zębatych*. V Krajowa Konferencja Diagnostyka Techniczna Urządzeń i Systemów 2003.
[9] Yang B. S., Kim K.: *Application of Dempster–Shafer theory in fault diagnosis of induction motors using vibration and current signals*. Mechanical Systems and Signal Processing 20/2006 (str. 403-420).
[10] Yang B.S., Han T., An J.L.: *ART–KOHONEN neural network for fault diagnosis of rotating machinery.* Mechanical Systems and Signal Processing 18/2004 (str. 645-657).
[11] Zhu F., Guan S.: *Feature selection for modular GA-based classification.* Applied Soft Computing 4/2004 (str. 381–393).

Łukasz JEDLIŃSKI, MSc, Eng., is a lecturer at the Department of Machine Design at the Mechanical Faculty at Lublin University of Technology. His fields are signal processing and analysis, and gear diagnostics.

Prof. **Józef JONAK**, PhD, Eng., is the Head of the Department of Machine Design at Lublin University of Technology. In his projects, he concentrates on the following issues: adaptive control of heavy-duty machines, fracture mechanics and fracture process simulation of composite materials, the construction, operation and diagnostics of mechanical gears (especially helicopter gearboxes) and computer-aided design of machines and devices.

FIELD TESTS OF THE SCISSOR-AVLB TYPE BRIDGE

Wiesław KRASOŃ

Department of Mechanics and Applied Computer Science
Gen. Sylwestra Kaliskiego 2, 00-908 Warsaw, Poland,
fax: +48 22 6839353, e-mail: wkrason@wat.edu.pl

Summary

Scissor-AVLB type bridges are subject of studies presented in a paper. The bridge span is extended automatically by means of a mechanical bridge-laying gear carried together with bridge sections on a self-propelled chassis. The single-span scissors-type BLG (a manufacturer's designation) bridge length available is up to 20m and the load bearing capacity is of 500kN. In connection to the BLG bridge modernization (bridge deck widening), there arose the need to conduct basic engineering analyses in order to verify the structure's correctness. Some aspects of an experimental test of the single-span scissors-type BLG bridge operation were presented. Displacements and strains in particular sections of the structure were measured during field tests with different load modes. Results of load tests performed on a modernized BLG bridge structure made it possible to verify the correctness of the BLG numerical models.

Keywords: modernized AVLB scissors-type bridge, load tests.

BADANIA POLIGONOWE MOSTU TOWARZYSZĄCEGO TYPU NOŻYCOWEGO

Streszczenie

Przedmiotem badań przedstawionych w pracy jest most nożycowy AVLB. Przęsło mostu nożycowego rozkładane jest automatycznie za pomocą układacza mechanicznego transportowanego razem ze złożonym przęsłem mostu na podwoziu gąsienicowym. Długość pojedynczego przęsła mostu nożycowego wynosi 20m, a nośność 500kN. W związku z modernizacją mostu BLG (poszerzenie pasa jezdni) powstała potrzeba przeprowadzenia podstawowych analiz inżynierskich w celu zweryfikowania poprawności konstrukcji. W pracy omówiono próby poligonowe pojedynczego przęsła mostu BLG. Podczas badań poligonowych zmierzono przemieszczenia i odkształcenia mostu poddanego działaniu różnych wariantów obciążeń. Wyniki prób obciążeniowych umożliwiły weryfikację poprawności modeli numerycznych mostu BLG.

Słowa kluczowe: modernizowany most towarzyszący typu nożycowego, próby obciążeniowe.

1. INTRODUCTION

Scissor-AVLB type bridges are subject of studies presented in a paper. These bridges are characterized by high mobility and modular structure [1, 5, 7, 8]. Single module-span consists of two spanning parts of the bridge; two main trucks and support structure joined with a coupling pin. The bridge span is extended automatically by means of a mechanical bridge-laying gear carried together with bridge sections on a self-propelled chassis. The single-span scissors-type BLG (a manufacturer's designation) bridge length available is up to 20m and the load bearing capacity is of 500kN. The bridges offer obstacle/gap-crossing capability to tracked and wheeled vehicles [1, 4].

In connection to the BLG-67 bridge modernization (bridge deck widening), there arose the need to conduct basic engineering analyses in order to verify the structure's correctness. Considering the fact that the structure of a BLG bridge is a typical thin-walled one of a complex internal structure, innovative engineering systems (CAD/CAE) were implemented in analyses [2, 3, 6].

Some aspects of an experimental test of the single-span scissors-type BLG bridge operation were presented here. Displacements and strains in particular sections of the structure were measured during field tests with different load modes.

2. I STAGE OF THE FIELD TEST – MEASUREMENTS OF DISPLACEMENTS

Field tests on an actual structure of a BLG scissors-type bridge were performed in Military Engineering Works. A fully efficient BLG bridge that underwent a general overhaul in Military Engineering Works was used for that purpose (see Fig. 1). The bridge was deployed to a crossing position on a test stand intended for tests and examinations of bridge structures that are repaired, modernized and produced in Military Engineering

Works. The test stand in the form of a dry pool with concrete abutments located on the premises of Military Engineering Works is illustrated in Fig. 1.
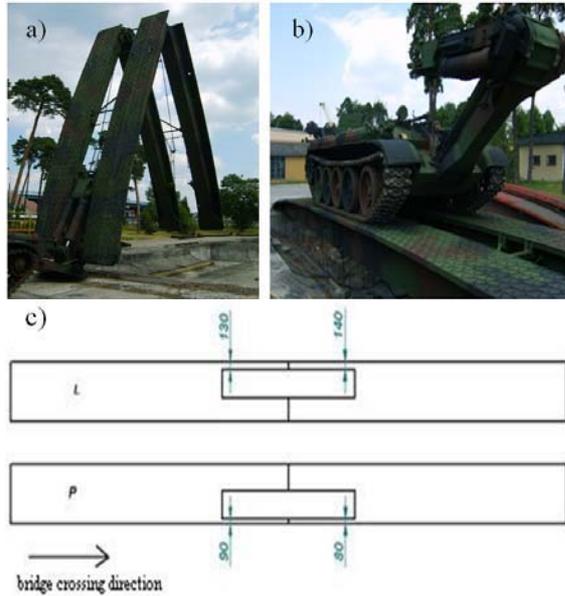
Fig. 1. a) A view of the tested BLG bridge during the deployment process,
b) BLG tracked carrying chassis without the transported span during the load test,
c) A schematic of the location of the contact between caterpillar tracks and the bridge span at the point where the vehicle had stopped

Prior to beginning actual load tests on a span of the BLG bridge, a test drive of a BLG tracked carrying chassis onto the bridge span laid on concrete pool abutments was realized (see Fig. 1, 2). The purpose of the operation was to initially locate metal anchorages built at the bottom of the abutments of the bridge girders on pool edges under the influence of an external load. Once the chassis/carrier had left the bridge span, there was performed a calibration of the measuring apparatus that corresponded with the state of being loaded only by the deadweight of the span structure. Subsequently, load tests on the BLG span were performed. A BLG tracked carrying chassis without the transported span constituted load in this test. A vehicle in such a configuration, which is presented in Fig. 1b), has a mass of 33.3 tons.

Displacements were measured by means of mechanical indicators located in the section that corresponded to the half-length of the bridge, and by means of potentiometric indicators located in the selected section of girder (see Fig. 2).

In addition to span bending, there simultaneously occurred girders' torsion both during a normal operation of the scissors-type bridge and a load test conducted on the test stand. The presence of an additional load in the transverse plane of the tested structure is the consequence of the eccentricity of the external load which occurs as a result of the

displacement of the center of gravity of the vehicle that crosses the bridge relative to the longitudinal axis of the bridge.
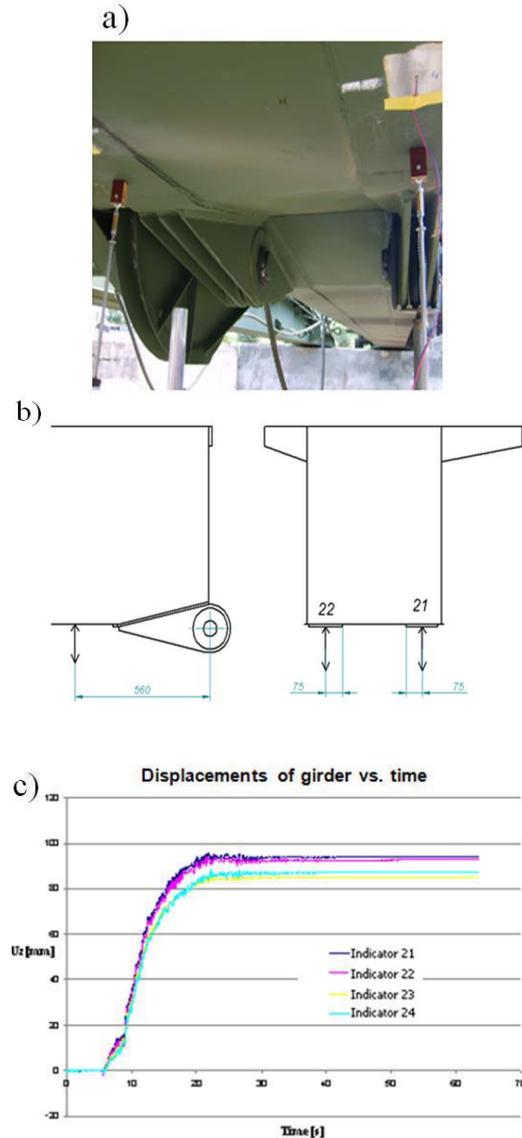
Fig. 2. a) A view of the location of potentiometric indicators used for measuring displacements,
b) A schematic that interprets the location of indicators on the right girder of the bridge, c) Diagram of vertical displacements vs. time recorded during load test

The above-described measurement of the deflection alone by means of mechanical indicators makes it possible to assess the operation of the bridge in the plane of longitudinal bending but is insufficient to estimate the torsion of the structure's members which results from imprecise driving of the vehicle across the bridge and the occurrence of the eccentricity of the external load.

In order to gather sufficient data and prepare a more complete description of the deformations, four potentiometric indicators (two indicators per each girder/deck of the tested bridge) were additionally

used. A schematic of the location of the potentiometric indicators on the right girder as well as the view of them on an actual object is presented in the schematic in Fig 2b) and the photograph shown in Fig 2a)

Since indicators were placed on both sides of the girder, the difference between vertical displacements recorded with the use of them will make it possible to assess the torsional deformation of the girder in the analyzed section accurately. It will allow a more precise interpretation and assessment of the correctness of the results of simulations obtained with the use of the numerical model and the actual BLG bridge structure.

Displacement values measured by means of particular potentiometric indicators were recorded while the tracked chassis was driving across the bridge. Displacements process in the function of the duration of load action on the bridge is shown in diagram presented in Fig. 2c).

The maximum deflection value was recorded for the right span and was equal to 94mm in the analyzed section. The value the reading of which was taken from the scale of the mechanical indicator for the right girder was 95mm. For the left girder, the maximum deflection value measured by means of the mechanical indicator was 87mm and was equal to the value recorded with the use of potentiometric indicators.

3. II STAGE OF THE FIELD TEST – MEASUREMENTS OF STRAINS

Electro-resistant extensometers were used for measuring strains. Extensometers were stuck up on two sections selected on the basis of the assessment of failures that occurred in the process of bridge operations (see Fig. 3).

EA-06-060LZ-120/E electro-resistant extensometers and EA-06-060RZ-120/E rosettes manufactured by Measurements Group Vishay were used for measuring deformations. Measurement signals were recorded by means of an ESAM Traveller EPP Plus extensometric bridge manufactured by ESA-Meßtechnik GmbH as well as a computer with a specialist software for extensometric measurements (Fig. 3a).
Extensometers were stuck up on two sections selected on the basis of the assessment of failures that occurred in the process of bridge operation. Locations of sections are illustrated in figure 3. The section A and B (see Fig. 3b) is located between the 4th and the 5th bulkhead of the girder. In the aforementioned area, there were recorded cracks in the structure that appeared during the bridge operation.
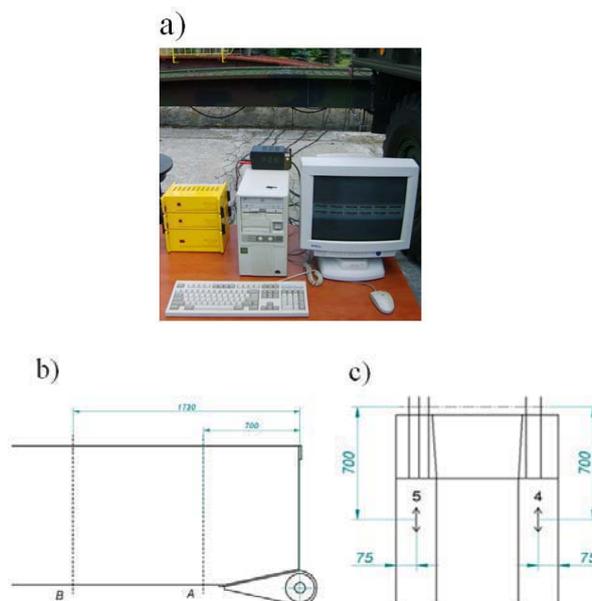
Fig. 3. a) Measuring position used in load test of the AVLB-bridge, b) A schematic of the locations of sections on the left and the right girders, in which deformations were recorded,
c) A schematic that illustrates the locations of extensometers No. 4, 5 on the bottom strips of the right bridge girders

Extensometers were stuck up on symmetrically located sections for the right and the left bridge birders. Strain values were measured simultaneously in 16 points during load tests.

Stress values determined on the basis of the results of measurements the readings of which were taken once the vehicle had stopped at the mid-length of the bridge were 187MPa for extensometer No. 4 and 129MPa for extensometer No. 5. Stress values obtained from numerical analyses were 175MPa and 141MPa for extensometers No. 4 and 5 respectively. Relative differences between the aforementioned stress values were 7% for extensometer No. 4, which was located on the outer strengthening strip, and 8.5% for extensometer No. 5. Table 1 contains correlated normal stress values obtained from the numerical analysis and determined on the basis of the values of deformations recorded during extensometric tests. Relative differences between the aforementioned values are also given in the table.

Table 1

Extensometer No.	Experiment [MPa]	FEM [MPa]	Difference [%]
4	187	175	7
5	129	141	8.5

Exemplary stress curves determined on the basis of the results of measurements recorded by extensometers No. 4 and 5 (section A) are presented in Figure 4.
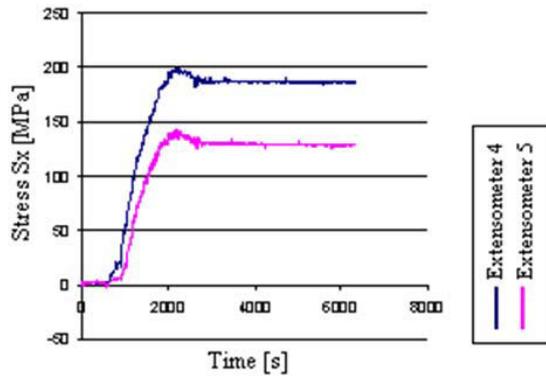
Fig. 4 The diagram with exemplary stress
curves determined on the basis of the results
of strains measurements

4.   CONCLUSIONS

Load tests performed on a modernized BLG
bridge structure made it possible to verify the
correctness of numerical models, which will be used
for assessing stress distribution in the analyzed
structure as well as analyzing the bridge in different
configurations in special uses, taking crisis situations
into particular consideration. Verification of the
correctness of models was performed by comparing
deflections obtained in load mode that corresponded
with the test performed on the test stand.

Displacements were measured by means of
mechanical indicators located in the section that
corresponded to the half-length of the bridge, and by
means of potentiometric indicators located in the
selected section of girder. In the considered load
mode, the maximum difference between
experimental results and the results developed by
means of numerical analyses was approximately 9%.

REFERENCES

[1] Ministry of National Defence in Poland. 1994:
     Military Bridges. Manual published by MND in
     Poland, (in Polish).
[2] Krason, W., Wieczorek, M., 2004: *Strength of
     the Floating Bridges - Computer Aspect*.
     Published   by   Military   University   of
     Technology, Warsaw: 269 p., (in Polish).
[3] Krason, W., Filiks, L., 2008: *Rigid and
     Deformable Models in the Numeriacal Strength
     Tests of Scissor Bridge.* Biuletyn WAT, Vol.
     LVII, No. 2 (650), 2008, pp. 103-116. (in
     Polish).
[4] Operational Manual, 1996: *Trilateral Designe
     and Test Code for Military Bridging and Gap-
     Crossing Equipment.* Published in the United
     Statets.
[5] Fowler J. E., Resio D. T., Pratt J. N., Boc S. J.,:
     Innovation for future gap-crossing operations.
     Engineer and Development Research Center
     Vicksburg, MS39180.
[6] Zielinska A.: *Strength verification of the vehicle
     frame for horizontal launched bridge girder.*
     Przegląd Mechaniczny, Z. 9/2006, LXV.
[7] Leading Military Bridge technology: *LEGUAN
     Bridge on SISU Truck for the Finnish Army.*
     Military Technology, oct 2006, 30, 10, ProQuest
     Science Journals, pp107
[8] Chen S., Petro S., Venkatappa S., GangaRao H.,
     Moody J.: *Modal testing of an AVLB bridge.*
     Experimental Techniques, Nov/Dec 2002, 26, 6,
     ProQuest Science Journals, pp43-46.

SIMULATION VERIFICATION OF DAMAGE DETECTION ALGORYTHM

Krzysztof MENDROK

AGH University of Science and Technology, Department of Robotics and Mechatronics,
al. Mickiewicza 30, 30-059 Krakow, Poland, e-mail: mendrok@agh.edu.pl

Summary

A modal filter is an excellent indicator of damage detection, with such advantages as low computational effort due to data reduction, ease of automation and low sensitivity to environmental changes [4,5]. However to apply it in a real SHM system, it first needs to be extensively tested to verify its sensitivity to damage location, inaccuracy of sensor location in the consecutive experiments, measurements noise as well as changes in ambient conditions, such as temperature and humidity. This paper presents the results of numerical simulations that test the sensitivity of the modal filter based damage detection method to the factors listed above. For this purpose three numerical models of the physical systems were created and applied.

Keywords: modal filter, damage detection, ambient conditions.

WERYFIKACJA SYMULACYJNA ALGORYTMU WYKRYWANIA USZKODZEŃ

Streszczenie

Filtr modalny jest bardzo dobrym wskaźnikiem wykrywającym uszkodzenie, posiadającym takie zalety jak niewielkie wymagania obliczeniowe, łatwość automatyzacji procedury i niska wrażliwość na zmiany warunków zewnętrznych [4,5]. Jednakże, aby zastosować go w rzeczywistym układzie monitoringu musi najpierw przejść szczegółowe badania symulacyjne w celu weryfikacji jego wrażliwości na takie czynniki jak lokalizację uszkodzenia, niedokładność umieszczania czujników w kolejnych pomiarach, zakłócenia toru pomiarowego oraz zmiany warunków otoczenia takich jak temperatura i wilgotność. W pracy tej przedstawiono wyniki weryfikacji symulacyjnej, sprawdzającej wpływ powyższych czynników na wyniki filtracji modalnej. W tym celu sporządzone zostały i zastosowane trzy modele numeryczne.

Słowa kluczowe: filtr modalny, wykrywanie uszkodzeń, warunki otoczenia.

1. INTRODUCTION

A modal filter is a tool used to extract the modal coordinates of each individual mode from a system's output [2, 3]. It decomposes the system's responses into modal coordinates, and thus, on the output of the filter, the frequency response with only one peak, corresponding to the natural frequency to which the filter was tuned, can be obtained. Very interesting way of using modal filtering to structural health monitoring was presented by Deraemaeker and Preumont in 2006 [4] Frequency response function of an object filtered with a modal filter has only one peak corresponding to the natural frequency to which the filter is tuned. When a local change occurs in the object – in stiffness or in mass (this mainly happens when damage in the object arises), the filter stops working and on the output characteristic other peaks start to appear, corresponding to other, not perfectly filtered natural frequencies. On the other hand, global change of entire stiffness or mass matrix (due to changes in ambient temperature or humidity) does not corrupt the filter and the filtered characteristic has still one

peak but slightly moved in the frequency domain. The method apart from the earlier mentioned advantages, which results from its low sensitivity to environmental conditions has very low computational cost, and can operate in autonomous regime. Only the final data interpretation could be left to the personnel. This interpretation is anyhow not difficult and it does not require much experience. Another advantage of the method results from the fact that it can operate on the output only data.

Method described above was in 2008 extended to damage localization by K. Mendrok [5]. The idea for extension of the method by adding damage localization, bases on the fact, that damage, in most of the cases, disturbs the mode shapes only locally. That is why many methods of damage localization use mode shapes as an input data. It is then possible to divide an object into areas measured with use of several sensors and build separate modal filters for data coming from these sensors only. In areas without damage, the shape of modes does not change and modal filter keeps working – no additional peaks on the filter output. When group of sensors placed near the damage is considered, mode

shape is disturb locally due to damage and modal filter does not filters perfectly characteristics measured by these sensors.

Because the method looks promising it can be applied in a real SHM system, however it first needs to be extensively tested to verify its sensitivity to damage location, inaccuracy of sensor location in the consecutive experiments, measurement noise as well as changes in ambient conditions, such as temperature and humidity.

2. MODELS USED FOR SIMULATIONS

As stated above, three different models of the physical systems were created for the verification procedure. All the models were created using the finite element methodology. The first model was used to verify its sensitivity to damage location, inaccuracy of the sensors' location in the consecutive experiments and the noise of the measured characteristics. The FEM model was created directly using MSC.Patran 2008 R1 software. It represents a steel beam with dimensions of 20 x 4 x 1 m supported at its free ends. It was modeled with 69,000 solid elements and 68,500 nodes. Such a dense mesh was required for tests on the inaccuracy of the sensor location. For the influence of damage location analysis, 4 cracks were modeled as discontinuity of a finite element mesh in different locations on the beam. For the purpose of further analyses, the following normal mode analysis scenarios were considered: beam without crack (reference state), beam with crack numbers 1, 2, 3, and 4 consecutively. In Figure 1 the locations of the cracks are presented.
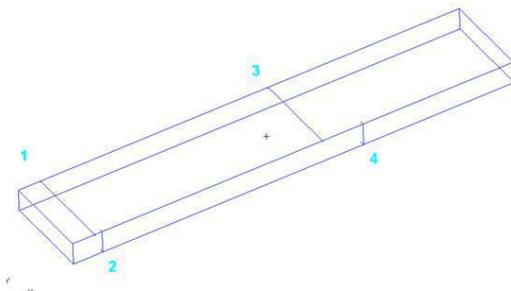
Fig. 1. Cracks in the beam model

The second model used for analysis was a metal frame and is presented in Figure 2. The model had a complex geometrical shape, was non-homogeneous (steel - aluminum), had realistic boundary conditions and thermal expansion was included. The main goal of this simulation was to investigate the influence of different temperature loads on the modal filtration and to compare it with the effect of damage. It was also modeled in MSC.Patran and meshed with 10,000 hex-8 elements (the number of nodes - approximately 14,000).
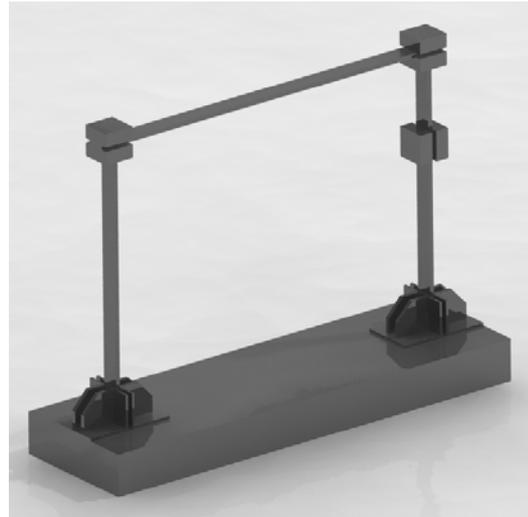
Fig. 2. 3D model of the frame

In order to investigate the behavior of a damaged frame, a horizontal beam crack was modeled as node disconnectivity. There were two crack stadiums - 5% and 10% of the cross-section area. The material properties applied to the model are listed in Table 1.

Table. 1. Material properties selected for simulation

	Steel (20°C)	Aluminum (20°C)
Young modulus [MPa]	$2.1*10^5$	$0.69*10^5$
Poisson's ratio	0.3	0.33
Density [g/cm^3]	7.85	2.71
Thermal expansion coefficient [1/K]	$1.5*10^{-5}$	$2.35*10^{-5}$
Thermal conductivity [W/m*K]	47	193
Specific heat capacity [J/kg*K]	420	880

Because the Young modulus varies with temperature, temperature-dependent material properties were applied. The material properties of aluminum were applied only to the horizontal beam. To take into account temperature-dependent material properties, each design scenario was carried out in two sub-stages; first – coupled mechanical-thermal analysis to obtain the temperature distribution, second – normal mode analysis. The following cases were analyzed: frame without crack – ambient temperature 20 °C (reference state), frame with 10% crack on upper beam, frame without crack – ambient temperature 25, 30, 35, 40, 50, 0 and -50 °C, frame without crack – upper beam heating (30 s) with 50 °C, frame without crack – local heating of the right vertical bar (30 s) with 50 °C.

The last model of a railway bridge used for the analysis of the damage detection procedure effectiveness was developed for two reasons. Firstly, to examine how the ambient humidity can disturb

the procedure, and secondly, to verify how it will work for such a complex structure. The CAD model was based on documentation of a real structure. The bridge is 27 meters long and consists of steel (beams, barriers, rails, and reinforcement of main plate), concrete (main plate and pavements), soil and wood (sleepers) elements. The CAD model is shown in Figure 3. Afterwards, based on the CAD model, a FEM model was built in MSC.Patran. This consists of approximately 28,500 elements and 30,500 nodes. Solid, shell and beam elements were used in the model. The FEM model is shown in Figure 2b. There were three cracks introduced in the model. The first and second are vertical cracks in the web, the third is a flange crack. Crack localization was based on linear-static stress analysis. The crack was modeled as discontinuity of the finite element mesh. Localization of the cracks is shown in Figure 4.
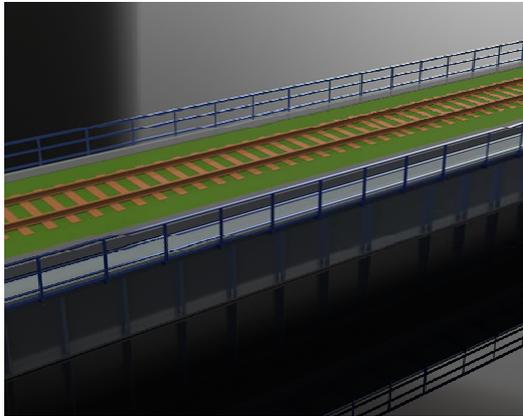
Fig. 3. CAD model of the bridge
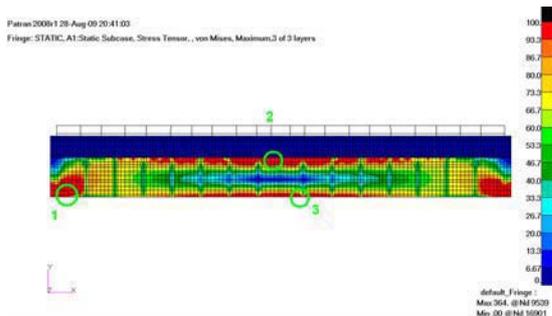
Fig. 4. FE mesh of the bridge model
with cracks localization

To take into account the influence of moisture, different material densities were used. Dependent on the analysis, material densities were appropriately adjusted. The following normal mode analysis scenarios were considered: bridge without crack – dry (reference state), bridge without crack – moist, bridge without crack – wet, bridge with crack numbers 1, 2, and 3 consecutively.

3. TESTING PROCEDURE

To test the influence of the factors listed in previous sections on the modal filter based damage detection procedure, the following operations were conducted. Firstly, the frequency response functions (FRFs) synthesis was performed for the models in reference states. The characteristics were synthesized for selected nodes of the models which simulated virtual measuring sensors with use of the following equation [6]:

$$H_{ij}(j\omega) = \sum_{r=1}^{n} \frac{2 \cdot j \cdot \omega_r \cdot \phi_{ir} \cdot \phi_{jr}}{\omega_r^2 - \omega^2} \quad (1)$$

where: ω_r – r-th natural frequency,
ϕ_{ir} – i-th element of r-th modal vector

Based on the reference modal model and synthesized FRFs of the reference systems, the reciprocal modal vectors were calculated – modal filter coefficients. With use of these coefficients, sets of FRFs for the reference states and for consecutive derogations from these states were filtered. For the obtained results, damage index values were calculated according to the formula [7]:

$$DI_4 = \frac{\int_{\omega_s}^{\omega_f} |x_i(\omega) - x_{ref}(\omega)|^2 d\omega}{\int_{\omega_s}^{\omega_f} x_{ref}(\omega)^2 d\omega} \quad (2)$$

where: ω_s, ω_f – starting and closing frequency of the analyzed band,
x_i, x_{ref} – characteristic in the current and reference state respectively..

The damage index was calculated only for frequency regions, which are the direct neighborhood of the model's natural frequencies, except the one to which the modal filter was tuned. The bandwidth of the consecutive frequency intervals was established at 5 Hz.

4. RESULTS OF ANALYSES

In this section the results of analyses will be presented. Due to the small amount of space available for the paper, no plots of modally filtered characteristics will be shown. The damage index values are presented only for the modal filter tuned to the mode shapes for which the indication of the modeled crack was the best.

In the first stage of simulation, the influence of the damage location on its detectability was examined. In the beam model 4 cracks were introduced at different locations (see Fig. 1). The size of each crack amounted to 5 % of the beam's cross-section area. In addition, in this section the authors checked which natural frequency the modal filter should be tuned to, in order to best detect the

expected damage. In Table 2, the maximal values of the damage index calculated for the consecutive damages are presented, together with information about the natural frequency to which the modal filter was tuned. In Figure 5 results of modal filtration performed for this simulation are presented. of damage is subjected to the largest deformation.

Table 2. Damage index for different damage locations

No. of Damage	Max Value of DI	No. of MF
1	3.5	7
2	13.5	5
3	12	1
4	810	1
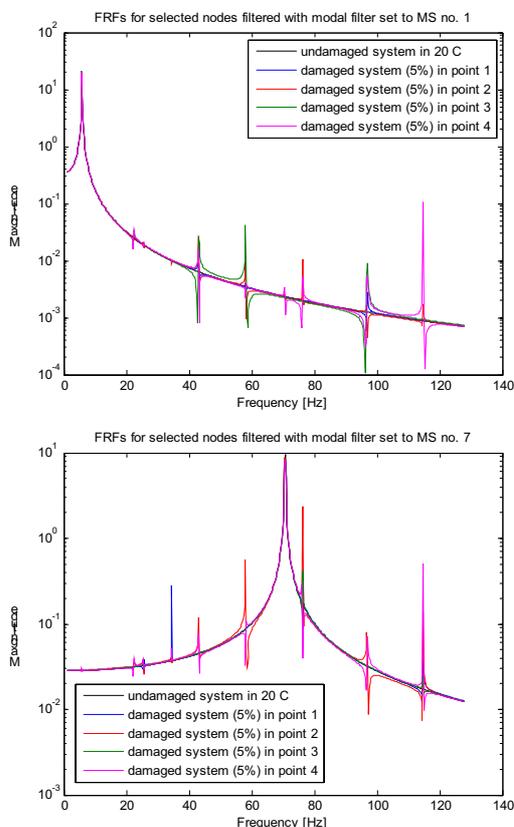
Fig. 5. Results of modal filtration tor different crack locations – modal filter set to natural frequency no.1 and 7

Best detectable damage is Crack 4 – in the middle of the beam, along the short side. The large difference in the damage index value between Crack 4 and the others results from the method of the damage index calculation – the square of the characteristics' difference is considered (1). The far worse results obtained for Damage 3 arise from the fact that it is much shallower than No. 4 (constant area with a much greater width). This is confirmed by the fact that among Cracks 1 and 2 the deeper one also gives higher values of the damage index. For

Cracks 1 and 2, the highest damage index values were noted for filters tuned to Natural Frequencies 4, 7, 9 and 10, with a clear dominance of Natural Frequency 7. These frequencies correspond to torsional modes and higher bending modes. Cracks 3 and 4 are definitely best detected by Modal Filter 1 (tuned to Natural Frequency 1) - by far the highest amplitude of vibration in the fracture region. From the conducted analyses, it can be concluded that the detection of cracks should be performed with use of a filter which is set to the mode in which the region.

To carry out the next verification test, it was assumed that in the consecutive measurements the sensors are slightly shifted against the reference position. The values of these shifts were defined as 1.5%, 1% and 0.5% of the beam length. It was assumed that the sensor position error can be committed only along the X axis - to the right or the left and that, in a single measurement, sensors will be positioned with a constant error value (e.g. 1%). Taking 8 virtual sensors, there were 256 combinations to analyze for each considered value of inaccuracy. Modal filtering errors for all cases at the same assumed sensor shift value were at a similar level and the highest values were achieved by Modal Filter 1. In Figure 6 results of modal filtration are shown. For presentation in Table 3, the worst cases were chosen, that is, those where the accuracy of modal filtering was the worst. These results were compared with Damage 4.

Table 3. Damage index for incorrect sensors location

Simulation Scenario	Max Value of DI
Damage no. 4	810
Sensors Sift 0.5 %	890
Sensors Sift 1.0 %	2480
Sensors Sift 1.5 %	9920
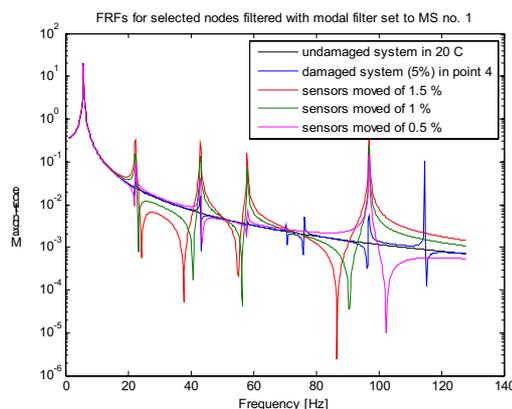


Fig. 6. Results of modal filtration tor incorrect sensors location – modal filter set to natural frequency no.1

The calculated values of the damage index confirm the significant impact of damage to the accuracy of the sensor location in the subsequent measurements on the results of modal filtration, and

thus the effectiveness of the method. In the case of the analyzed beam, the smallest sensor shift gives a comparable value of the index to 5% crack at the point where it is easiest to detect. The obtained results allow the following conclusions to be formulated:

- since the method depends on the mode shape, it requires high repeatability for the location of sensors, and therefore it is recommended for systems where a network of sensors is permanently attached to the object - a classic SHM system,

- if the method is used as an NDT technique, attention should be paid to the repeatable placement of sensors. Additionally, the level of damage that could be detected in this way should be raised to about 10% in order to avoid false alarms.

In the third stage of the simulation study, the impact of noise on the modal filtration results was tested. The simulations will test the influence of interference generated by the measuring equipment on the modal filtering errors. Considering the characteristics of the sensors, their attachment (character - not location), as well as disruptions in wires and recording devices, the signal to noise ratio for the entire measurement path is set at 40 dB, which corresponds to the noise of 0.01% recorded signal amplitude. To ensure a large enough margin error, it was decided to introduce noise of a normal distribution, zero mean and amplitude of 5% of noised characteristics. Results of modal filtration for this case are shown in Figure 7. In Table 4, the values of the damage index for the noised characteristics and Crack 1 were compared, both for Modal Filter 7.

Table 4. Damage index for noisy data

| Simulation Scenario	Max Value of DI
Damage no. 1	3.5
5 % Noise on the Data	0.39
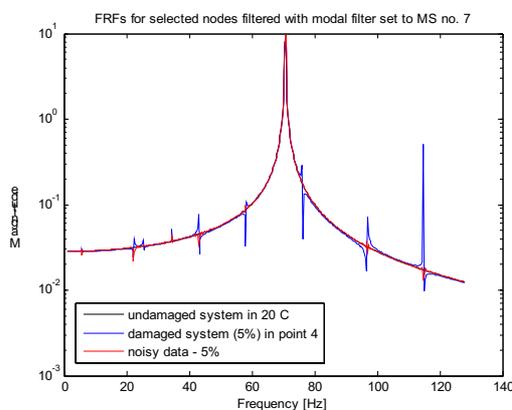
Fig. 7. Results of modal filtration tor noisy data – modal filter set to natural frequency no.7

On the basis of this part of the simulations, it can be concluded that the noise associated with the

measuring path does not affect the operation of the proposed method of damage detection

One of the most important issues in the analysis of damage detection method properties is their sensitivity to changes in external conditions, especially ambient temperature. Therefore, it was decided to carry out extensive simulation studies devoted to the influence of ambient temperature changes on the results of the modal filtration. The tests were performed for various values of ambient temperature where the entire object had the same temperature as the environment, and for two special cases. The first one reflects the situation where the sun heats one of the parts of the object, while the others remain in the shade or are additionally cooled by their proximity to the river. In this scenario, the simulated model was heated from above at the time, which prevented its total warming. The second special case is the situation where the temperature changes only in one fragment of an object as the result of some artificial source of heat. In Figure 8 results of modal filtration performed for this simulation are presented. Table 5 shows the damage index values collected for all changes in temperature as well as for the damage of 5% and 10%. In all cases the modal filter was tuned to Natural Frequency 2.

Table 5. Damage index for temperature changes

Simulation Scenario	Max Value of DI
Damage 5 %	5.8×10^6
Damage 10 %	3.6×10^8
Ambient Temp. 25 ^{O}C	2.7×10^5
Ambient Temp. 30 ^{O}C	9.2×10^5
Ambient Temp. 35 ^{O}C	2.5×10^7
Ambient Temp. 40 ^{O}C	15.6×10^7
Ambient Temp. 50 ^{O}C	1.9×10^8
Ambient Temp. 0 ^{O}C	8.8×10^6
Ambient Temp. -50 ^{O}C	2.3×10^9
Upper Heating 50 ^{O}C	4.5×10^7
Local Heating of the Right Bar 50 °C	5.7×10^9

After analysis of the damage index values, it can be seen that the impact of 5% damage is greater than a temperature change of 5 ^{O}C. However, if one wants to use the method for a wider ambient temperature range, it is suggested some kind of modal filter bank should be built. In such a bank, one would have the reference model of the system identified for various ambient temperatures. In order to decide on the bank of filters designated for every 10 ^{O}C, it is recommended to increase the minimum size of recognizable damage to about 10%. The damage index calculated for such damage is higher than the value of the difference in temperatures reaching up to 30 ^{O}C. In addition, the heating frame from the top gives a lower value of the damage index than the damage. The worst of the simulated cases were the temperature change of 70 ^{O}C

(ambient temperature -50 ^{O}C) and heating only the vertical bar of the frame. Both of these cases, however, do not disqualify the method, since the 70 ^{O}C difference in temperature using even a small bank of filters should not occur, and local high temperature change should be detected, because it can be regarded as a failure.
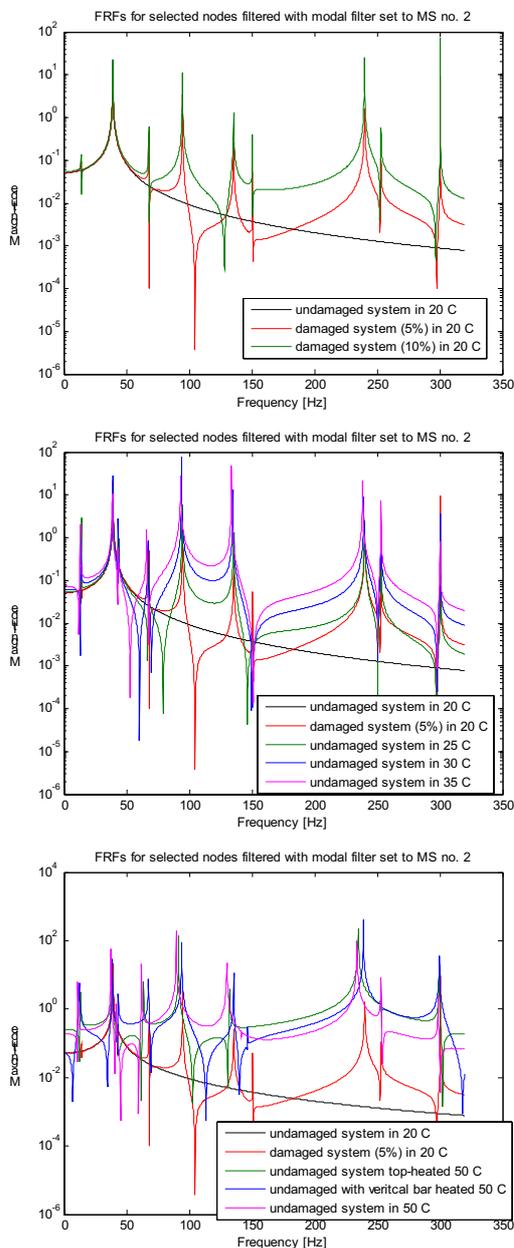
Fig. 8. Results of modal filtration for temperature changes – modal filter set to natural frequency no.2

To examine the operation of the method for a complex civil engineering object (real structure), and check the effect of humidity on the efficiency of the damage detection method again, the modal filter coefficients were calculated for the reference model, which is a dry bridge without any damage. Results of modal filtration for the bridge are shown

in Figure 9. In Table 6, one can find the damage index values for 3 cracks introduced to the bridge consecutively and for a moist (relative humidity 99%) and wet (after intense rainfall) bridge. All results are for Modal Filter 10.

Table 6. Damage index for bridge simulations

Simulation Scenario	Max Value of DI
Damage no. 1	7210
Damage no. 2	2.7×10^4
Damage no. 3	7.3×10^7
Moist Bridge	1670
Wet Bridge	3.2×10^9
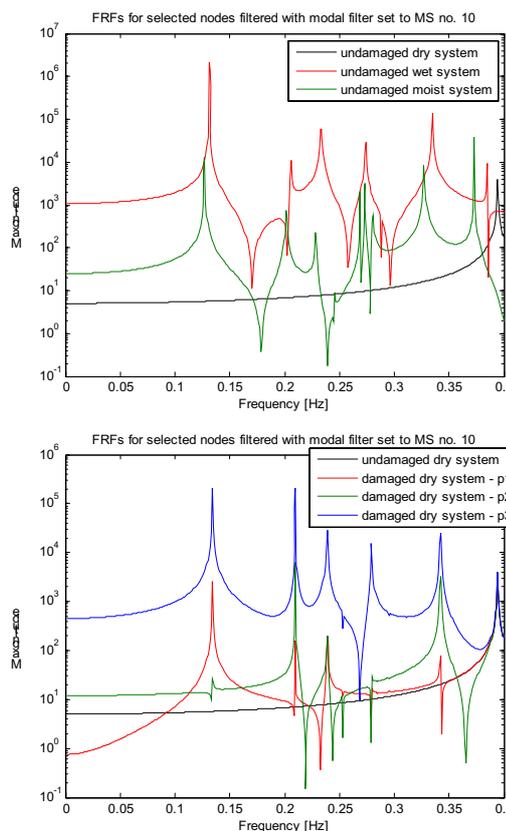
Fig. 9. Results of modal filtration for bridge simulations – modal filter set to natural frequency no.10

The analysis of the damage index values confirmed the lowest detectability of Damage 1 - close to the support. To obtain the higher values of the damage index for this crack, one should take into account the modal filters tuned to higher modes – the ones which greater deform the region of Damage 1. Regarding the impact of humidity changes, it is quite significant - the weight of soil and wood changes by over 10 percent and is a significant share of the object's total mass. On this basis, it is concluded that the method should not be applied to objects which change their mass so heavily due to moisture. On the other hand, the method has shown its effectiveness in detecting small-scale damage for such a highly complex technical facility.

5. SUMMARY

The paper presents the results of numerical tests for a damage detection procedure based on modal filtration. The following cases has been considered: verification of the method sensitivity to damage location, inaccuracy of sensor location in the consecutive experiments, measurement noise and changes in ambient conditions, such as temperature and humidity. Additionally the applicability of the method was examined for very complex structure – rail viaduct with elements made of steel, concrete, wood and soil. Partial conclusions were presented in the last section after the results of each study. A general conclusion is that the method detects damage with good sensitivity but users have to be aware that, since the method is based on the modal model, it can be influenced by other factors which change the modal model parameters. On the other hand basing on the results of the earlier studies of the authors [1] it can be stated that the method is much less sensitive to environmental changes than other modal model based methods.

ACKNOWLEDGEMENT

REFERENCES

[1] Mendrok K., Uhl T.: *Overview of modal model based damage detection methods.* Proceedings of 2004 ISMA, Leuven, Belgium, (2004).

[2] Zhang Q., Allemang, R.J., Brown, D.L.: *Modal Filter: Concept and Applications.* Proceedings of International Modal Analysis Conference, pp. 487-496, (1990).

[3] Meirovitch L., Baruh H.: *Control of self-adjoint distributed parameter system.* Journal of Guidance Control and Dynamics, 8 (6), 60-66, (1982).

[4] Deraemaeker A., Preumont A..: *Vibration based damage detection using large array sensors and spatial filters.* Mechanical Systems and Signal Processing, Volume 20, Issue 7, 1615-1630, (2006).

[5] Mendrok K., Uhl. T.: *Modal filtration for damage detection and localization.* Proceedings of 4th EWoSHM, Krakow, (2008).

[6] Uhl T.: *Komputerowo wspomagana identyfikacja modeli konstrukcji mechanicznych.* WNT, Warszawa, (1997).

[7] Mendrok K., Uhl T.: *The application of modal filters for damage detection.* Smart Structures and Systems, Vol. 6, No. 2 (2010).

PhD. Eng. **Krzysztof MENDROK**
Is a senior researcher in the Department of Robotics and Mechatronice of the AGH University of Science and Technology. He is interested in development and application of various structural health monitoring algorithms. He mainly deals with low frequency vibration based methods for damage detection and inverse dynamic problem for operational load identification.

METHODOLOGY OF THE DEFECT MAPS AND ITS APPLICATION FOR REPRESENTATION OF VIBRATIONAL EFFECTS OF BEARING MISALIGNMENT

Józef RYBCZYŃSKI

Institute of Fluid-Flow Machinery, Polish Academy of Sciences, 80-952 Gdańsk, Fiszera 14,
Tel.: (+48) 058-6995273, E-Mail: ryb@imp.gda.pl   rybczynskij2@asme.org

Summary

The essence of the present work is an innovative methodology consisting in creation and presentation of complex diagnostic relations in the form of "defect maps", which allow mapping the machine technical state in certain domain of random events represented by defects. In the case of the bearing misalignment defect, which is the subject of the present article, the "domain of events" is the area of possible bearing dislocations and the "technical state" may be expressed e.g. by vibrations of the machine elements. The effect of this work is complete set of maps, which present distribution of bearing vibration as functions of individual bearing displacements. Within this work various types of bearing misalignment maps were constructed, intended for various applications in the turbogenerator diagnostic system. The defect maps methodology applied here for presentation of the bearing misalignment effects has been generalized and proposed as the idea of presentation of a machine response to certain class of defects.

Keywords: technical diagnostics, rotating machine, mechanical vibration, misalignment.

METODYKA MAP DEFEKTÓW W ZASTOSOWANIU DO PREZENTACJI DRGANIOWYCH SKUTKÓW ROZOSIOWANIA ŁOŻYSK

Streszczenie

Istotą niniejszej pracy jest innowacyjna metodyka polegająca na tworzeniu i prezentacji złożonych relacji diagnostycznych w formie „map defektów", które pozwalają odwzorowywać stan techniczny maszyny w pewnym obszarze zdarzeń losowych reprezentowanych przez defekty. W przypadku defektu rozosiowania łożysk, który jest przedmiotem niniejszego artykułu „obszar zdarzeń" może być wyrażony np. przez drgania elementów maszyny. Efektem pracy jest kompletny zestaw map, które prezentują rozkład drgań łożysk jako funkcję indywidualnych przemieszczeń łożysk. W ramach tej pracy zostały utworzone różne rodzaje map skutków przemieszczeń łożysk, przeznaczone dla różnorodnych zastosowań w systemie diagnostycznym turbogeneratora. Metodyka map defektów, zastosowana tu do prezentacji efektów rozosiowania łożysk została uogólniona i zaproponowana jako sposób prezentacji odpowiedzi maszyny na pewną klasę defektów.

Słowa kluczowe: diagnostyka techniczna, maszyna wirnikowa, drgania mechaniczne, rozosiowanie.

1. INTRODUCTION

For turbo-generators of great power developed are extended diagnostic systems, which need proper diagnostic knowledge for safer operation. For continuous evaluation of the machine condition employed are self-acting diagnostic systems. The diagnostic systems need formulated previously "diagnostic relations", which link type and intensity of defects with their measurable effects [1-4].

We have worked for many years on the diagnostics of power turbo-generators, especially in the aspect of bearing misalignment defect. During this activity we found, that misalignment of bearings has great effect on the dynamic state of large rotating machines with a long shaft line supported in numerous bearings [5-8]. Location of particular bearings in relation to other bearings determines the bearing load distribution, therefore determines the shaft line shape and, as a consequence, operation of all bearings and, as a consequence, also rotors. The observations confirm numerous literature positions, e.g. [9-13]. According to Bognatz [14], the bearing misalignment defect may cause even 70% of vibration problems, which are recorded in rotating machines. Numerous phenomena observed in turbo-sets, which frequently grow stronger or vanish without a visible reason and are difficult to explain, are expected to have their origin in bearing misalignment [2, 5, 9-11, 14]. It is noteworthy and
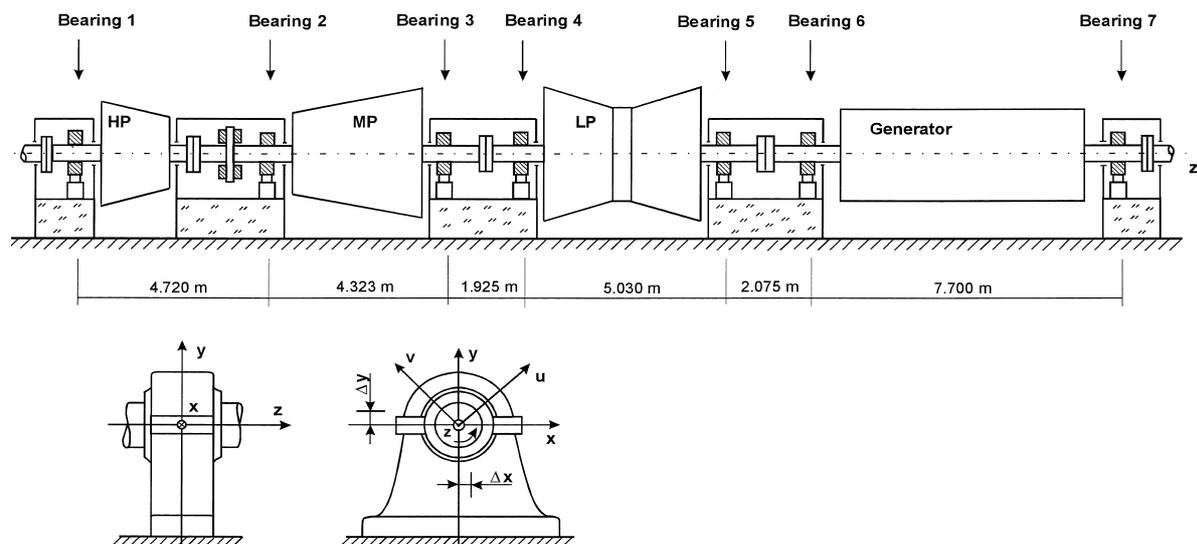
Fig. 1. Scheme of the 13K215 turbogenerator, which shows location of bearings and orientation of the machine in the coordinate system used in the analyses

underlined by majority of authors of papers on the subject that the literature on the bearing misalignment defect is anyway rather poor [9, 10, 13, 15, 16]. Especially Muszynska in [9] stresses it very strongly. In multi-support machines like the analyzed turbogenerator particular bearings are arranged in such a way that the shaft line consti-tutes a catenary. It helps to reduce shaft bending at the couplings. The catenary is determined theoretically in the design phase and then practically implemented in the process of machine assembly by proper positioning of axes of particular bearings with respect to the geodesic line [2, 9, 10]. Displacement of any turboset bearing from its optimum position, defined by the designed shaft catenary, changes conditions of operation of the hydrodynamic bearings and rotors supported on them. The distribution of the static load of particular bearings changes, and vibrations can be generated [2, 5, 9-11, 13-16]. Reasons for bearing displacements from the designed catenary can be of various natures, mainly connected with machine assembly and operation processes, and/or possible failures [7, 10].

During our work connected with the bearing misalignment defect we encountered troubles with gathering and interpreting great quantity of information, which were the results of computer simulation [6, 8]. The effect of seeking the method for proper arrangement of the acquired data is the idea of "maps of defect effects". The defect maps make possible presentation of response of a machine to defects in the comprehensible and easy interpretable form. The utilitarian effect of the work is the complete set of maps, which present distributions of the bearing vibration and the bearing

load as a function of individual bearing displacements in relation to bearing proper position. The mapping may be regarded as the set of diagnostic relations or may be used for creation of the relations [1, 3, 4, 8]. Practical significance of the presented here investigations consists in possibility of direct application of the simulation results in a turbo-set diagnostic or advisory system, namely, the diagnostic relations may be included to the turbo-generator diagnostic knowledge base. Results of the work were intended for a certain specific 13K215 power turbo-generator, which works in the power station; therefore all results may find direct application to this real machine.

2. CALCULATION PROCEDURE AND OBJECT OF ANALYSIS

The object of calculations and following analysis is the 13K215 turbogenerator of 200MW power, which works in one of Polish power plants. The obtained results and conclusions may be directly applied to this specific machine as this machine was modelled and to this machine the model was tuned up. The machine consists of the three-stage steam turbine and the electric generator. Its scheme, showing the arrangement of shafts and distribution of bearings, is given in Fig. 1. Rotors of the four-casing machine are supported on seven bearings. Main dimensions and other characteristic features of the bearings are included in Table 1.
All calculations we carried out using a set of computer codes composing the system MESWIR. It is a package of codes, which has been developed for many years in the Institute of Fluid-Flow Machinery

Table 1. Characteristics of the turbo-set bearings and main operation parameters for the base case

Parameter	Denotation	Bear. 1	Bear. 2	Bear. 3	Bear. 4	Bear. 5	Bear. 6	Bear. 7
Diameter	D [m]	0.300	0.330	0.360	0.450	0.450	0.400	0.400
Length	L [m]	0.210	0.270	0.290	0.358	0.358	0.500	0.400
Clearance, horiz.	ΔR_H [mm]	0.643	0.650	0.745	0.880	0.885	0.885	0.245
Ellipticity ratio	m [-]	0.7309	0.700	0.7342	0.3886	0.3898	0.4520	0.0408
Eccentricity	ε [-]	0.3360	0.2684	0.3587	0.5226	0.5636	0.5095	0.3653
Attitude angle	γ [deg]	350.6	354.6	351.7	329.3	327.9	334.1	333.7
Oil abs. viscosity	μ [N*s/m^2]	0.0233	0.0276	0.0272	0.0296	0.0296	0.0283	0.0188
Bearing load – hor.	Q_x [N]	-1,042	-603	-7,133	7,473	-4,108	3,523	-741
Bearing load – vert.	Q_y [N]	41337	62351	164430	186740	255100	293520	253880
Relative vibr. – hor.	$A_{pp\,u}$ [µm]	49.3	60.8	29.8	30.7	31.7	44.2	17.9
Relative vibr. – vert.	$A_{pp\,v}$ [µm]	43.4	50.8	20.9	6.7	13.7	16.9	11.3
Absolute vibr. – hor.	V_x [mm/s]	0.54	1.04	0.80	0.18	0.39	1.51	0.87
Absolute vibr. – vert.	V_y [mm/s]	0.31	1.65	0.61	0.83	1.62	1.88	1.11

intended for calculating dynamics of rotors supported on oil bearings. The MESWIR is not specific for presented here calculations, but it was adopted for bearing misalignment simulation. Its detailed description and features are published among others in [17, 18] and its application to bearing misalignment is presented in [6-8]. Post-processing and visualisation were performed using MATLAB. The bearing static characteristics were obtained as a solution to the two-dimensional Reynolds equation by making use of Reynolds' boundary conditions. In the calculation model the bearings are treated as hydrodynamic oil bearings of finite width.

The reference point for our analysis is the "base case" – a numerical model of the machine free of defects. The model particular description is described e.g. in [7, 8, 17, 18]. The base model was created and tuned based on the results of measurements done in a real power plant by the turbogenerator diagnostic system. The measurements were performed in steady state and nominal conditions of turbo-set operation, at the rotational speed 3000 rev/min and at full power output 211 MW. It was assumed that the data recorded in the power plant in these operational conditions illustrate the machine without defects, i.e. that they describe the reference case to be used for comparison with the machine with implemented defect. Table 1 contains most important parameters, which characterize operation of the turbogenerator for the base case. The bearing static loads and bearing shaft positions characterize the bearing operation and amplitudes of relative shaft vibration and RMS velocity of bush absolute vibration characterize the machine dynamic state.
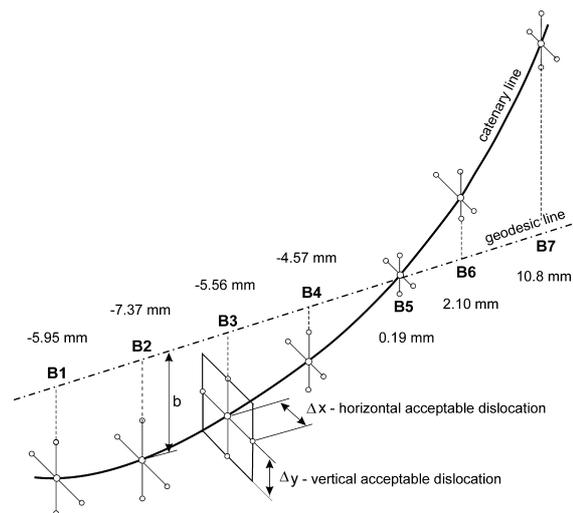
Fig. 2. Scheme of turboset shaft catenary on the background of the geodesic line, and the interpretation of bearing misalignment. b – displacement of a bearing positioned in the catenary with respect to the geodesic line, Δx, Δy – additional bearing displacement with respect to the catenary (defect)

An analysis concept of bearing misalignment defect is schematically shown in Fig. 2. The scheme presents the shape of the catenary line of rotors and against the background of the reference geodesic line. The bearing locations with respect to the geodesic line are denoted as "b" on the Fig. 2. Additional dislocations of the bearings, Δx, Δy representing the "defects" of the machine, were added to the basic dislocation values. In the codes

used for calculations, the locations of particular bearings were introduced as their dislocations with respect to the geodesic line in the bearing data files [6, 17, 18].

For the purpose of creation the maps of bearing misalignment defect, which show vibrational effects of various bearing displacements, an area of simulated bearing dislocations has been defined. The area of possible bearing dislocations defined in the plane perpendicular to rotor axis is presented in Fig. 2 and the Fig. 3. The centre of this area is the base bearing position on the catenary line of the rotors, precisely defined by the turbo-set designer. Assuming the centre position as a base is justified by the fact that bearing dislocations reveal random nature, therefore dislocation of an arbitrary bearing in arbitrary direction is equally possible. Assuming that simultaneous dislocations in vertical and horizontal directions are possible, calculations of the effects of bearing dislocations were performed within the range:

–5mm < < 5mm, with 0,2mm horizontal step,

–5mm < Δy < 5mm, with 0,2mm vertical step.

Consequently, a 51 x 51 grid shown in Fig. 3 was defined, which gave 2601 possible positions of the bearing centre on the dislocation area. Distribution of the calculation points within the 10x10 mm square is marked in the figure with small circles. The base position of bearings on the shaft line catenary is represented in the Fig. 3 by the central point in of the dislocation square. Each point within the square represents a defect consisting in dislocation of a bearing from its base position to this point, that means dislocation of the bearing by Δx, Δy. For every of the 2601points the calculations of the turbogenerator numerical model were carried out by means of the MESWIR codes. For the needs of the present work the following quantities were calculated, every of them in two reciprocally perpendicular directions:

– A_u, A_v, the amplitudes of relative journal-bush vibrations, expressed by the p-p dislocation amplitude in two directions u and v, inclined by 45° to the vertical,

– V_x, V_y, the RMS velocities of absolute bush vibrations, expressed by RMS vibration velocities in the horizontal and vertical directions, x and y.

A machine works properly and safely, when some operation parameters, defined for a given machine as the most important, do not exceed permissible values. For the purpose of here presented work the following criteria are adopted:

A_u, A_v < A_{lim} = 165 μm, where A_{lim} is the limit of relative journal-bush vibrations,

$V_{RMS\,x}$, $V_{RMS\,y}$ < $V_{RMS\,lim}$ = 7,5 mm/s, where $V_{RMS\,lim}$ is the limit of absolute bearing vibrations.
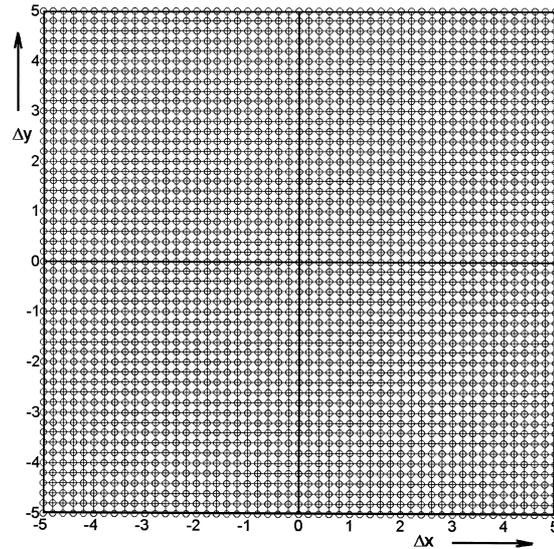

Fig. 3. The area of possible bearing dislocations with grid containing 51 x 51 nodes representing the bearing dislocations for which calculations were carried out

The axes x, y, u, v are interpreted in Fig. 1. The limiting vibration parameters and their values were taken from ISO standards: the relative vibration amplitudes from the standard 7919-2, and the absolute vibration velocities – from the standard 10816-2. The limits correspond to the „warning state". Table 1 shows that for the base case all vibration parameters are much lower than the defined above limits.

3. VARIOUS WAYS OF PRESENTATION OF THE BEARING MISALGNMENT DEFET

The maps of bearing misalignment effects are created automatically by special graphic software written in Matlab. Data for the maps consist of the results of simulating calculations of the machine model with implemented defects. To create a single map, the series of calculations for all the points shown in Fig. 3, which represent the defects, had to be done. Every single map presents distribution of only one vibration parameter concerning one particular bearing as the effect of dislocation of only one bearing within the defined area of dislocations. But vibrational effects of misalignment of a single bearing can be observed in every of seven machine bearings. This means that effects of misalignment of all seven bearings on all seven bearings characteristics can be presented using 49 maps showing the distribution of one single parameter. What is more, characterisation of the machine operation condition need a set of 4 graphs, presenting distribution of 4 parameters, defined in the previous section: A_u, A_v, V_x, V_y. The sample set of such graphs, which is one of the 49 possible sets, is given in Fig. 4.

Each set of graphs, like this in Fig. 4 contains four three-dimensional diagrams illustrating effect of dislocation of one particular bearing on the following parameters observed in one of the machine bearings:

$A_x = f(\Delta x, \Delta y)$ – u-dir. relative vibration amplitude,
$A_y = f(\Delta x, \Delta y)$ – v-dir. relative vibration amplitude,
$V_x = f(\Delta x, \Delta y)$ – x-dir. velocities of absolute vibration,
$V_y = f(\Delta x, \Delta y)$ – y-dir. velocities of absolute vibration.

To order the great number of maps, every particular figure is labelled by a pair of numbers {N_d N_e}, where:

N_d =1...7 is the number of the bearing, in which the defect is present,

N_e =1...7 is the number of the bearing, in which the response (effect) to the above defect is observed.

According to the above denotation the graphs presented in Fig. 4 are labelled by {5,5} and show the effect of dislocation of bearing 5 on the vibration parameters in the same bearing 5. In the diagrams the area of examined dislocations of a bearing is located in the x-y plane and is limited by the square $-5mm < x < 5mm$, $-5mm < y < 5mm$. In the Fig. 2 this area is seen as the square perpendicular to the shaft axis. The base bearing position on the catenary, (i.e. when the misalignment defect is missing), is marked in the Fig. 4 with the vertical line starting

from the centre of the dislocation plane, $\Delta x=0$, $\Delta y=0$. To an arbitrary bearing dislocation by a vector [Δx, Δy] corresponds a certain value of the parameters: A_x, A_y, V_x, V_y. These values for the base case, i.e. for $\Delta x=0$, $\Delta y=0$, are gathered in Table 1. On the vertical axis the level representing the corresponding parameter limit, A_{lim}, $V_{RMS \, lim}$ is marked. Crossing of the plane parallel to the x-y plane and situated at the limit level with the surface representing one of the functions *effect* = $f(\Delta x, \Delta y)$, gives the level line shown in each figure. The steep slopes noticeable on the vibration graphs testify that the gradient of vibration over the dislocation plane is high. The gradient is especially high in the vicinity of limit vibration level, which is marked in the figure with the thick line.

Figures of this type may be presented also in a modified form. Fig. 5 presents sample of the modified diagrams, which correspond to the diagrams shown in Fig. 4 after cutting them off at the level of the adequate parameter limit. The vertical axes of these graphs are properly rescaled. The areas limited by the level lines are marked dark. In these graphs the prohibited bearing dislocations are better visible and distribution of the analysed
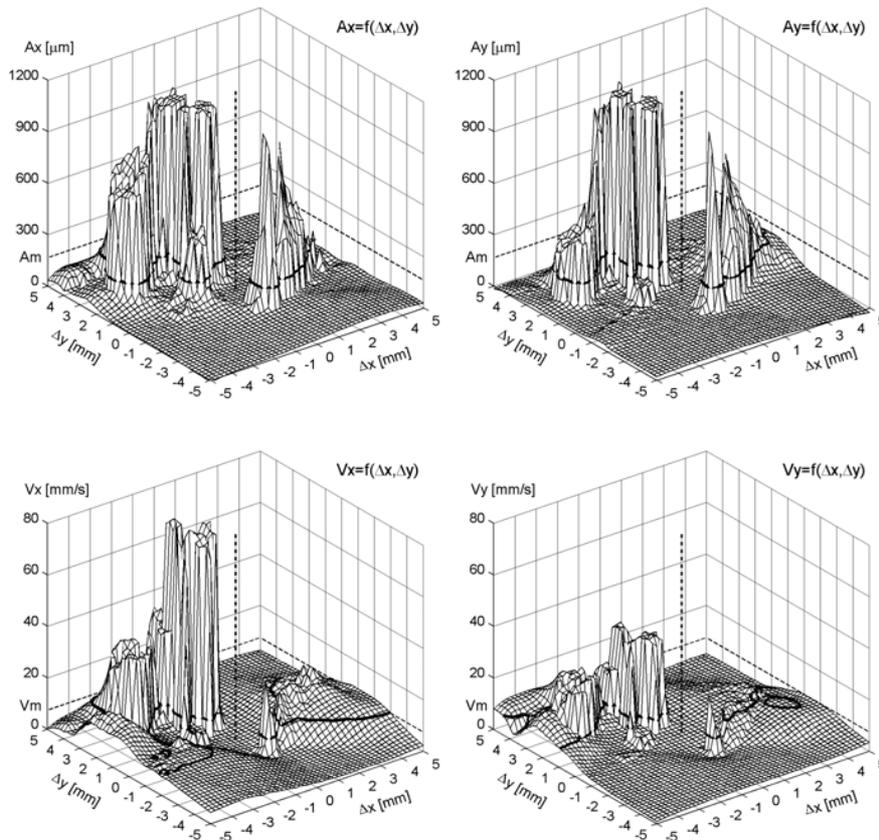

Fig. 4. The set of six three-dimensional diagrams, coded {5,5}, which illustrates effects of dislocation of the bearing 5 on the bearing 5 parameters: amplitude of relative vibration and velocity of absolute vibration, all in horizontal and vertical directions

parameters on the *x-y* plane is more readable. Projection of the limit level lines onto the dislocation plane x-y defines the region of prohibited bearing dislocations. When, in any way, the bearing bush centre falls into this prohibited region (marked dark in the figure), the machine should be stopped from operation as it means that the permissible limit for one of operating parameters was exceeded in at least one bearing.

Fig. 6 presents 2-dimensional but multiple valued graphical representations of the graphs presented in Figs. 4 and 5. The graphs have the form of contour lines filled with colours like geographical maps. Broken lines in the maps envelope the area, where appropriate parameters are greater then limiting values defined in Section 3.

From the practical point of view, of high usability are simplified figures of this type, showing the division of the area of the expected bearing dislocations into only two sub-areas: permissible

dislocations and prohibited dislocations. Samples of such diagrams are shown in Fig. 7. The prohibited and permissible dislocation areas are separated by lines, which are the projections of the limit level lines drawn in Figs. 4 and 5 onto the x-y dislocation plane. In Fig. 7 the areas of prohibited bearing dislocations are marked dark, while the white area represents permissible dislocations. Dislocating the bearing to an arbitrary point located within the white area does not provoke effects, which could be considered unacceptable from the point of view of machine operation.

It is seen, that many miscellaneous representations of the defect maps can be created, depending on needs. Figs 4-7 present the maps of bearing misalignment effects in various degree of complexity. Figs. 4 and 5 present the 3-dimensional graphs and Figs. 6 and 7 present their two-value plane representations. It should be added, that all defect maps in their original version are colourful.
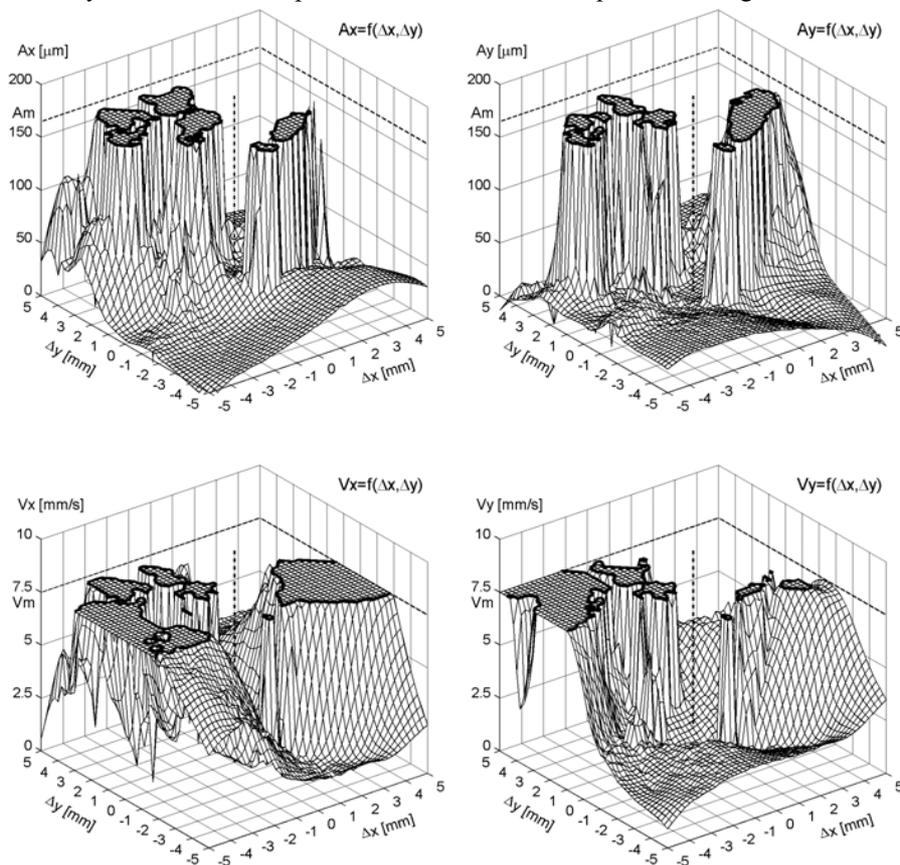

Fig. 5. The set of three-dimensional diagrams corresponding to the graphs from the Fig. 3, cut off at the level of the adequate parameter limiting value

4. ANALYSIS OF THE BEARING MISALIGNMENT DEFECT MAPS

The three-dimensional maps of bearing dislocation effects shown in Figs. 4 reveal that the amplitudes of relative vibrations of the bearing journals as well as velocities of absolute vibrations of the bearing bushes rapidly increase in some areas of bearing dislocations. Comparison of the vibration magnitudes with the contour lines drown on the permissible levels shows, that vibration may exceed many times the permissible limits. It is seen also in the Fig. 4 that the amplitudes of relative vibrations of the bearing journals are limited to about 1000 μm (peak to peak). The diagrams are cut off at this level. The maximum double vibration amplitude $A_{pp} = 1000$ μm seen in Fig. 4 corresponds approximately to the average bearing clearance in the direction of vibration measurements (vibration amplitudes are calculated here in the directions being the bisectors of the coordinate axes). Limitations placed on the amplitudes of the relative journal-bush vibrations result from physical limitations of the bush surface, since journal movements are limited to the bearing

clearance circle. This testifies to the fact that after reaching the maximum amplitude the journal slides along the bush surface, or hits into it.

This suggest the presence of vibrational instability of the rotors or bearings, manifesting itself in the fact that relatively small intensification in bearing misalignment in some directions leads to rapid increase in vibration. The appearance of the instability in bearing operation due to the bearing misalignment is confirmed by shapes of trajectories of the bearing journals. Analysis of the bearing journal trajectories corresponding to bearing misalignment directions and magnitude was the subject of the author earlier papers [7].

The bearing misalignment defect maps can be useful for the diagnostic purposes in two ways:
- they can provide information on machine vibrational state if the bearing misalignment is known,
- they can provide opportunities for drawing conclusion on the location and magnitude of the bearing misalignment basing on the recorded vibration patterns of the bearing journals and bushes.
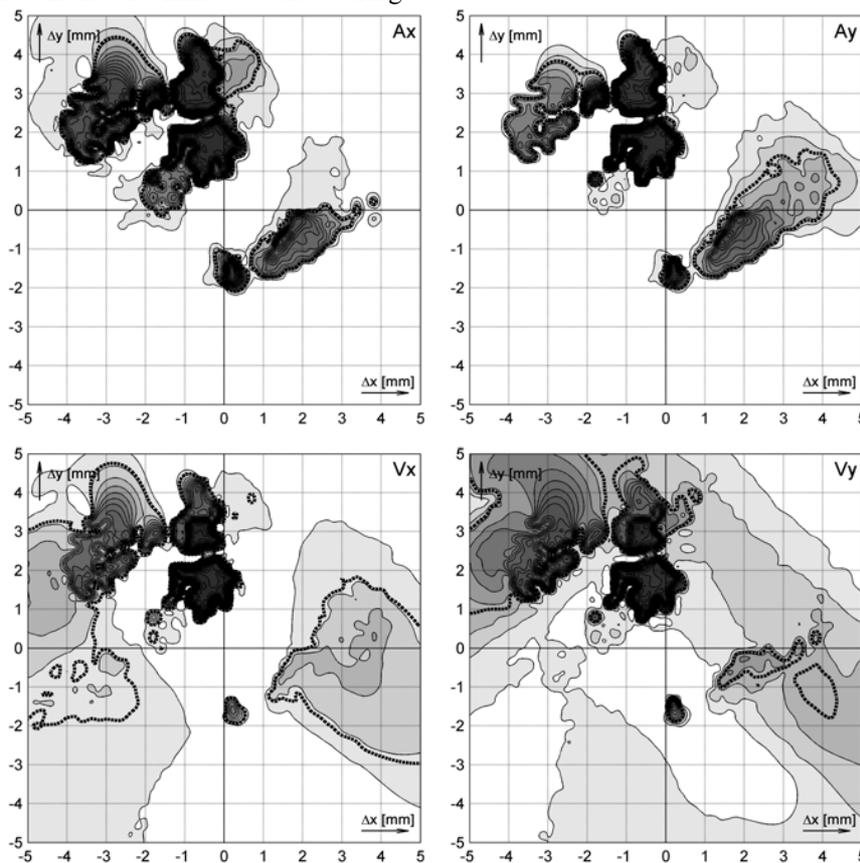

Fig. 6. The two-dimensional representations of the diagrams from the Fig. 3 in the form of contour lines. The broken lines link the points where presented parameters are equal to the limiting values
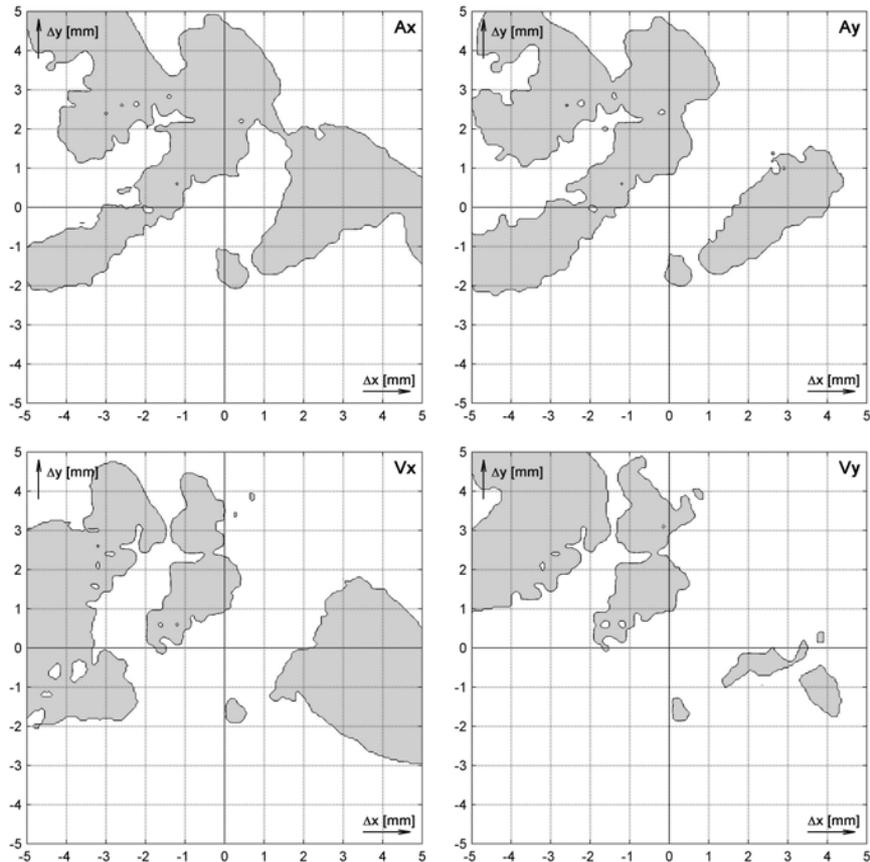
Fig. 7. The two-value, two-dimensional graphs, which show the division of the possible bearing dislocation area
to the area of prohibited dislocations (marked dark) and area of permissible dislocations (white)

In the former case, an assessment is possible whether the known bearing misalignment, e.g. bearing dislocation measured by the diagnostic system, is safe, and, what effects generates this misalignment. In the latter case we can conclude about the scale and form of a bearing misalignment by comparative analysis of the machine vibration pattern recorded by the diagnostic system with vibration magnitude characteristics for a given misalignment readout on the maps. Moreover, the set of bearing dislocation maps enables distinction between bearing misalignment and other defects manifesting themselves in bearing vibrations despite the fact, that effects of bearing misalignment are not specific for this defect. The correct distinction is more possible if vibration parameters of many bearings may be analyzed altogether. Probability of the right diagnosis is very high if vibration patterns of all bearings agree with samples, which are readout from bearing misalignment maps. The distinction is also easier if additional symptoms may be taken into account, e.g. bearing oil temperature.

It is quite obvious, that a rotating multi-bearing machine should be considered unserviceable as a whole when only a certain single parameter is exceeded even in only one bearing due to misalignment of any bearing. But a single set of maps, like the sets shown in Figs 4 – 7, contain graphs for only one vibration parameter and for only one particular bearing. Moreover, the graphs present functions of displacements of only one particular bearing. The problem may be overcome on the ground of operations on sets. It is easy to note, that in the sense of the algebra of sets the area of prohibited dislocations of a given bearing is the sum of the areas of prohibited dislocations of this one bearing calculated with the viewpoint of fulfilment of given criterion in every particular bearing separately. For instance, when taking into account only the relative vibration criterion, the area of prohibited dislocations of the bearing 5 covers all these dislocations of the bearing 5, which generate unacceptable relative vibrations in any of bearings 1… 7. In similar way, the area of allowable and prohibited dislocations can be linked together via the abovementioned operations on sets also with respect to other criteria. Thus, based on numerous detailed maps, it is possible to find areas of bearing dislocations provoking certain generalised effects. Such operations on sets are very easy in relation to the defect maps in the numerical form. What is more, the maps in numerical form may be easy put into use in automatic diagnostic systems. Basing on so created numerical maps also graphical maps can

be created for different combinations of criteria, for example with respect to vibration in one particular bearing, or with respect to particular kind of vibration. However this cause, that the number of graphs grows and their analysis becomes difficult.

5. THE GENERAL IDEA OF DEFECT MAPS

The primary idea of the presented work consists in specific methodology of presentation of the machine response to a certain class of defects. The idea of defect maps consists in mapping a machine technical state in certain domain of random events, which are represented by defects. In relation to the presented here defect of bearing misalignment the "domain of events" is an area of possible dislocations of bearings in relation to their base location. The "technical state" may be expressed e.g. by vibration intensity of the machine elements, which is subject of this article, but also by the bearing oil temperature, by the bearing load etc.

In general approach the "maps of defects" are represented by ordered sets of parameters, which determine technical status of the machine as the function of parameters, which ambiguously characterise defect in respect of type, location and intensity. The maps express intensity of machine reaction to defect as the function of parameters, which characterize the defect. According to this approach maps may be of graphical or numerical form. The numerical maps are the matrixes, which contain discrete parameter values but may be approximated for intermediate parameter values characterizing a defect. Maps in this form may find application in self-operated diagnostic and expert systems. The graphical maps are the plots made on the basis of the corresponding numerical maps. The form of graphical maps may be adapted to the intended application. The graphical maps may have a form of two- or three-dimensional plots illustrating intensity of analysed parameters. A level of the parameter may be shown in the maps e.g. as the diagram ordinate or using a colour scale. Various types of the graphical maps are illustrated in Section 4.

The method of the defect maps is especially suitable in the case of complex mechanical systems, where reducing diagnostic relations to simple logical sentences of defect-symptom type is not possible in practice. What is more, in some cases creation of predefined defect maps is the only possible solution. This is why methodology of the defect maps has been practically applied to bearing misalignment defect of the real power turbo-generator. In this particular application the maps characterize relative and absolute vibration of bearings as a function of bearing displacements in relation to their proper, base position. The practical result of the described above investigations is complete and ready to use knowledge base on the defect consisting in misalignment of all bearings of the 13K215 turbogenerator.

It should be remembered, that the knowledge base that is the object of this paper contain the effects of an individual bearing dislocations, i.e. situation in which the misalignment defect takes place in only one bearing, while the remaining bearings are still in their base positions. The defects consisting in simultaneous dislocations of two or more bearings couldn't be presented in the form of the ready-to-use base of knowledge, as the expected volume of resulting base and corresponding effort for its preparation would be too high. If necessary, however, arbitrarily selected individual cases of simultaneous dislocations of a number of bearings may be calculated and interpreted.

CONCLUSIONS

- The idea of presentation of a machine response to defects in the form of defect maps has been proposed. The maps allow presentation of the machine response to a set of defects in comprehensible, easy readable and usable form. The maps express intensity of machine reaction to defect as the function of parameters, which characterize the defect.
- The complex set of maps, which present response of the turbo-generator to the bearing dislocations has been created by computer simulation of the defect implemented in numerical model of the machine. The maps present relative journal vibrations and absolute bush vibrations, thus giving a general view on the machine resistance to misalignment of particular bearings from the viewpoint of defined criteria.
- The maps of bearing misalignment defect reveal, that vibrational response of the complex machine to the bearing misalignment is difficult to predict intuitively, as it can be rapid and unexpected. Vibration intensification gradient is especially high at the border between the areas of permissible and prohibited bearing dislocations.
- In some areas of possible bearing misalignments small increase in bearing displacement may lead to sudden appearance of extremely high vibrations, which many times exceed the permissible limits. In those situations the limitations for relative vibration amplitudes are physical restrictions resulting from the size of bearing clearance. This suggests the presence of vibrational instability of the rotors or bearings.
- The set of maps containing information on effects of the tutbogenerator bearing misalignment can be interpreted as the base of knowledge on this defect and may be implemented in the turbogenerator diagnostic system. The presented work is an example of practical realisation of a concept of creating a pre-defined base of diagnostic

knowledge using the model based computer simulation.

Acknowledgement

REFERENCES

[1] Natke H., Cempel C.: *Model Aided Diagnosis of Mechanical Systems*. Springer Verlag, 1997, Berlin.

[2] J. S. Rao J. S.,: *Vibratory Condition Monitoring of Machines*. Narosa Publishing House, New Delhi, Chennai, Mumboi, Calcuta, 1999, London.

[3] Cempel C.: *Multidimensional Condition Monitoring of Mechanical Systems in Operation.* Mechanical Systems and Signal Processing, 2003, Vol. 17, pp.1291-1303.

[4] Moczulski W., Szulim R.: *On Case-based Control of Dynamic Industrial Processes with the Use of Fuzzy Representation.* Engineering Application of Artificial Intelligence, 2004, Vol. 17 (4), pp. 371-381.

[5] Rybczynski J.: *Attempts of Explanation of the Reasons of Vibrations of Three-supported Rotor Recorded on the Research Rig for Investigations of Rotor Dynamics.* Proceedings of II International Congress of Technical Diagnostics, Sept. 19 – 22, 2000, Warsaw, Vol. 2, p. 219.

[6] Rybczynski J.: *Acceptable Dislocation of Bearings of the Turbine Set Considering Permissible Vibration and Load of the Bearings.* Key Engineering Materials, 2005, Vol. 293-294, pp. 433-440.

[7] Rybczynski J.: *The Effect of Turboset Bearing Misalignment Defect on the Bearing Journal and Bush Trajectory Pattern.* No. IMECE2007-43330, Proc. of ASME International Mechanical Engineering Congress, Seattle, 2007, WA.

[8] Rybczynski J.: *Maps of vibrational symptoms of bearing misalignment defects in large power turboset.* No. GT2008-50558, Proc. of ASME Turbo Expo 2008, Berlin.

[9] Muszynska A.: *Rotordynamics*, CRC Press, Taylor & Francis Group, 2005, London, New York.

[10] Piotrowski J.: *Shaft Alignment Handbook*, CRC Press, Taylor & Francis Group, 2007, London, New York.

[11] Lees A. W.: *Misalignment in rigidly coupled rotors.* Journal of Sound and Vibration, 2007, No. 305, pp. 261-271.

[12] Vance J. M.: *Rotordynamics of Turbomachinery*, A Wiley – Interscience Publications, 1985, New York.

[13] Rao J. S., Sreenivas R.: *Dynamic Analysis of Misaligned Rotor Systems.* Proceedings of VETOMAC-1 Conference, Oct. 25-27, 2000, Bangalore, India

[14] Bognatz S. R.: *Alignment of critical and non-critical machines.* Orbit, 1995, pp. 23-25.

[15] Sekhar A. S., Prabhu B. S.: *Effects of Coupling Misalignment on Vibrations of Rotating Machinery.* Journal of Sound and Vibration, 1995, Vol. 185 (4), pp. 655-671.

[16] Patel T. H., Darpie A. K.: *Experimental Investigations on Vibration Response of Misaligned Rotors.* Mechanical Systems and Signal Processing, 2009, Vol. 23, pp. 2236-2252.

[17] Kicinski J., Drozdowski R., Materny P.: *The non-linear analysis of the effect of support construction properties on the dynamic properties of multi support rotor systems.* Journal of Sound and Vibration, 2006, Vol. 4, pp. 523-539.

[18] Kicinski J., Drozdowski R., Materny P.: *Nonlinear model of vibrations in a rotor - bearings system.* Journal of Vibration & Control, 1998, Vol. 4 (5), pp. 519-540.

Dr inż.
Józef RYBCZYŃSKI
Graduated from Gdansk University of Technology at Mechanical Engineering Faculty in 1971 in technical science. PhD since 1988 in mechanics. Employed since 1972 at The Institute of Fluid Flow Machinery, PASci in Gdansk. Area of interest: dynamics of rotors, oil bearings, machine diagnostics, experimental investigations into rotor and foundation vibrations, measurement techniques. Member of Polish Association of Technical Diagnostics and American Society of Mechanical Engineers.

UTILIZATION OF COMPONENTS OF SIGNALS FROM HIGH FREQUENCY RANGE IN CONDITION MONITORING OF BEARINGS

Adam GAŁĘZIA

The Institute of Automotive Engineering, Warsaw University of Technology
84, Narbutta St., 02-524 Warsaw, Poland
e-mail: agalezia@simr.pw.edu.pl

Summary

The paper describes the utilization of high frequency range of vibro-acoustic signals in condition monitoring of bearings. High frequency components of signals, generated by a bearing working under operational conditions, contain low energy disturbances which might carry information related to the technical condition of the bearing. These high frequency signal components are most probably related to friction effects and the effects related to the behaviour of structure in mesoscale. The emergence of cracks leads to the changes in the friction of mating elements in bearings and has an influence on the structure in mesoscale. This in turn causes changes in high frequency range of the signal. Based on the monitoring of high frequency structure of signals, it is possible to draw conclusions about the changes in the technical condition of a bearing. The paper describes the application of measures, typical for acoustic emission, to acoustic signals recorded from bearings working on a laboratory stand. The measurements were performed with the uses of an ultrasonic microphone.

Keywords: acoustic emission parameters, ultrasonic, spectral moments, condition monitoring.

WYKORZYSTANIE SKŁADOWYCH SYGNAŁU Z WYSOKIEGO PASMA CZĘSTOTLIWOSCI W DIAGNOSTYCE ŁOŻYSK

Streszczenie

Publikacja przedstawia wykorzystanie wysokoczęstotliwościowych sygnałów wibroakustycznych w diagnostyce technicznej łożysk. Wysokoczęstotliwościowe składowe sygnałów, emitowanych przez pracujące łożysko, zawierają niskoenergetyczne zaburzenia, które mogą nieść informację związane ze stanem technicznym łożyska. Te wysokoczęstotliwościowe składowe sygnałów są najprawdopodobniej związane ze zjawiskami tarcia i zjawiskami zachowania struktury w mezoskali. Powstanie uszkodzenia prowadzi do zmian w tarciu współpracujących powierzchni łożyska i ma wpływ na zachowanie struktury w mezoskali. W wyniku tego następują zmiany w wysokoczęstotliwościowym paśmie sygnału. Wykorzystując monitoring wysokoczęstotliwościowej struktury sygnału, możliwe jest wnioskowanie o zmianach stanu technicznego łożyska. Publikacja przedstawia wykorzystanie miar, typowych dla emisji akustycznej, w analizie sygnałów akustycznych pracujących łożysk na stanowisku badawczym. Pomiary zostały przeprowadzone z wykorzystaniem mikrofonów ultradźwiękowych.

Słowa kluczowe: parametry emisji akustycznej, ultradźwięki, momenty widmowe, diagnostyka techniczna.

1. INTRODUCTION

The condition monitoring of bearings allows, on the one hand, to reduce the probability of a catastrophic failure of a machine and costs related to it and, on the other hand, to increase the reliability and extended working time of a machine. Economic and ecological factors exert an increased pressure on the development of new, more reliable techniques which would allow to determine the technical state of a machine, predict changes in its technical state, and to estimate the remaining useful life of a machine. The correct and reliable assessment of the technical state is an important issue in condition monitoring and it allows to define future operating strategies in order to minimise the operating costs and the hazard of failure. The change in the technical state of equipment is usually related to the changes in kinematics of an object, its degradation, and changes in cooperation of kinematic pairs.

Common bearing diagnostic techniques are based on vibro-acoustic signals that range from few to 10,000 Hz. The frequency analysis of recorded

signals is the basic method of signal analysis. An early detection of the time of the origination of a defect allows to control its build-up and to plan repairs and optimal operation conditions.

Present research in the filed of condition monitoring of bearings is often related to the development and application of technologies used in other domains of technical diagnostics, signal processing and analysis techniques, as well as building of diagnostic models and systems.

The development and application of techniques related to acoustic emission [1, 2, 3] and stress-wave technology [4] is of increased interest to scientist and maintenance engineers. These technologies base on the detection of transient elastic waves generated by a rapid release of a strain of energy caused by a deformation or damage within or on the surface of a material [5]. The transient elastic waves can be also generated by the interaction of two surfaces in relative motion e.g. the interaction of the surface of a rolling element and the race of a bearing. The acoustic emission detects events from a very high range of frequencies such as 100,000-1,000,000 Hz.

Signal processing and analysis techniques such as higher order spectral analysis, Teager-Kaiser energy operator, cepstrum analysis, time-frequency analysis are widely used to obtain diagnostically useful information, based on which it is possible to determine the technical state and to make decisions regarding further operation of machine [6, 7].

Based on diagnostic knowledge and information obtained from signals, it is possible to build a model of degradation process or to establish a decision-support system. Such solutions can be based on neural networks or expert's knowledge [8].

The paper presents results and conclusions from a preliminary research, made by the author, which aimed at retrieving useful diagnostic information in the high frequency bands of an acoustic signal. As a result, it was possible to identify the band of signal, in which the highest differences were observed for different technical stages. Different signal analysis techniques were used to identify signal parameters, some of which will be used in further research to build the hidden Markov model for bearing degradation process.

2. TEST STAND AND MEASUREMENT SETUP

The test stand presented below (Figure 1) was used to record signals during the experiment.
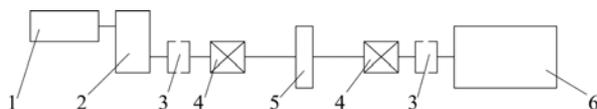

Fig. 1. Sketch of the test stand (description in text)

The test stand consisted of: 1. driving motor, 2. gearbox, 3. coupling, 4. bearings in housings, 5. unbalance disk, 6. electric dynamometer, (numbers according to sketch).

The driving motor (1), via the gearbox (2) and the coupling (3), set in motion the shaft with the unbalance disk (5) placed on it. The shaft was supported on bearings in housings (4). The energy from the shaft was dissipated by an electric dynamometer (6). Two self-aligning ball bearings (SKF 1205 EKTN9) were mounted in bearing housings. The unbalance disk allowed to introduce different unbalance states by screwing in grub screws. The bearing placed closer to the gearbox was subject to artificially introduced damage, that is described in the next section. The applied gearbox was a one-stage gearbox, with reduction ratio i=2.84. The nominal input power of the gearbox was 0.37 kW, the power of the applied driving motor was 0.25 kW. The technical condition of the gearbox during the measurements was good. The gearbox was after the grind-in of co-acting parts and its working time was short. Working conditions of the gearbox can be described as under its nominal load. Vibrations of the gearbox were low and did not affected diagnostic results.

Measurements of the acoustic signals from the bearings were made using NI PXI computer with NI PXI-4462 measurement card. The signals generated by the bearings were recorded with the use of VIS-311 vibration sensors and G.R.A.S. 40BE ultrasonic microphones. These one-direction vibration sensors, with the frequency range of 0.5-10,000 Hz, were used to measure vertical vibrations carried out by the bearing's housing. The ultrasonic microphones with the frequency range from 10 Hz up to 100,000 Hz were mounted on stands close to the shaft opening in the bearing housing. Their aim was to record the acoustic signals generated by the working bearing. The sampling frequency of the measurement card was set to 200,000 Hz, which, according to Nyquist–Shannon sampling theory, allowed to record the signals components up to 100,000 Hz.

3. MEASUREMENTS

During the experiment, measurements were carried out for three types of unbalance and three simulated stages of bearing degradation. All together, there were 9 measurement sessions: one for each combination of unbalance and degradation stage. The unbalance was obtained by installing a number of grub screws in the disk. In a set of measurements, the unbalance disc was rotating without screws, with one and with six screws. The degradation stage was changed by artificially introduced cracks. There were three stages of degradation considered: 1. bearing without an artificial defect, 2. bearing with a "small" defect introduced in the inner race, approximately: 1 mm in

diameter and 0.5 mm deep, 3. bearing with a "big" defect introduced in the inner race, approximately: 4 mm long, 1 mm wide, and 1 mm deep.

During the experiment, the speed of the shaft was constant and equal to 986 rpm. Each measurement session consisted of ten one-second measurements. The measurements in a given session were held at 1-second intervals. In this way a set of data was recorded which allowed for averaging the results.

4. MEASUREMENT RESULTS

4.1. Preliminary analysis

The review of the measurement results started with the analysis of a signal spectrum. The signals' spectra, watched in linear scale in full range of frequencies, did not reveal any particular phenomena. Except for peaks in the frequency band up to 10,000 Hz, it seemed that the rest of the spectrum contains only components related to noise.

However, the comparison of spectra presented in logarithmic scale of values, revealed an interesting phenomenon, which was an incentive for further research (Figure 2).

Figure 2 presents comparison between spectra of signals recorded for the analysed bearings with different stages of unbalance, but without an artificial defect. The first plot presents the signal from the bearing with no screws in the unbalance disk, the second - with one unbalance screw, the third one - with six screws. An interesting phenomenon could be observed in the frequency band ranging from 40,000 Hz to 60,000 Hz. It was possible to notice that in this frequency band, an observable change of spectrum occurred in relation to the change of the degree of unbalance. It was noted that a local increase of spectrums magnitude, as compared to the full spectrum, was shifting and changing its distribution in reaction to the increase of the stage of unbalance. An important observation is that all signals from a given measurement session look similar and observed effect is repetitive.
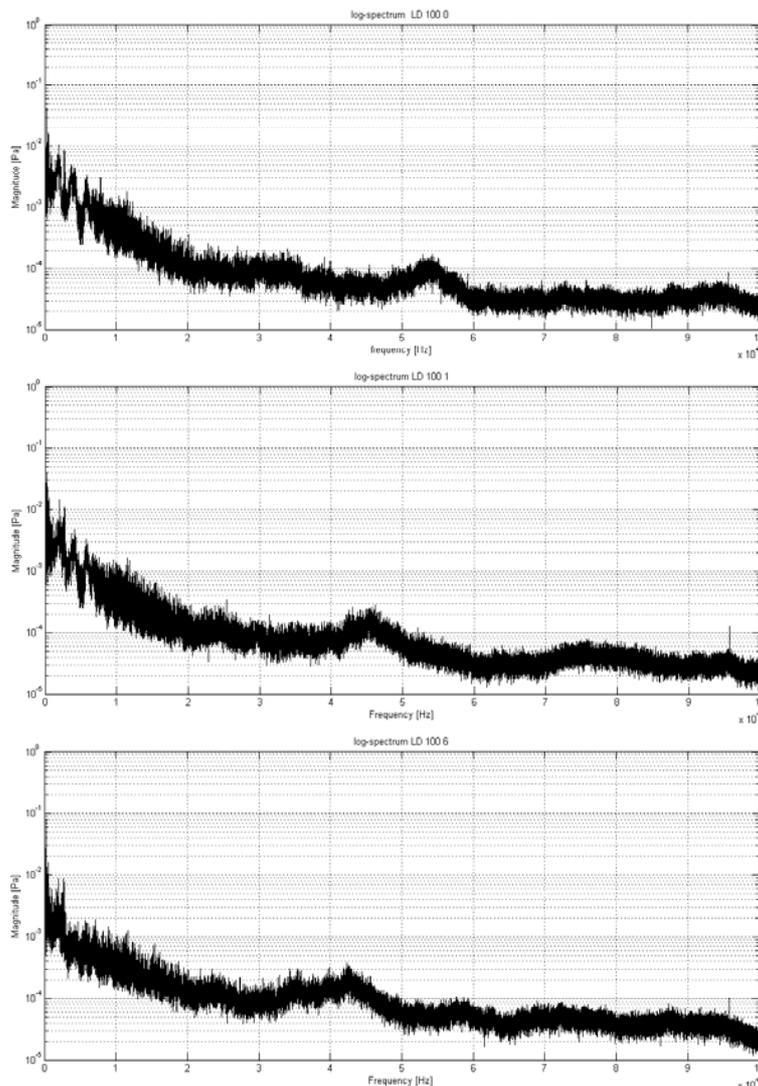

Fig. 2. Log-spectra of signals recorded for bearing with different stages of unbalance

Also comparisons of other log-spectra calculated from different measurement sessions reveal changes in the high frequency band from 40,000 to 60,000 Hz. It must be pointed out that changes in the band mentioned above were different in shape, range or distribution for individual comparative measurements – the different stages of degradation and unbalance. Each time it was possible to conclude that some kind of change had taken place in the technical state of the bearing. Following the observation, spectral moments were calculated. This was done in order to extract information which could describe the changes, observed in the spectrum, with the use of specific parameters.

4.2 Spectral moments

Spectral moments are the measures describing parameters of spectrum's shape such as centre of gravity, standard deviation, skewness and kurtosis [9]. Spectral moment of order **m** is:

$$M(m) = \sum_{f_i=f_d}^{f_i=f_g} |G(f_i)| [f_i]^m \qquad (1)$$

where: $G(f_i)$ - signal's spectrum f_i,

f_i - centre frequency of analysed band,

f_d, f_g - lower and upper frequencies of band.

Most commonly, normalised spectral moments are used:

$$M_u(m) = \frac{M(m)}{M(0)} \qquad (2)$$

Calculation of the first four normalised spectral moments was performed for frequency bands of the width of 10,000 Hz, from 0 up to 100,000 Hz. All spectral moments for all measurements in a given measurement session were concentrated around the mean value. Performed calculations and analysis of the spectral moments for all measurement sessions reveal no significant differences in values of averaged spectral moments in frequency bands of interest. Also the distribution of values did not reveal any particular trend. The main reason for this might be a very low magnitude of the signal components in a given frequency band, compared to the width of the band. Therefore, the spectral moments defined by (1) and (2), tuned out to be improper measures for detecting and inferring on changes of the technical state of the tested object (unbalance and defect).

Due to the fact that the spectral moments did not provide expected reliable information, the attention was directed to the analysis of the time signal and measures characteristic for the acoustic emission.

4.3. Acoustic emission measures

Acoustic emission (AE) is a decaying elastic wave that results from a vehement release of energy concentrated in material by propagating micro defect (increase of micro gaps, movement of dislocations) in material [10]. In non-destructive testing (NDT) of materials, acoustic emission is a passive listening technique, which is very sensitive and can detect defects such as the movement of a few atoms. Usually during tests, these waves can be separated into two types of behaviour: (1) burst emission, which is a discrete packet of waves associated with a single event or a small number of events and (2) a continuous emission, which tends to be a cluster of many small interlinked events. The basic measures used in acoustic emission are: the number of events, the number of counts, energy of the event, duration of the event. Figure 3 presents a sketch of AE event and its basic measures. [10].

In case of signals emitted by a working bearing, no typical acoustic emission events were expected. However, it was expected to find a continuous train of transient waves. Figure 4 presents, as an example, part of signal, filtered from 40,000 up to 60,000 Hz, recorded for a bearing under working conditions.

For further analysis of the signals, recorded for all measurement sessions, a uniform discrimination level was chosen, which allowed to compare parameters of signals from different measurements. For a detailed analysis of signals, the following parameters were calculated: the number of events in a measurement, energy of the event, duration of the event, time between events, maximum height of the event, height to width ratio of the event, skewness of the event, kurtosis of the event. The analysis of parameters was carried out in order to determine, which of these parameters can be used to identify the technical states of an analysed machine.
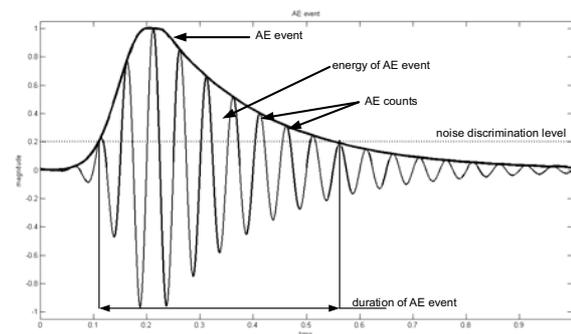

Fig. 3. AE event and its basic measures.
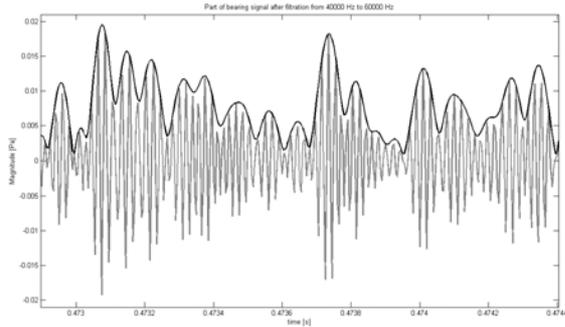
Fig. 4. Part of bearing signal after filtration from
40,000 Hz to 60,000 Hz with its envelope

As a result of calculations and analysis it was
noted that only the number of events and the energy
of the event seemed to be diagnostically useful.
Their analysis is presented in detail in the further
part of this paper. Neither the duration of the event
nor its kurtosis revealed such a trend in the
distribution of values which could be unequivocally
connected with changes in the technical state of the
tested object.

The number of events during the measurement
was the first parameter to be analysed. Figure 5
presents the distributions of the numbers of events
for each measurement for each combination of the
degree of unbalance and degradation. The value of
the analysed parameter is indicated on the horizontal
axis. The vertical axis represents the bearing's
technical state. The bearing is described by a
combination of two characters separated by an
underscore. First letter informs about the degree of
degradation were "G", "SC", "C" respectively mean:
bearing without an artificial failure, bearing with a
"small" failure introduced in the inner race
(approximately: 1 mm in diameter and 0.5 mm in
depth), bearing with a "big" failure introduced in
inner race (approximately: 4 mm long, 1 mm wide, 1
mm deep). The number standing next to the letter U
informs about the stage of unbalance: 0 – without
grub screw, 1 – with one grub screw, 6 – with six
grub screws (Table 1).

Each circle on Figure 5 represents the number of
events for one measurement. This presentation
allows to observe how numbers of events differ in
measurement sessions and in which regions they
overlap. For the bearing without an artificial failure,
the change of unbalance had the highest influence on
the number of events during the measurement. For a
bearing with an introduced defect, the change of
unbalance did not have an equally strong impact.
However, in these cases, the changes are still
observable and what is more, the distribution of
values of the analysed parameter is more
concentrated.

Table 1. Indicators of technical state used in article

Technical state indicator	Failure	Unbalance
G_U0	no	no
G_U1	no	one unbalance screw
G_U6	no	six unbalance screws
SC_U0	"small" defect	no
SC_U1	"small" defect	one unbalance screw
SC_U6	"small" defect	six unbalance screws
C_U0	"big" defect	no
C_U1	"big" defect	one unbalance screw
C_U6	"big" defect	six unbalance screws

Energy of the event was another analysed
parameter. Although the energy was calculated for
every event, during each of ten measurements
performed during the measurement session, the
mean value of energy from each measurement was
used for further calculations. Figure 6 presents the
distribution of mean values for different technical
stages of bearings.
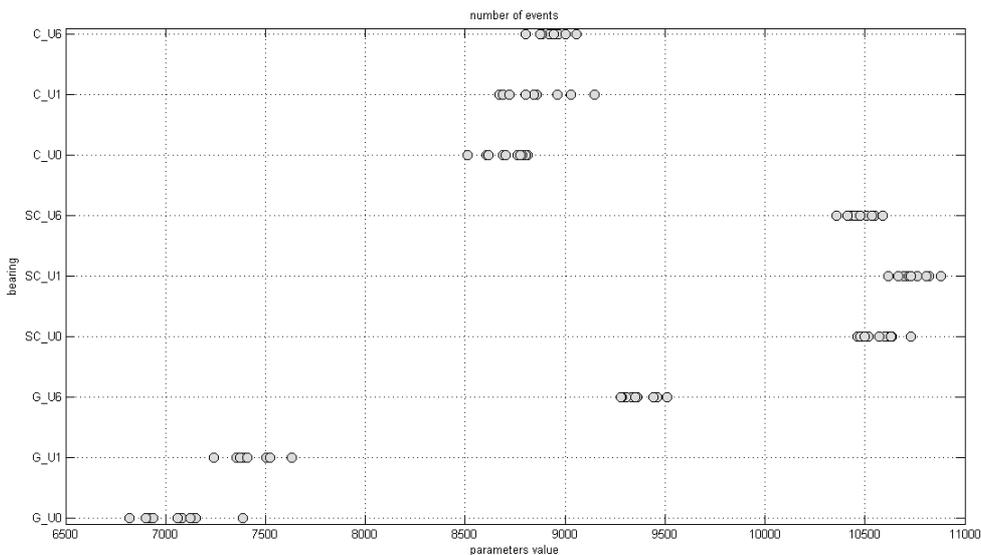
Fig. 5. Distribution of numbers of events for each measurement for each combination
of the degree of unbalance and degradation
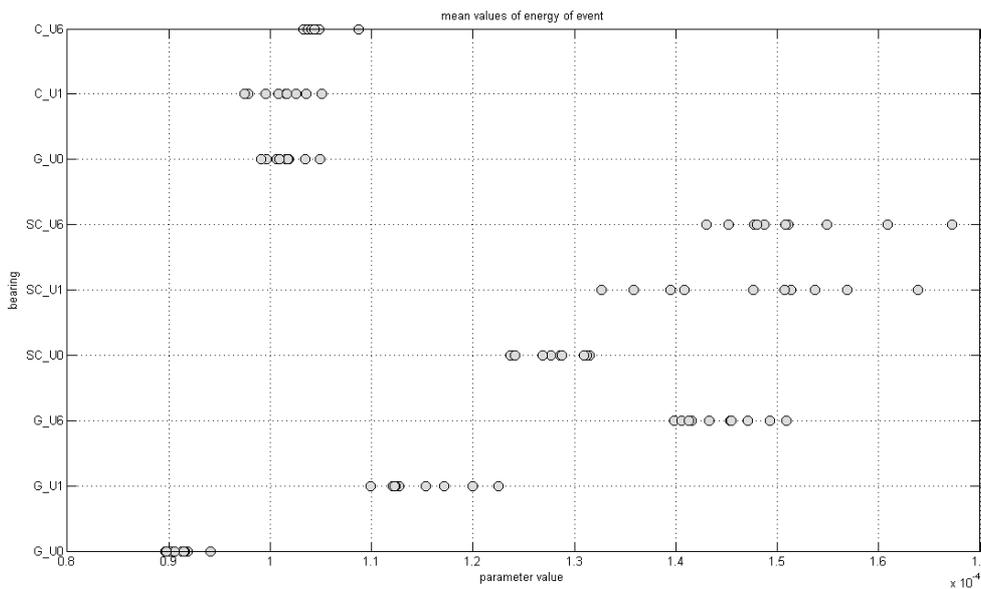
Fig. 6. Distribution of mean values of event energy for different technical stages of bearings

For the bearing without an introduced failure and with introduced small crack (small degree of degradation) it is possible to observe that the higher the degree of unbalance, the higher are the values of energy and the higher is their dispersion. A closer analysis of the dispersion of values reveals interesting trends. Figure 7 and 8 present comparisons of dispersion of values of energy of events for bearings without and with an artificial fault. For measurements made for the bearing without failure, the change of the degree of unbalance causes a shift and change in the distribution of values of energy of the event. Such effect is not so clearly observable in the case of the bearing with a small introduced failure. For the bearing with highest degree of degradation, this effect is not observable at all.
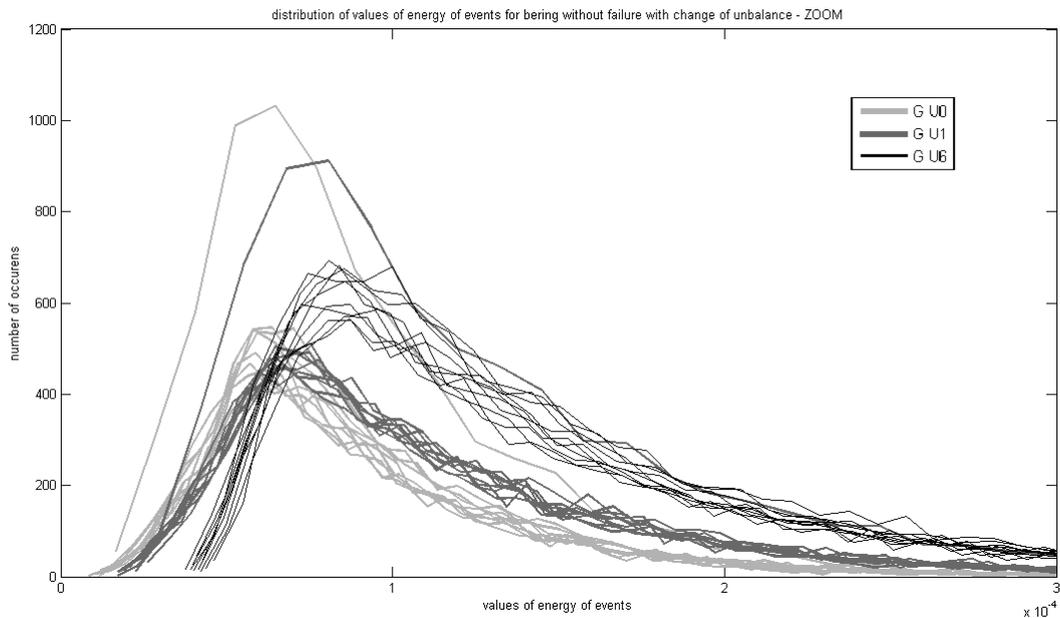
Fig. 7. Comparison of dispersion of values of energy of events for bearings without introduced crack
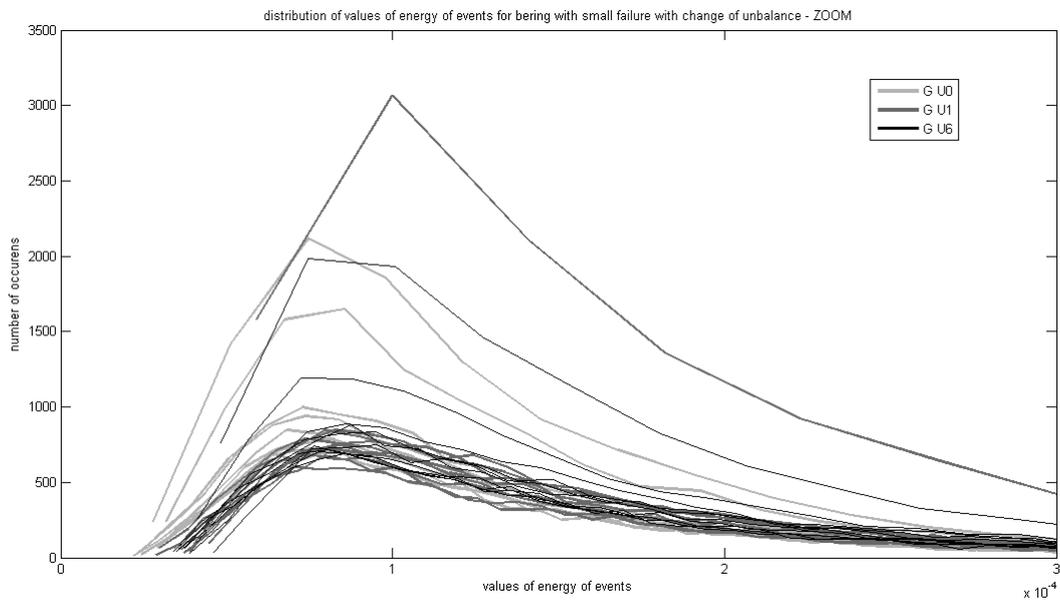

Fig. 8. Comparison of dispersion of values of energy of events for bearings with introduced "small" crack

Figure 9 presents comparison of the distribution of values of energy of an event calculated for each measurement session. For measurement sessions performed for the bearing without introduced failure (G_U0, G_U1, G_U6), the increase of unbalance caused the widening of the distribution with simultaneous shift of its maximum value. No such behaviour was observed for the results of other measurement sessions – sessions form bearing with "small" defect (SC_U0, SC_U1, SC_U6) and "big" defect (C_U0, C_U1, C_U6). Changes in the energy of the events occurring for measurement sessions for the bearings with defect had no strict trend. This is most probably related to the fact that the bearing's failure causes strong impulses during the passing of roller elements through the damaged area. These strong impulses demonstrate themselves in the low band of frequencies and can be observed there.

For a signal from the bearing in which no defect was introduced, changes of unbalance have stronger observable influence on high bands of signals, which can be related to the friction effects and effects related to the behaviour of structure in mesoscale.

Other parameters such as the height of the event (its maximum value) reveal correlation with the energy of the event and therefore, they were not analysed in detail. Neither the number of events during measurement nor the mean energy of events or any other parameter demonstrated unique changes that would be sufficient to indicate changes in the technical state of the tested object.
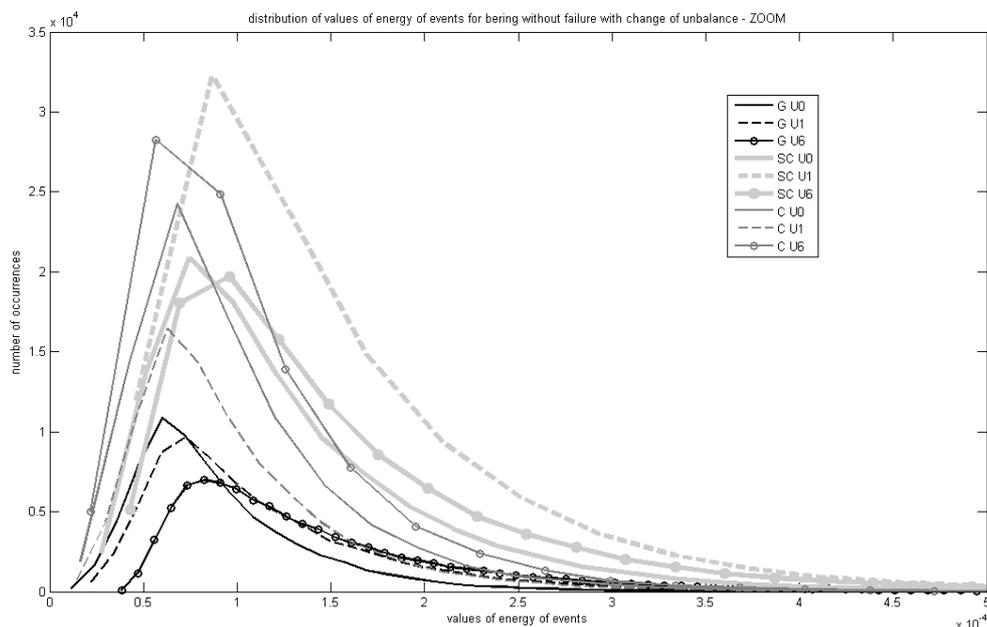

Fig. 9. Comparison of distribution of values of energy of event calculated for measurement sessions

To enhance the probability of correct determination of technical state of the bearing, distributions of values of pairs of parameters were analysed. This was made to verify whether it is possible to find such a pairs of parameters, observation of which would allow to classify the technical state of a bearing.

The analysis of distributions of values of pairs of parameters were made on two-dimensional parameter-plane with the axes reflecting the values of analysed parameters. From all possible combinations of parameters pairs, figure 10 and 11 presents the ones that best represented different technical states. For the clarity of the presentation, the technical state is reflected by numbers from 1 to 9 (Table 2). The location of a number is determined by the values of the analysed parameters.

It can be seen that both pairs of parameters have similar distribution and allow to use a simple technique to distribute the space of the technical state. For bearing without introduced failure, a strong diversification is observed with the change of unbalance. These states are well separated and can be determined based on the analysed parameters. For bearings with both stages of defect there is no such a good separation of data based on measurements for different stages of unbalance. During the analysis of different pairs of parameters, no such combination was found which would allow for easy separation of stages of unbalance of bearing with failures. In order to reach such a separation, it would be necessary to use other parameters and also other frequency bands.

Table 2. Number indicator of technical state for figures 10 and 11

| Numerical indicator	Technical state indicator	Failure	Unbalance
1	G_U0	no	no
2	G_U1	no	one unbalance screw
3	G_U6	no	six unbalance screws
4	SC_U0	"small" defect	no
5	SC_U1	"small" defect	one unbalance screw
6	SC_U6	"small" defect	six unbalance screws
7	C_U0	"big" defect	no
8	C_U1	"big" defect	one unbalance screw
9	C_U6	"big" defect	six unbalance screws
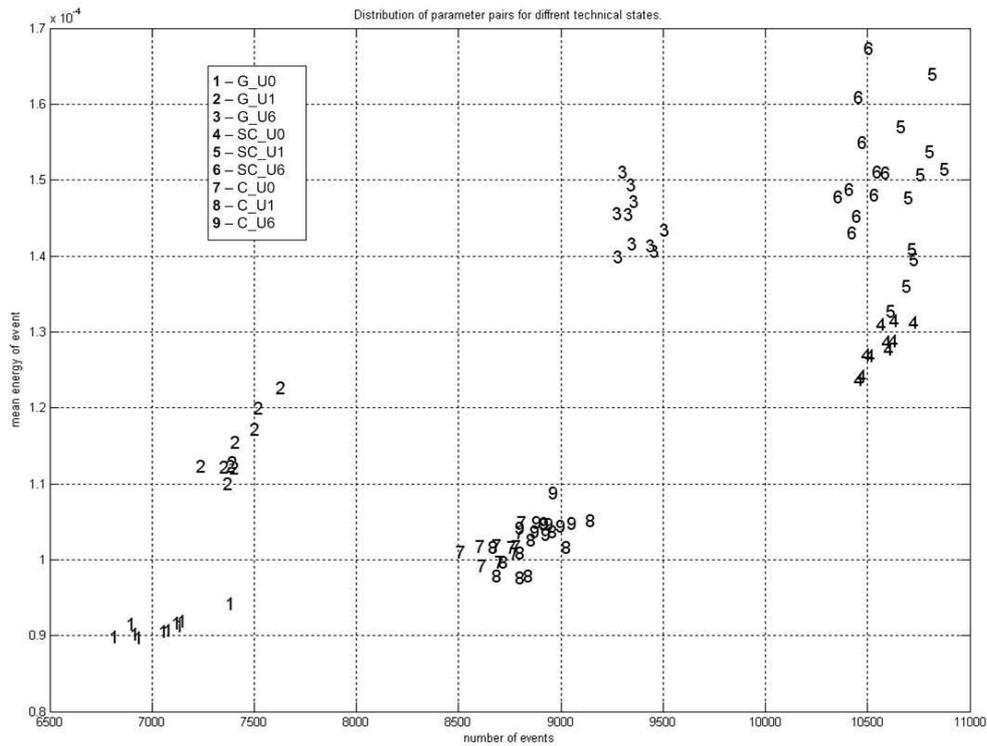
Fig. 10. Distribution of mean energy of event and number of events pairs on parameter plane
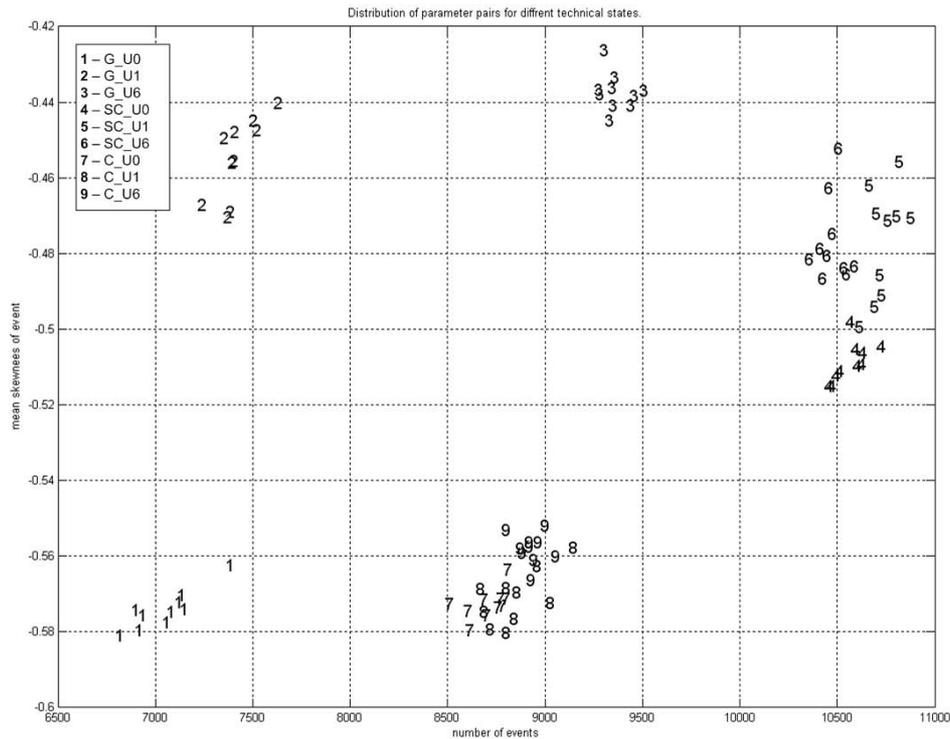

Fig. 11. Distribution of mean skewness of event and number of events pairs on parameter plane

To perform the separation process, subspaces must be defined for each separable state. The separation process can be performed as an iteration process. The depth of this process can be related to the number of accessible parameters and the degree of problem complexity. In the analysed case, a two-iteration separation can be used. In the first iteration, the parameter plane, which gives the best separation of data for degradation degree is used. After determination of the degree of degradation, depending on the need, different parameters, from different frequency bands, are used for analysis of the degree of unbalance. Markov models or neural networks can be then used as a tool for

determination of the degradation scenario [11]. In case of big number of analysed parameters combinations it is possible to use neural classifiers such as SVM or NBV [12, 13] to increase quality of classification of technical state.

5. CONCLUSIONS

The performed analysis proves that high frequency components of signals recorded for working bearings can be used to determine its technical state. It was demonstrated that based on acoustic emission parameters calculated for the acoustic time signal, it is possible to conclude about changes in the technical state of a bearing. The separation performed on parameter plane allows to determine the state of unbalance. Further research will be carried out for higher number of different technical stages and types of degradation.

Additionally work related to implementation of the hidden Markov models, as tools to determine the degradation stage and degradation scenario, will be preformed in the future.

REFERENCES

[1] A. Morhain, D. Mba: *Bearing defect diagnosis and acoustic emission.* Proceedings of the Institution of Mechanical Engineers, Part J, Journal of Engineering Tribology, Vol. 217, No. 4, pp: 275–272, 2003.

[2] A. Choudhury, N. Tandon: *Application of acoustic emission technique for the detection of defects in rolling element bearings.* Tribology International 33, pp: 39–45, 2000.

[3] M. S. Patil, J. Mathew, P. K. Rajendra-Kumar: *Bearing Signature Analysis as a Medium for Fault Detection: A Review.* Journal of Tribology, Vol. 130, Jan. 2008.

[4] V. Lough: *Acoustic energy driven machinery failure process planning,* Proceedings of the International Conference on Condition Monitoring CM2009/MFPT2009 Dublin 2009, pp: 259–268, 2009

[5] J. R. Mathews: *Acoustic emission,* Gordon and Breach Science Publishers Inc., New York. 1983.

[6] A. Gałęzia, S. Radkowski: *Teager-Kaiser energy operator and Hilbert transform approach to vibroacoustic signal demodulation,* Proceedings of the VI International Technical Systems Degradation Seminar, Liptovský Mikuláš 2007, pp: 113–119, 2007

[7] R. B. Randal: *The application of cepstrum analysis to machine diagnostics,* Proceedings of 36th meeting of the mechanical failures prevention group, Cambridge University Press, pp. 64–72, 1983

[8] J. Dybała, S. Radkowski: *Use of CP neural networks in vibroacoustic diagnostics of failures of gearbox.* Diagnostyka, vol. 31, 59–66, 2004.

[9] E. Eriksson, L. Cepeday, R. Rodmany, K. Sullivan, D. McAllister, D. Bitzer, P. Arroway: *Robustness of Spectral Moments: a Study using Voice Imitations,* Proceedings of the 10th Australian International Conference on Speech Science & Technology Macquarie University, Sydney, Australia 2004, pp. 259–264, 2004

[10] C. Cempel: Diagnostyka wibroakustyczna maszyn, (Vibroacoustic diagnostics of machines), PWN, Warszawa, 1989, (in Polish).

[11] A. Gałęzia, S. Radkowski: *Hidden Markov models in task of condition monitoring,* Proceedings of the International Conference on Condition Monitoring CM2009/MFPT2009 Dublin 2009, pp. 198–208, 2009.

[12] J. Dybała, *Rozpoznawanie obrazów z wykorzystaniem neuronowego klasyfikatora NBV, (Pattern recognition using NBV neural classifier),* Diagnostyka, No. 3(51), 2009, pp. 105–112, (in Polish).

[13] J. Dybała: *Wykrywanie wczesnych faz uszkodzeń metodami sztucznej inteligencji, (Detection of the early stages of damages using methods of artificial intelligence),* Wydawnictwo Naukowe Instytutu Technologii Eksploatacji, Warszawa – Radom, 2008, (in Polish).

M.Sc. **Adam GAŁĘZIA** is worker of Integrated Laboratory of Automotive Mechatronics Systems, Warsaw University of Technology. His scientific interests are related with condition monitoring of machines and vehicles, structure analysis.

THE ANALYSIS OF MULTI-SECTION CONCEPT FOR AN ACTIVE AIR HEADREST

Marek JAŚKIEWICZ, Tomasz L. STAŃCZYK

Kielce University of Technology, Department of Vehicle and Mechanical Equipment,
7 Tysiąclecia Państwa Polskiego Ave., PL – 25 314 Kielce, Poland

Summary

In the following paper there was built a mathematical model of 13 degrees of freedom which shows a man-driver model in a sitting position with a fastened seatbelt. Next a multi-section concept of a headrest was shown, and in fact an ideal protection of the back of head and spine. There was conducted a simulation of protective activity of a headrest with the use of a man-model. Obtained results have been used to conduct the analysis which show the influence of headrest activation time and the level of its filling-in on its protective features.

Key words: passive safety, collisions.

ANALIZA KONCEPCJI WIELOSEKCYJNEGO POWIETRZNEGO ZAGŁÓWKA AKTYWNEGO

Streszczenie

W pracy zbudowano model matematyczny o 13 stopniach swobody przedstawiający człowieka-kierowcę w pozycji siedzącej, zapiętego pasami. Następnie przedstawiono koncepcję wielosekcyjnego zagłówka a w zasadzie idealnej tylnej ochrony głowy i kręgosłupa. Wykonano symulację ochronnego działania tego zagłówka z wykorzystaniem opracowanego modelu człowieka. Uzyskane wyniki wykorzystano do przeprowadzenia analiz pokazujących wpływ czasu uruchomienia zagłówka oraz stopnia jego napełnienia na właściwości ochronne zagłówka.

Słowa kluczowe: bezpieczeństwo bierne, zderzenia.

1. INTRODUCTION

In papers [3] and [11] was shown that air headrests are better protection during a front collision than mechanical headrests. During the contact of head with a headrest the collision event does not occur and head is smoothly stopped [2, 4, 9]. However, such headrests have their disadvantages, too. Firstly, horizontal displacement of headrests is little, therefore head further on for longer period of time of its back movement is not protected. Secondly, their activation time (deployment) has to be adjusted to anthropometric features of a driver. You cannot use average headrest activation time because for one group it will be too early and for another too late.

Apart from the above-mentioned disadvantages, a big drawback for all headrests is the fact that they have to be placed at the same height as head. If their height varies from head, they do not provide sufficient protection [1, 5, 7]. Much worse is lower position of a headrest to the position of head because in such a case not only it does not fulfil its function but it is instrumental in (intensifies) contusion of an upper spine part [6, 8, 10].

2. CONSTRUCTION OF MAN-DRIVER MODEL

The following assumptions have been taken into consideration during the construction of a mathematical model of a man-driver sitting in a seat, fastened with seatbelts, for car collision computer simulation:
– flat model (movements in an XOZ car plane in further considerations marked as X_oOY_o plane),
– model elements (particular solids) are treated as perfectly stiff,
– the arrangement of stiff solids that corresponds to particular parts of the body,
– the location of weight centres and moments of inertia of particular solids are known,
– solids are linked by joints with a linear stiffness and damping, which can turn,
– no spaces occur among particular solids,
– the only input influencing the system is Vx initial speed,
– chest bend has not been taken into consideration,
– belts are modelled as linear spring-damping elements of Kelvin-Voigt,
air bag has been modelled as a linear spring-damping element of Kelvin-Voigt.
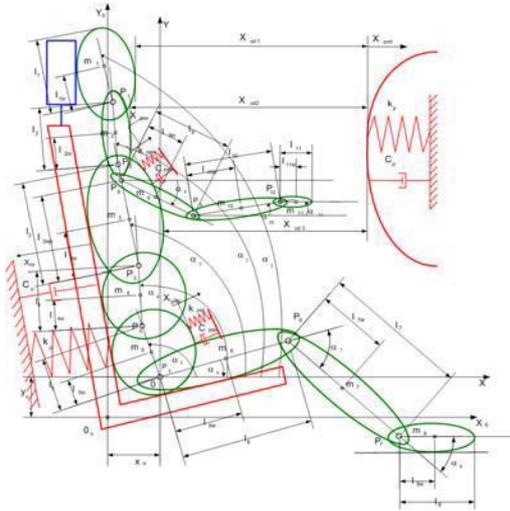
Fig. 1. The structure of a man-driver
model of 13 degrees of freedom

For the above-mentioned model movement equations were formulated with the use of Lagrange's II type equations. These equations are presented in paper [3]. Full identification of stiffness and damping parameters which occur in the models has been presented in papers [3,12].

3. CONSTRUCTION AND FUNCTIONING CONCEPT OF A HEADREST

The following three pictures present the concept of air-bag functioning, which ideally protects against injuries of a head-on collision. Such an air-bag is divided into sections. The number and activation time of particular sections are steered dependent on real driver body movement. Its functioning would be the following: when a driver body moves to a certain distance forward the headrest (air-bags) is activated. The level of X direction displacement would be a key indicator deciding on the number of air-bag sections opened. The number of activated sections would be determined by a managing processor depending on a registered impulse during car collision or the signals from micro-sensors which register body movements. During little displacement, for instance only two sections would be activated (fig. 2) whereas during a bigger head displacement and very little displacement of the trunk – three upper sections (fig. 3), etc. The further forward human body is displaced, the more air-bag sections are filled resulting in further displacement forward. Such an air-bag would not only influence head but also protect neck and trunk. The damping force would be obtained by means of opened valves. The amount of such force would be measured and depend on the number of opened valves. During a big driver displacement forward all sections of an air-bag would be opened (fig.4). The concept of protection system functioning has been presented in

the photos from a crash test conducted in the Automotive Industry Institute where particular number of opening air-bag sections were drawn into the photos between car seat back and dummy depending on dummy and car seat location. A fully opened 5-section air-bag would allow for longer dispersion of kinetic energy of human body, thus with longer way of stopping the body, decelerations would be much smaller.
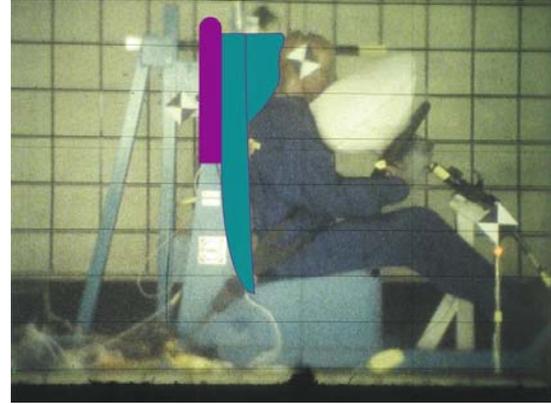

Fig. 2. The concept of the functioning
of head back and spine ideal
protection – 2 sections activated
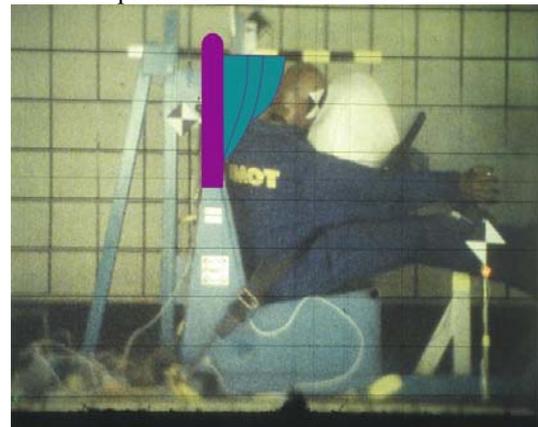
Fig. 3. The concept of the functioning of head
back and spine ideal protection – 3 upper
sections activated
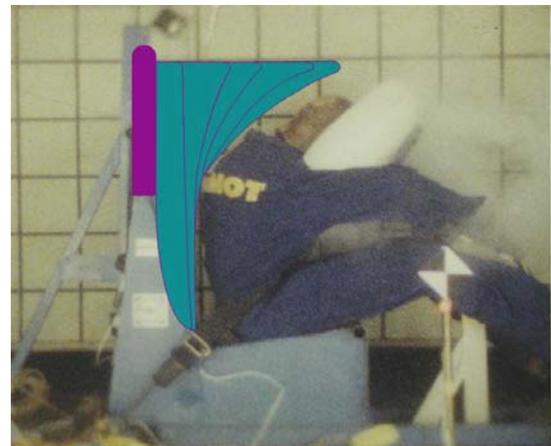
Fig. 4. The concept of the functioning of head
back and spine ideal protection – 5 sections
activated

4. THE ANALYSIS OF HEADREST FUNCTIONING

4.1. The cooperation of headrest with head

For air headrests it is crucial to select optimal activation time. To facilitate the analysis and the interpretation of displacement routes presented in figures 7, 8, 9 and 10 in fig. 5, were shown four typical situations which can occur in cooperation with a headrest ($X_{headrest}$ blue line) with head (X_{head} red line). Arrows show head and headrest displacement directions. We shall consider four examples of the cooperation between head and headrest. 5a) example shows a case when a headrest is activated too late. A headrest being filled hit a returning head. This is the most dangerous case from the above-mentioned four. Headrest displacement is opposite to head displacement. 5b) example illustrates a case of correct headrest activation. The headrest managed to be filled and the phase of headrest emptying begins. Returning head lay gently on to the headrest. 5c) example shows a case when a headrest is activated too early. Returning head hits a partly filled headrest. Protection is much less than 5b) example. 5d) example illustrates a case of very early opening of a headrest. The headrest after opening already managed to empty itself and then the head hits an empty headrest. In such a case protection is less than in 5c) example.
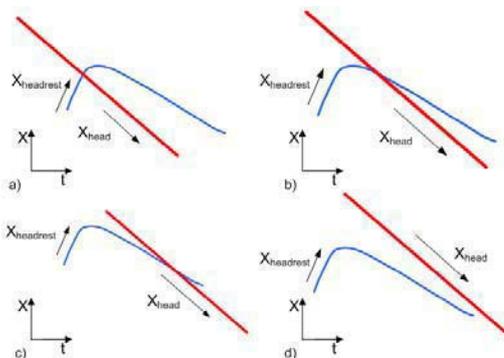

Fig. 5. Possible situations of the cooperation between headrest and head: a) too late headrest opening – a headrest hits head while being filled in (increase of X value in time function), b) correct opening – contact with head straight after full filling of a headrest, c) too early opening – a headrest contact head while being emptied, d) very early opening - a headrest will get emptied before head contacts it

4.2 The analysis of headrest protective functioning

Having analysed the functioning of multi-section air headrest it is recommended to show different values of its horizontal displacement (different levels of filling-in). Fig. 6 shows horizontal displacement of multi-section air headrest on the head level with indicated movement area.
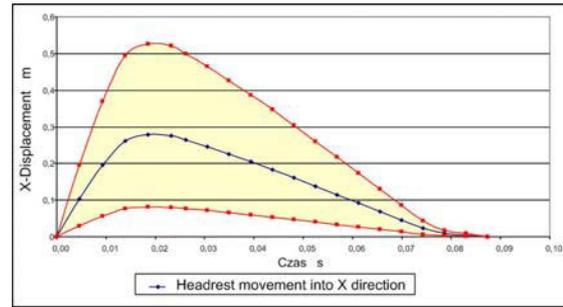

Fig. 6. Multi-section air headrest horizontal displacement with marked estimated movement area

Maximum horizontal headrest displacement amounts to 0.53m. It was assumed that minimum headrest opening amounts to 0.08m. For a maximum displacement, the time of headrest full opening equals t=0.02 s.

For a full estimation of its protective functioning, the above-mentioned headrest displacement needs to be set and compared with head displacements. To check how a protective functioning of such a headrest would look like, its displacement was indicated on a common graph with horizontal head displacements of a man-model. Fig. 7, 8, 9 and 10 set headrest displacements and horizontal head displacements of a man-model for different times of activation.
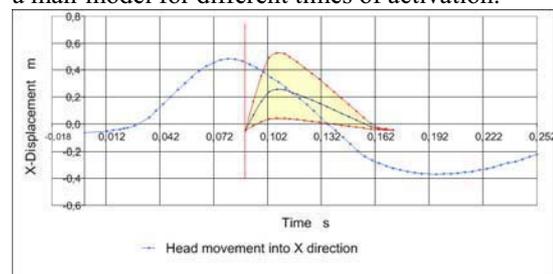
Fig. 7. Horizontal head displacements of a man-model and displacements of a multi-section air headrest at activation time t=0.090s

Fig. 7 shows an optimal protection for a head of a man-model at the second level of filling-in. The headrest displaces at the distance of 0.26m. At such a headrest displacement, knowing time for its full opening, to obtain full and optimal protection in such a case, a headrest should start its activity in time t=0.090 s. Such time will provide for the most efficient protection of the back of head and an upper spine part while 50% opening. At the maximum headrest displacement even an early opening of a headrest does not solve the problem as the headrest will simply get displaced further than a man-model which means that a deployed air-bag will hit the back of a man. If there was a need for protection at smaller displacement, then smaller number of deployed air-bag sections is not enough. There is a need for a better-determined activation time. At activation time t=0.090 s., an air-bag will get emptied before head leans on it.
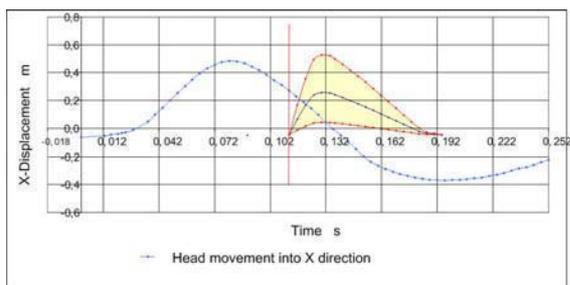
Fig. 8. Horizontal head displacements of a man-model and displacements of a multi-section air headrest for activation time t=0.112s

Fig. 8 shows optimal protection for man-model head at the least level of filling-in. A headrest displaces at the distance of 0.08m. In such a case to obtain optimal protection, a headrest should begin its activity in time t=0.112 s. Such time will provide the most effective protection of head and an upper spine part at its least filling-in level. For the rest of headrest filling-in levels, activation time will be too late. In all cases, a returning head will hit a headrest while being filled in.
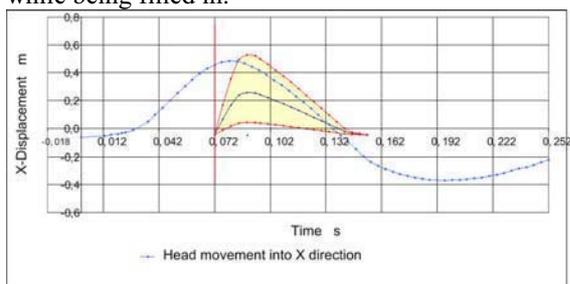

Fig. 9. Horizontal head displacements of a man-model and displacements of a multi-section air headrest at activation time t=0.072s
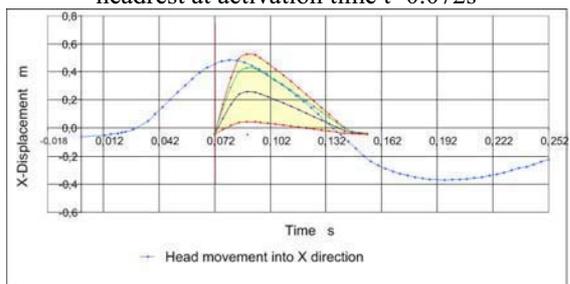
Fig. 10. Horizontal head displacements of a man-model and displacements of a multi-section air headrest at activation time t=0.072s with indicated level of filling-in

Fig. 9 shows a case where for average headrest filling-in, time of its activation is too early and for maximum headrest filling-in, both time and level of filling-in are not adjusted do head displacement. In fig. 10 additional level of headrest filling-in has been marked (green colour). For such a filling-in level, activation time of t= 0.072s is right time of correct activation of a headrest which provides for optimal protection of man-model head.

5. CONCLUSIONS

The concept of multi-section air headrest presented in the paper in not only a theoretical one but a possible to be realized in current technical conditions. The above-mentioned analysis show that for right protection of an upper spine part it is not always enough to limit horizontal headrest displacement. It is also needed to adjust its opening time. Too early opening results in a headrest being emptied before head contacts it and too late will lead to collision with the back of head.

6. LITERATURE

[1] Wicher J.: *Bezpieczeństwo samochodów i ruchu drogowego. (Safety of cars and road traffic)* WKiŁ. Warszawa 2002 (in Polish).

[2] Viano D. C., Olsen S., Locke G. S., Humer M.: *Neck biomechanical responses with active head restraints: rear barrier tests with BioRID and sled tests with Hybrid III.* SAE, Inc., Warrendale 2002.

[3] Jaśkiewicz M.: *Symulacyjne badanie działania ochronnego zagłówków aktywnych.* Rozprawa Doktorska. *(Simulation research of active headrests protective functioning)* Politechnika Świętokrzyska, Kielce 2007 (in Polish).

[4] Rokosch U.: *Airbag und Gurtstraffer. Vogel Industrie Medien GmbH & Co.* KG, Würzburg 2002.

[5] *Aktive Kopfstütze mindert das Risiko von Nackenverletzungen.* Verkehrsunfall und Fahrzeugtechnik, Januar 2006.

[6] Schmitt K. U., Niederer P., Walz F.: *Trauma Biomechanics. Introduction to Accidental Injury.* Springer-Verlag Berlin Heidelberg New York 2004.

[7] Segui-Gomez M.: *Driver airbag effectiveness by severity of the crash.* American Journal of Public Health, October 2000, Volume 90, Number 10.

[8] Seiffert U., Wech L.: *Automotive safety handbook.* SAE, Inc., Warrendale 2003.

[9] Viano D. C.: *Role of the seat in rear crash safety.* SAE, Inc., Warrendale 2002.

[10] Klanner W., Ambos R., Hummel T., Langwieder K.: *Unfallverletzungen in Fahrzeugen mit Airbag.* Bergisch Glandbach, November 2004.

[11] Jaśkiewicz M., Stańczyk T. L.: *Ocena działania aktywnych zagłówków gazowych poprzez porównanie kinematyki ruchu zagłówków i manekina w próbie zderzeniowej (The evaluation of gas active headrests by comparing the kinematics of headrest and dummy movement in a crash test)* Teka Komisji Motoryzacji Zeszyt Nr 33-34, s. 159 - 168, 2008 (in Polish).

[12] Jaśkiewicz M., Stańczyk T. L.: *The identification of damping and stiffnes*

parameters of a driver model on the basis of crash tests, Journal of KONES Powertrain and Transport Vol. 16, No. 1, pp. 229-238, 2009.

Tomasz Lech STAŃCZYK - doktor habilitowany nauk technicznych – 1994 r. - budowa i eksploatacja maszyn, spec. dynamika maszyn - Wojskowa Akademia Techniczna, Wydział Mechaniczny. Profesor nadzwyczajny Politechniki Świętokrzy-skiej od 1.04.1996 do chwili obecnej. Kierownik Katedry Pojazdów Samochodowych i Transportu.

Marek JAŚKIEWICZ – doktor nauk technicznych – 2007 – Budowa i Eksploatacja maszyn, w specjalności Dynamika i Budowa Pojazdów Samo-chodowych – PŚk / WMiBM. Adiunkt Polite-chniki Świętokrzyskiej od 1.11.2007 do chwili obecnej. Od 01.02. 2008 Sekretarz PTMTS oddział Kielce

DETERMINATIONS OF SHOCK ABSORBER DUMPING CHARACTERISTICS TAKING STROKE VALUE INTO CONSIDERATION ACCOUNT

Łukasz KONIECZNY, Rafał BURDZIK, Jan WARCZEK

The Silesian University of Technology, Faculty of Transport
Krasińskiego 8, 40-019 Katowice, Poland fax./tel. 6034166 lukasz.konieczny@polsl.pl

Summary

The paper presents the results of the hydraulic vehicle shock absorbers' researches on indicator test stand. The front twin tube hydraulic shock absorber for Fiat Punto was researched. The aim of this investigation was to determine the dumping characteristics (points of force for maximum linear velocity) taking stroke value into account. The stroke and rotary velocities were selected so that to different combinations the same maximum linear velocity was taken. For that extortion parameters the influence of stroke value on force versus displacement and force versus velocity diagrams was determined. The dumping surface in stoke and linear velocity function was determined too.

Keywords: shock-absorbers, dumping characteristics.

WYZNACZENIE CHARAKTERYSTYK TŁUMIENIA AMORTYZATORA
SAMOCHODOWEGO PRZY UWZGLĘDNIENIU WARTOŚCI SKOKU

Streszczenie

W ramach pracy przeprowadzono badania hydraulicznego amortyzatora samochodowego na stanowisku indykatorowym. Obiektem badań był bezciśnieniowy dwururowy amortyzator hydrauliczny stosowany w zawieszeniu przednim samochodu marki Fiat Punto. Celem przeprowadzonych badań było wyznaczenie punktowych charakterystyk tłumienia (wartości sił tłumienia dla maksymalnych wartości prędkości liniowej) przy dodatkowym uwzględnieniu wartości skoku roboczego. Wartości skoku i prędkości kątowej zostały tak dobrane, aby przy różnych kombinacjach otrzymać zbliżone wartości maksymalnej prędkości liniowej. Dla tak dobranych parametrów wymuszenia określono wpływ skoku na kształt przebiegów wykresów prędkościowych i charakterystyk punktowych. Wyznaczono także powierzchnię sił tłumienia w funkcji prędkości liniowej i skoku.

Słowa kluczowe: amortyzatory samochodowe, charakterystyki tłumienia.

1. INTRODUCTION

In simulation research of suspension dynamic the vehicle shock absorber is described as the element of viscosity dumping and the dumping force depends only on linear velocity function. For low frequency extortion apparent stiffness effect and the influence of stroke value on dumping characteristic are not taken for consideration.

In real conditions of shock absorber work the axel resonance frequency is higher than the body resonance frequency and the amplitude of these vibrations is small. In these conditions the direction of piston move is often changed and small quantity of oil is flowed by valve. This is cause the differences in dumping force in case of higher amplitude and lower frequency to lower amplitude and higher frequency. On indicator test stand with the sinusoidal extortion the change of maximum linear velocity can be got in two ways: constant stroke and changeable rotary velocity (frequency) or constant rotary velocity and changeable stroke. In scientific literature the authors often insist on thesis

that these two ways lead to this same results. This thesis is true for low frequency of extortions. In real conditions, frequency of extortions has got wide range so for different amplitudes the linear velocity can be over few m/s. The forms of loop determined on indicator test stand differ considerable from theoretical elliptic loop describing viscosity dumpers. These differences are connected with many factors: cavitations, valve inertia, oil properties, friction between moving parts and many other. These factors show that the dumping characteristics are dependent from stroke too. The example of investigations where results (dumping force) are presented as surface in stoke and linear velocity function [9] shows fig 1.
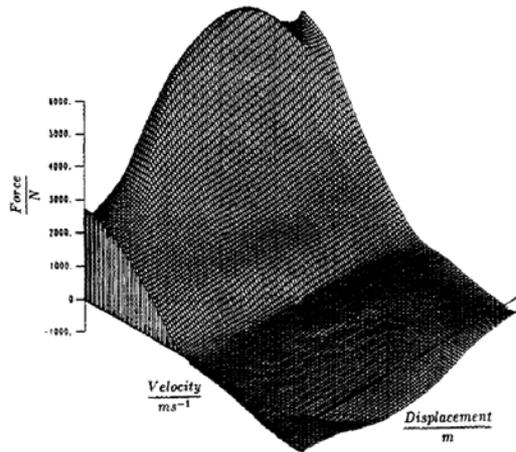
Fig. 1. Dumping surface in stoke and linear velocity
function [9]

2. INDICATOR TEST STAND AND RESEARCH OBJECT

The researches were made on indicator test stand. On this stand can be determined force versus displacement and force versus velocity diagrams for selecting strokes and velocities[1, 3, 6, 7, 8]. The Faculty of Transport at the Silesian University of Technology is in the possession of mechanical indicator test stand [2, 4, 5]. The view of indicator test stand and kinematic scheme of this stand presents fig 2.
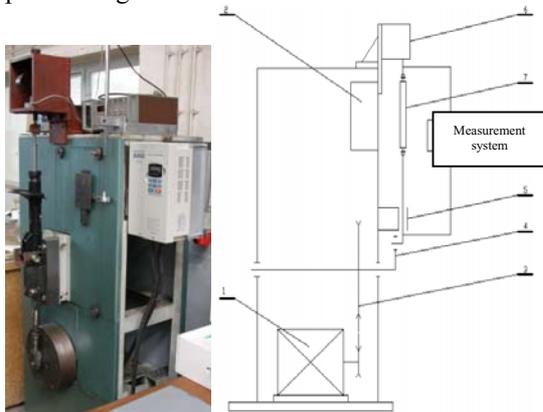

Fig. 2. The indicator test stand view and kinematic scheme: 1- electric motor, 2- frequency converter, 3- belt transmission, 4- eccentric system, 5- slider ways, 6- force sensor, 7- shock absorber.

This test stand is electric engine driven. The rotary velocity of engine is controlled by frequency converter. The belt transmission with cog belt connects the engine and the eccentric system with arm. Length of this arm determines the stroke in research and can by changeable by steps about 4 [mm]. The rotary move of eccentric system is changed into linear move of slider.

The lower end of shock absorber is mounted in slider. The piston rod is mounted in force sensor where the dumping force is measured.

To measure of forces the bi-directional extensometer sensor was used (range of sensor was 5 kN). The linear displacement of shock absorbers lower end is measured too. To measure linear displacement inductive displacement sensor PTx 200 was used. The analog signal from these sensors are recorded using SigLab 20-22A with high frequency sampling (2048 [Hz]).The minimum 15-th stress cycle (bound and rebound) was recorded every time. The analog signals were filtering with FIR (finite impulse response) filter and the force-displacement diagrams are the average of all recorded cycles.

The twin tube hydraulic shock absorber for front suspension of Fiat Punto was researched (fig.3). Before the measurement procedure the shock absorber was initially heated up to temperature stabilization.

Fig. 3. The twin tube hydraulic shock absorber for front suspension of Fiat Punto

3. ANALYSE OF RESEARCH RESULTS

For determining set of shock absorber dumping characteristics, series of researches for different combinations of stroke value and rotary velocity was made. For every stoke, the frequency of extortion was chosen so as to set the same maximum linear velocity every time.

The results of researches show the cumulative force versus displacement (fig.4) and force versus velocity diagrams (fig.5)

The shape of loop on force versus velocity diagrams is changed in stroke function. For higher strokes and higher frequency they are visibility curvature. These curvatures are made adequately to time moment of open bump and rebound values. For low stroke this curvatures aren't visible and the shape of loop is similar to elliptic curve.
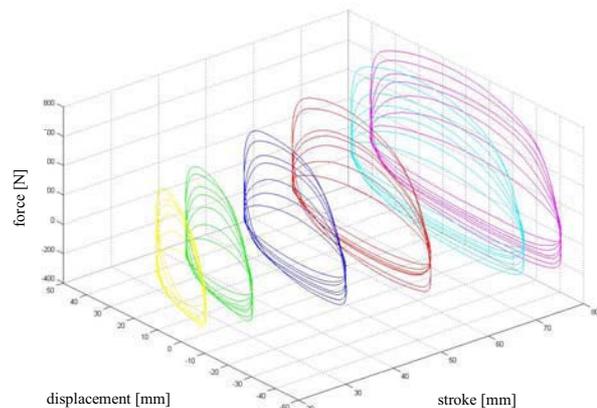

Fig. 4. Force versus displacement diagrams (each color for different stroke)
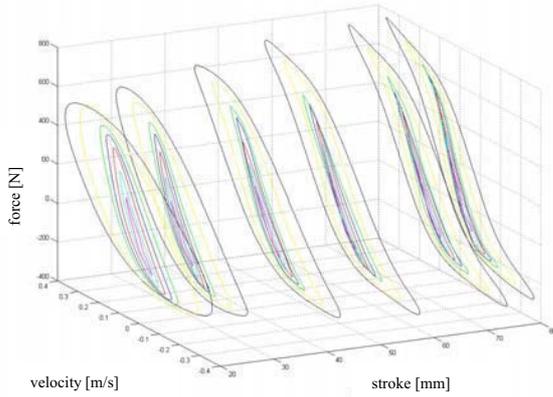
Fig. 5. Force versus velocity diagrams (each color for different maximum linear velocity)


Fig. 6. Force versus velocity diagrams for chosen maximum linear velocity 0.1 [m/s] (each color for different stroke)

Fig. 7. Force versus velocity diagrams for chosen maximum linear velocity 0.3 [m/s] (each color for different stroke)

On fig 6 and 7 there are shown diagrams for different strokes. For maximum linear velocity above 0.1 m/s there are not any visible differences. For maximum linear velocity above 0.3 m/s there are visible differences related to time moment of open bump and rebound values. The next fig. 8 and 9 show set of shock absorber dumping characteristics series (force points for maximum linear velocity for different strokes).

Fig. 8. Dumping force characteristic for bump (each color for different stroke)

Fig. 9. Dumping force characteristic for rebound (each color for different stroke)

Analyse of obtaining points dumping characteristics for bound and rebound let state that for low strokes and higher maximum linear velocities the force of dumping is lower for bump and for rebound.
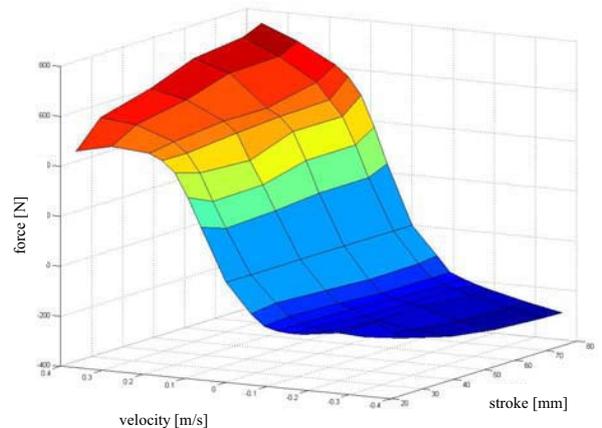

Fig.10. Dumping force surface in stroke and linear velocity function

The dumping characteristics for bump and rebound presented on fig 8 and 9 were expanded in second parameter (stroke) so this way the dumping surface in stroke and linear velocity function was made (fig10).

4. CONCLUSION

The results presented in paper show some disadvantages and simplification resulting from taking dumping characteristics of shock absorber only as a function of maximum linear velocity. Particularly that form of describing of shock absorber dumping characteristics is used in simulation research of vehicle dynamic. The analyse of presented results put emphasis on the influence of some factors like cavitations or valve inertia on shape of loop on force versus velocity diagrams and dumping forces on dumping characteristics. For higher maximum linear velocity and short stroke on dumping characteristics the dumping forces are lower than forces for long short for bump and rebound. These results will be used in simulation researches while taking into account dumping force as surface.

6. LITERATURE

[1] Dixon J. C.: *The shock absorber handbook.* Society of Automotive Engineers, USA 1999.
[2] Gardulski J., Warczek J.*: Investigation on force in frictional kinematic pairs to assess their influence on shock absorber characteristic.* Transport Problems, volume 3, Issue 1, Gliwice 2008 s.19-24.
[3] Kamiński E.: *Dynamika pojazdów i teoria zawieszeń.* WPW, Warszawa 1977.
[4] Konieczny Ł.: *Badania amortyzatorów hydraulicznych na zmodyfikowanym stanowisku indykatorowym.* Zeszyty Naukowe Politechniki Śląskiej, s. Transport, z.61 Wydawnictwo Politechnik Śląskiej, Gliwice 2007 s.151-156.
[5] Konieczny Ł., Śleziak B.: *Wpływ wybranych parametrów na charakterystyki tłumienia amortyzatorów hydraulicznych.* Zeszyty Naukowe Politechniki Śląskiej, s. Transport, z.64 Wydawnictwo Politechnik Śląskiej, Gliwice 2008 s.145-150.
[6] Lanzendoerfer J.: *.Badania pojazdów samochodowych.* WKiŁ, Warszawa 1977.
[7] Reipell J., Betzler J.: *Podwozia samochodów – podstawy konstrukcji.* WKiŁ Warszawa, 2001,
[8] Sikorski J.: Amortyzatory – budowa – badania – naprawa. WKiŁ, Warszawa 1984.
[9] Worden K, Hickey D, Haroon M, Adams D.: *Nonlinear System Identification of Automotive Dampers: A Time and Frequency-Domain Analisys*, Mechanical Systems and Signal Processing, nr 23/2009.

Łukasz KONIECZNY is Ph.D. in Department of Automotive Vehicle Construction, Faculty of Transport, Silesian University of Technology. His research interests are: machinery diagnostic, digital analyse of signals, simulation researches of vehicle dynamic, hydro-pneumatic suspensions

Rafał BURDZIK is Ph.D. in Department of Automotive Vehicle Construction, Faculty of Transport, Silesian University of Technology. His research interests are: machinery diagnostic, digital analyse of signals, logistics and forwarding

PhD Eng. **Jan WARCZEK** is a researcher in Department of Vehicle Car Construction, Faculty of Transport Silesian Technical University Research interests: diagnostics and experimental simulation using vibroacoustics methods, dynamics of vehicle suspensions, method of active vibration reduction.

PROPOSAL FOR THE METHOD OF DETERMINING THE MOST INTENSIVE FRAGMENTS RIVET JOINS APPEARING THE SHELL AIR PANELS WORKING UNDER THE INFLUENCE OF TENSION FIELD

Jarosław MAŃKOWSKI, Jerzy OSIŃSKI, Przemysław RUMIANEK

Instytut Podstaw Budowy Maszyn, Politechnika Warszawska
ul. Narbutta 84, 02-524 Warszawa, fax: (+48 22) 234 86 22, email: jarosław.mankowski@simr.pw.edu.pl

Jerzy JACHIMOWICZ

Katedra Mechaniki i Informatyki Stosowanej, Wojskowa Akademia Techniczna

Summary

This article presents the methodology for determining seam rivet fragments most exposed to fatigue damage caused by buckling cover sheet occurring in the semi-monocoque structures. The present study is focused on determining the impact of the tension field, which is one of the cases of buckling, the state of the burden and strain of riveted joints occurring in shell structures. The conditions in which tension field arise for example two-flange girder were also examined. Analysis was also performed to explore micro-slides between the rivet and the hole in the conditions of normal and torsional loads of combined sheets.

The presented method allows both the determination of dangerous places, susceptible to the tension field for the whole structure, as well as a detailed analysis of selected parts of the structure - which can be useful, especially in the design of structures on the basis of supervising durability.

Keywords: shell structures, semi-monocoque structures, riveted joints, tension field, FEM.

PROPOZYCJA METODY WYZNACZANIA NAJBARDZIEJ WYTĘŻONYCH FRAGMENTÓW SZWÓW NITOWYCH WYSTĘPUJĄCYCH W CIENKOŚCIENNYCH PANELACH LOTNICZYCH PRACUJĄCYCH POD WPŁYWEM POLA CIĄGNIEŃ

Streszczenie

Celem artykułu jest przedstawienie metodyki określania najbardziej narażonych na zniszczenie zmęczeniowe, spowodowane wybaczaniem blach pokrycia, fragmentów szwów nitowych występujących w konstrukcjach półskorupowych. W niniejszej pracy skupiono się na określeniu wpływu pola ciągnień, które jest jednym z przypadków wyboczenia, na stan obciążeń i odkształceń połączeń nitowych występujących w konstrukcjach cienkościennych. Zbadano warunki powstawania pola ciągnień na przykładzie dźwigara dwupasowego. Wykonano również analizy mające na celu zbadanie mikropoślizgów pomiędzy nitem a otworem w warunkach obciążeń normalnych i skrętnych łączonych blach.

Przedstawiona w pracy metoda, pozwala zarówno na określenie miejsc niebezpiecznych, podatnych na działanie pola ciągnień, dla całej konstrukcji; jak i przeprowadzenie szczegółowej analizy wybranych fragmentów konstrukcji - co może być przydatne, zwłaszcza przy projektowaniu konstrukcji na trwałość dozorowaną.

Słowa kluczowe: konstrukcje cienkościenne, półskorupowe, połączenia nitowe, pole ciągnień, MES.

1. INTRODUCTION

Riveted joints are classified as persistent connections, in which parts do not change their positions relative to each other. Therefore, design of riveted joints usually comes down to check the basic conditions, such as strength of shear and pressure. This is a simplification in which the residual stresses resulting from the technological process are not taken into account, in which there is rivet clenching [1-3]. The fact that the riveted joints

occurring in aircraft structures are overlooked, but in reality are at least partly rubbing joints [4, 5]. In this case, it appears that the basic conditions for checking the strength may be insufficient or may be in significant degree to limit the possibility of the development of a structure due to the need for additional factors of safety. In some special cases it can prove disastrous - as in the case of Boeing 737 Aloha Airlines in-flight No. 243 [6], in which the

main cause of the accident[1] was multi-focal coverage cracks along the riveted joint_and destruction of a big part of the hull. Examples of multi-focal fatigue cracks of air structures can be found for example in [7], where the authors present the results of shell structures made of natural scale.

Currently, in order to avoid accidents, properly designed shell construction is built with an appropriate[2] supply of safety in relation to the service loads and do not really have concerns that it will be destroyed suddenly during normal exploitation. Today, the struggle leads to an extension of overhaul life through: firstly - increasing the fatigue life, secondly - to increase safety by monitoring the damage - which allows the replacement of worn components and non-threatened exploitation of the whole object.

Air structures are subjected to very high and variable load in time. They are also differentiated with reference to the character of the amplitude and load - a combination of elements of these structures are the most vulnerable to damage as a result they must meet very high demands. Significant values of loads acting on the construction sites, often associated with the occurrence of large displacements parts of the structure, make the riveted seams move very large in value, and complex states of loading [8]. Since the life-time of an aircraft largely depends on the durability of its connections around the world, research on this topic has since intensifed [2, 3, 9-15]. On this basis it can be concluded that the occurrence of local stress concentrations, have a substantial impact relative displacement of joints components, caused by service loads. This applies especially to the semi-monocoque structures[3] where there is a definite change load conditions beyond the critical forces - leading to the formation of an additional burden of large gradients loads in the seam riveted joint length [8]. In such a situation, it becomes necessary to take it into account in the design process because of the relatively large cover deformations in the

---

[1] Described event is called the air accident - Regulation of the Minister of Transport from 18.01.2007 – in case about air accidents and incidents, Dz. U. 27.02.2007.

[2] The overall safety factor currently used in aviation, is 1.5.

[3] Semi-monocoque structure - it is such a shell structure in which elements of the cover is very thin in relation to elements of the framework, and therefore may be a local loss of stability of elastic recovery, while the structure for loads exceeding the maximum operating loads, due to the small thickness - cover elements can work rather than flexion membrane and bending moments and the local bending is taken over by elements of the framework (the bending stress in the elements of cover are very small and usually does not exceed 5%) [21, 22]

riveted joint accompanying the buckling of that cover.

2. COVER BUCKLING - PROBLEMS IN CONNECTION WITH ANALYSIS SHELL STRUCTURES WORKING IN OVER-CRITICAL STATE

The necessity to pay special attention to the structural analysis for the over-critical state, is also connected with another important, yet relatively new issue, which is the change in approach to determining the time to damage the structure. Keeping in mind that one of the characteristics features of aircraft structures, which affects the design process, is very long life of 20-30 years or more and taking into account their cost of production, extension of overhaul life and extension of their life this translates into very high costs. Thus, in aviation, is gaining great importance in determining the service life extension than at the time, but according to technical condition, for example by supervising durability using damage tolerance [16-19]. In this case, damage tolerance may be authorized for one or more elements.

A shortcoming of life according to time is a fact that it is not possible to foresee all possible cases of load and working conditions, and therefore assumes the most unfavourable conditions of work and will determine the time overhaul life. Exploitation by supervising durability can significantly prolong the safe operation. This approach to sustainability, however, requires carrying out many detailed research and analysis for determining which charges and what mechanisms cause the destruction. Examples of such activities could be found in [3, 10, 11, 20]. They presented the results of research and analysis of local and micro-local phenomena, occurring in rivet joints, caused by closing the rivet.

In the case of riveted construction, a very important problem is to identify dangerous places - places in the structure, which needs special attention. This implies a need to address many issues affecting the phenomena at the micro level, from which usually begins joints degradation. This is particularly important in the case of semi-monocoque structure, which is allowed to lose the cover stability in elastic range, which further complicates the problem. Structural analysis in the over-critical state, belong to a very complex and require both vast knowledge and experience, the implementation of a series of studies, as well as possession of computer equipment with very high computing power. The scale of the problem, in cases of complex shell structures, is shown clearly by the contents of the document published in 2002 by NASA[4] [23]. In this document, section 6.1.1.7

---

[4] NASA - National Aeronautics and Space Administration.

(buckling and destruction) describes the methodology of analysis and loading in cases of shell structures, which should include an analysis of buckling. Also indicates that for the analysis of thin-walled shell appropriate "reduction" factor should be applied that takes into account the differences between classical theory and experimental results of the burden, which causes loss of stability. Mainly due to the fact that the occurrence of tension field (one of the forms of buckling) cannot be ruled out.

3. TENSION FIELD

Tension field – special case buckling covered by the shell structures, formed by the action of tangential forces[5].

In 1928, H. Wagner presented the trial, in which a thin shell of the transverse stiffeners subjected to load, gave rise to a diagonal fold [24]. He demonstrated that uprising buckling of cover doesn't destroy constructions until transverse stiffeners work only on compression (until stability is lost). This had a huge impact on the approach to the design of shell structures.

The essence of tension field is that in spite of charging to cover only the tangential forces in coverage after exceeding the critical load, there is a complex state of stress in Fig. 1.
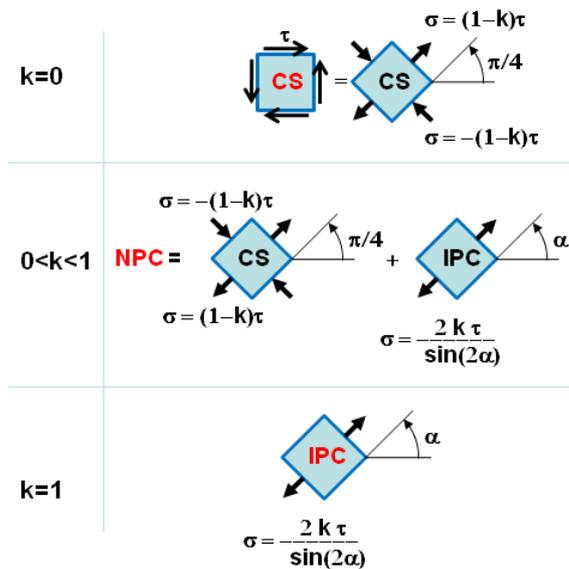

Fig. 1. State of stress in tension field

In the case of the tension field it should be divided into three phases depending on the value of the load:

- first phase, in which the load does not exceed the critical load, therefore, the coverage is only pure shear CS (1), in principle, should not even talk about the tension field:

$$\sigma_{PC} = \sigma_{CS} = \tau \qquad (1)$$

- second phase, in which the load exceeds the critical force in this case the state of stress in the coating is a superposition of pure shear CS and tensile stress resulting from folding the cover, so the tension field IPC (2), the second phase is called the incomplete tension field and identified NPC[6];

$$\sigma_{PC} = \sigma_{CS} + \sigma_{IPC} \qquad (2)$$

$$\sigma_{CS} = (1-k)\tau ; \quad \sigma_{IPC} = \frac{2k\tau}{\sin(2\alpha)} ;$$

- third phase, in which the load is so large that there is no longer just a clean cutting stress stretching IPC (3); of course this is a purely theoretical case, but may be taken into account for very thin covers.

$$\sigma_{PC} = \sigma_{IPC_{(k=1)}} = \frac{2\tau}{\sin(2\alpha)} \qquad (3)$$

Structural damage as a result of the tension field may occur when:

- the strength of the material covering the tension is exceeded - will tear the substance;
- the critical force for the elements of the skeleton is reached, due to the increasing normal force and the emergence of the load perpendicular to the axis of rods of the framework.
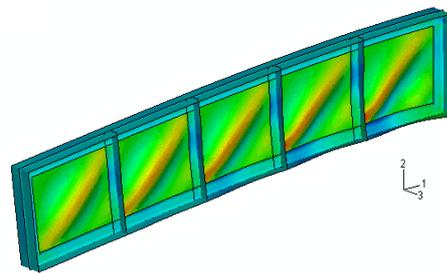

Fig. 2. Deformation of the cover was created in bended thin-walled girder
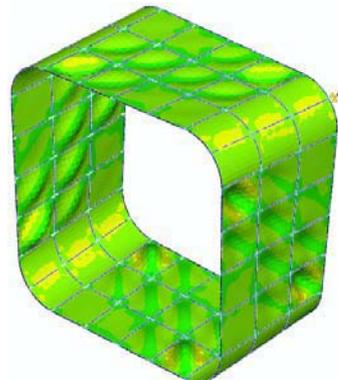

Fig. 3. Deformation of a cover in the simplified model of an aircraft fuselage section, which is subject to torsion

---

[5] Definition based on [28].

[6]NPC - incomplete tension field, the term introduced by Professor Zbigniew Brzoska [28].

In real structures, the problem of the tension field most often occurs in thin-walled girders (Fig. 2) and the external covering of aircraft, especially in covering the fuselage, which include subjection to torsion (Fig. 3).

A detailed summary of the phenomenon presented by Paul Kuhn of the National Advisory Committee for Aeronautics in 1952[7], and then fully structured description of this phenomenon, posted a comprehensive monograph on the analysis of shell structures [25], published in 1956. Other important items, which contain a number of details about the tension field, are: [24] published in 1960[8], [26] published in 1961[9] and [27] published in 1965[10]. In 1965 he appeared in revised and enlarged edition of the book, "Statics and stability of structures" [28]. The next thesis, which concerns the subject of tension field were based on the work of J. P. Timoshenko, P. Kuhn, and Z. Brzoska.

4. METHODOLOGY OF RESEARCH AND ANALYSIS

As already noted, the tension field is a phenomenon whose occurrence is closely associated with shell structures. It occurs both in the outer covering of shell structures and in shell girders covering. Therefore, in order to assess the impact of this specific type of buckling load on the state of riveted joints, a series of analysis or test of the proposed structure was performed.

Analysis can be divided into three groups depending on the scale of the model. The proposed models are:

- global model (entire structure or a sufficiently large part of it) - the analysis of such a model is to answer charges relating to merger riveted joint and the location of vulnerable parts of the structure [29, 30] (an example of a global model is shown on Fig. 4);
- local model (selected portion of the structure) - the analysis of this model is used in determining the movements of dangerous places (such as a local model is shown in Fig. 5);
- micro-local model - (appropriately sized fragment containing one or two rivets) - used to perform two studies:
  - analysis of closing the rivet, in order to determine the initial stresses and strains introduced into the model;
  - riveted joint call for an analysis of stresses and deformations introduced and applied

---

[7] A SUMMARY OF DIAGONAL TENSION, Kuhn Paul (information is posted on the basis of [23] First Edition)

[8] Autor: Hertel Heinrich, Dr. Ing. O. Professor an der Technischen Universitët Berli

[9] Autor: Zbigniew Brzoska Dr Inż. Profesor IPPT PAN, PW.

[10] Autor: Jerzy Teisseyre Dr Inż. Profesor IPPT PAN, Politechnika Wrocławska.

displacements obtained from the analysis of local model - in order to obtain answers about the stress concentrations and the size of the relative displacements of individual elements of the connection.
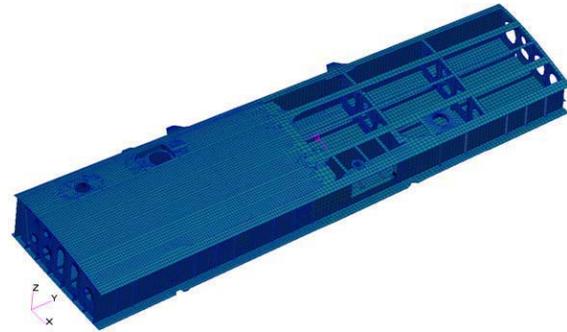
Rys. 4. FEM model of the fragment of the wing (the main torque box) PZL M28 Skytruck - for selected treated as a global analysis (to show the hidden internal structure to cover the upper part of torque box)

Most of the analysis of tension field of impact assessment on the state of riveted joints is carried out using FEM. FEM systems have many features in common - especially the basic elements and models of library materials and computational methods [31-33]. Results obtained from different FEM systems, using the same model (the number of elements, type of elements, the calculation method and material models), should be the same. This statement is purely theoretical. In practice, there is another very important factor: namely, the FEM is not the scientific method but approximate method - in conjunction with the accuracy of the results still depends on "numeric" - the applied methods of solving equations and methods for their software. Moreover, due to the sensitivity of this method for numerical errors, the impact on the outcome is also a class of computer equipment used for analysis. Thus, in addition to the need to adapt to the analysis of the available computer hardware and to resolve the problem selection of an appropriate methodology for modelling of riveted joints, it depends on: first, the scale model, and secondly on the requirements associated with the introduction of charges. Until that time, some interesting theses in which, special emphasis on the above issues.

The problem of modelling methods of riveted joints to the environment of one or more rivets were raised in [34, 35]. These theses contain examples of different ways of modelling riveted joints and guidance on the scope of applicability of the methods discussed in them. The problem of modelling global structures, which are riveted joints, has been addressed in [29, 36]. Particularly important is the thesis of [29], which has been shown that the influence of internal stresses caused by clenching a rivet is local and does not exceed 8-10 rivet diameters. Above this limit, the modelling process of the rivet does not matter. Based on the

results cited in the theses, we can conclude that building a local model for analysis, should be elected for more than a dozen area of the rivet diameter, and should be modelled, at least in a simplified manner, the phenomenon of contact. Micro-local model should be extended to cover from one to several rivets, including all contact pairs. However, building a global model construction, the rivet model can be replaced by a single beam element, or may be omitted. Today, despite major simplifications in global models, it puts ever greater demands on such analysis, because they allow for precise determination of risk areas and are the source of the data (stress, displacement) for analysis on a local scale and micro-local.

Therefore, it is necessary to carry out many studies, aimed at optimal finite element models for each stage of the analysis, because the same models will be used during subsequent analysis. The work can be divided into four stages.

4.1. Stage 1 - Preliminary analysis of construction - a global model

In the initial design phase to make a preliminary analysis of the construction to determine the basic dimensions of the carrying structure (cross-sections of skeletal elements, sheet thickness) and between other levels of burden riveted joints. The purpose of this analysis is also the general designation of the displacements and stresses in the structure, which is the starting point for many other detailed analyses. An example of this global analysis can be reduced tensions in the map coverage of the visible portion of the wing buckling coverage zones depicted in Fig. 5, obtained for one of the manoeuvring loads [29].

Fig. 5. Reduced stress (by H-M-H11) [MPa] and the displacement in the model wing. The apparent local loss of stability

In the course of this thesis, actions taken include the implementation of the initial design and analysis of sample designs. After reading a number

---

[11] H-M-H - reduced stress by hypothesis Huber - Mises - Hencky

of structural solutions, in which there are problems with the drawings on the field, three examples were selected: classical two-flange girder, two-belt girder with holes in coverage and the spatial structure of a fragment corresponding to the aircraft fuselage subjected to twisting, and then made their global models and conducted appropriate analysis. The obtained results allow, inter alia, to identify high-risk places in the structure which should be subjected to a thorough analysis. Over these results the analysis global-local models were used to determine charges, (step 2)[12]. The results of the thesis have been published in [37-39].

4.2. Stage 2 - Analysis of a chosen structure - local model

This phase includes analysis of the construction areas especially threatened by the stress concentration and buckling in the action from the tension field Fig. 6 Verification should especially burden the state and deformation of the rivet seams [29, 30].

Fig. 6. The combination of riveting, a local model of the wing - reduced stress (by H-M-H) [MPa] - frame and cover on the side of formed rivet heads

The remainder of the paper presents results of calculations of the air panel sample, for which we were a "classic" analysis of the connection and the riveted joint analysis of the FEM, with emphasis on the combination of riveting. Based on the results of the choice of the most loaded rivets for detailed analysis of a single rivet. Obtained at this stage, the results were used to determine the burden for the analysis of micro - local models (stage 4). They will also be used to prepare the test program (stage 3).

---

[12] The concept of a global model is contractual in nature and smooth, and is understood as a model superior to the other model, which in this case is considered to be local, or subordinate. Otherwise, the global model can be considered as a local example, presented as part of the wing is a local model for the entire model, or an entire wing of the aircraft.

4.3. Stage 3 - Research - Review FEM models

Due to the rapidly growing opportunities and the development of FEM software hardware, computing tools get more powerful. This allows the analysis of increasingly complex cases. At the same time, the field analysis of complex, nonlinear problems is relatively new and therefore there is a small number of publications with real test results. If these facts are combined with the fact that the FEM systems are excellent tools and the "by oneself" do not count, it becomes necessary to perform the test on real objects, to verify the FEM models - in this case, the analysis is used to calls riveted joint. At this stage the preparation of the assumptions and tests connections, whose results will be used to verify the calculation method. Another important factor is to design a test sample in such a way as to be representative and have as many features of a connection that will be present in the actual construction. In particular, attention should be paid to the selection of the load..

4.4. Stage 4 - Detailed analysis of the riveted joint calls - the micro-local model

At this stage, using data from the local model (stage 2) and assumptions for the implementation of the FEA model, as evidenced by test results (stage 3), followed by preparation of finite element models for detailed analysis of the riveted joint connection of the test structure. The results of the analysis on the model of micro-local, allow to determine the degree of stress concentration and to assess the intensity of co-movements of the surface - which allows for detailed and very accurate assessment of the test portion of the joint.

5. SUMMARY

Riveted seams occurring in shell structures, especially semi-monocoque structures, are exposed to the difficulty of determining the load caused by buckling of coverage. A special case of this type of load is a tension field.

The proposed method allows the selection of the most heavily loaded portion of rivet seams, and then to isolate a single rivet environment where stress is the greatest. This is particularly important in the design of structures on the stability of the supervised control of damage tolerance. Knowledge of the biggest areas of stress, pressure and relative displacement of elements is essential in determining potential sites for crack initiation, and the knowledge of the stress field can identify the direction and speed of propagation.

In the proposed method of performance analysis, based on the use of FEM. Please note that this method is approximate and, therefore, is required for experimental verification of models and analysis.

6. BIBLIOGRAPHY

[1] Derewońko A., Jachimowicz J., Szymczyk E.: *Analiza połączenia nitowego z uwzględnieniem naprężeń resztkowych i eksploatacyjnych*. VIII Międzynarodowa Konferencja Naukowa Computer Aided Engineering, Polanica, Oficyna Wydawnicza Politechniki Wrocławskiej, 2006.

[2] Derewońko A., Jachimowicz J., Szymczyk E.: *Numeryczna symulacja procesu nitowania*. IX Konferencja Naukowo-Techniczna „Programy MES w Komputerowym Wspomaganiu Analizy Projektowania i Wytwarzania", Giżycko, WAT, 2005. str. 19-22.

[3] Szymczyk E., Derewońko A., Jachimowicz J.: *Analysis of displacement and stress distributions in riveted joint*, III European Conference on Computational Mechanics Solids, Structures and Coupled Problems in Engineering, Lisbon, Portugal, C.A. Mota Soares et.al. (eds.), 2006.

[4] Łaguna J., Łypacewicz K.: *Połączenia śrubowe i nitowe*. Warszawa, Arkady, 1986.

[5] Jachimowicz J., Kaniowski J., Karliński W.: *Zmęczenie cierne w konstrukcjach lotniczych*, XVIII Sympozjum: Zmęczenie Materiałów i Konstrukcji , Bydgoszcz-Pieczyska, 2000.

[6] Hawaiian Steam Engineering: *Aloha Airlines Flight 243 - Aircraft Accident - Maui Hawaii*. [Online] 1997.
http://www.aloha.net/~icarus/index.htm.

[7] Boyd D., Howard and Co.: *Corrosion detection devices*, Department of Energy, 2003. Contract No. DE-AC09-96SR18500 U.S.

[8] Mańkowski J.: *Wpływ pola ciągnień na obciążenia połączeń nitowych występujących w konstrukcjach cienkościennych*. Warszawa, Politechnika Warszawska, 2009, rozprawa doktorska.

[9] Müller Richard P. G.: *An experimental and analitical investigation on the fatigue behaviour of fuselage riveted lap joint*. Delft University of Technology, 1995, rozprawa doktorska.

[10] Derewońko A., Jachimowicz J., Szymczyk E.: *Numeryczne szacowanie poziomu naprężeń resztkowych w zakuwanym połączeniu nitowym*. praca zbiorowa pod red. Tadeusza Niezgody „Analizy numeryczne wybranych zagadnień mechaniki" Warszawa, WAT, 2007, str. 329-350.

[11] Kubiak T., Młotkowski A., Niezgodziński T.: *Zastosowanie metody elementów skończonych do badania procesu nitowania*. t. 23 - Analizy numeryczne wybranych zagadnień mechaniki, Warszawa, 2007, str. 445-457.

[12] Jachimowicz J., Kajka R., Kaniowski J., Karliński W.: *Fretting w konstrukcjach lotniczych*. Tribologia: tarcie, zużycie, smarowanie Tom 201, 3/2005, 2005, str. 97–108.

[13] Jachimowicz J., Kajka R., Krysztofik J., Szachnowski W., Szymczyk E.: *Stan odkształceń i naprężeń w pobliżu nitu w konstrukcji lotniczej – analizy MES i badania*, IX Konferencja Naukowo-Techniczna „Programy MES w Komputerowym Wspomaganiu Analizy Projektowania i Wytwarzania", Giżycko, WAT, 2005.

[14] Gołoś K.: *Trwałość zmęczeniowa metali w ujęciu energetycznym*, Warszawa, Wydawnictwo Politechniki Warszawskiej, 1990.

[15] Dębski M. A., Dębski D. K., Gołoś K. M.: *Hypothesis of loads cycle reduction to equivalent fatigue cycle*, Prace Instytutu Lotnictwa, Warszawa, Wydawnictwo Naukowe Instytutu Lotnictwa, 2005. 4/2005 (183). praca zbiorowa. ISSN 0509-6669.

[16] Głowiński S.: *Identyfikacja stanu technicznego oraz podstawy prognozowania pracochłonności napraw urządzeń mechanicznych na przykładzie eksploatacji statków powietrznych*, Koszalin, Politechnika Koszalińska, 2004, rozprawa doktorska.

[17] Chang J. B., Rudd J. L.: *Damage Tolerance of Metallic Structures, Analysis Methods and Applications,* ASTM International, 1984. ISBN-EB: 978-0-8031-4908-3.

[18] Lewitowicz J.: *Podstawy eksploatacji statków powietrznych,* Tom 1. Statek powietrzny i elementy teorii, Warszawa, Wydawnictwo Instytutu Technicznego Wojsk Lotniczych, 2001. ISBN: 83-900817-4-1.

[19] LexTech, Inc.: *DTD Handbook, Handbook for Damage Tolerant Design.* 2008. http://www.afgrow.net/applications/DTDHandbook/default.aspx.

[20] Jachimowicz J.: *Ocena wytrzymałości konstrukcji,* Wewnętrzne materiały szkoleniowe. Warszawa, Instytut Lotnictwa, 1996.

[21] Jachimowicz J., Lamparski J.: *Przegląd materiałów z zakresu obliczeń metodą elementów skończonych cienkościennych konstrukcji lotniczych.* Warszawa: Instytut Lotnictwa, 1976. Sprawozdanie Instytutu Lotnictwa nr 6/BW/WS/76.

[22] Jachimowicz Jerzy i inni: *Opracowanie metody obliczeniowej oraz przykłady obliczeń rzeczywistych konstrukcji lotniczych.* Sprawozdanie Instytutu Lotnictwa. Warszawa: Instytut Lotnictwa, 1980. 21/RW/WO/80.

[23] National Aeronautics and Space Administration, International Space Station Program, Johnson Space Center: *Payload flight equipment requirements and guidelines for safety–critical structures,* Houston, Teras, NASA, 2002. Contract No. NAS9–02099 (PA16).

[24] Hertel H.: *Leichtbau flugzeuge und andere leichtbauwerke*, Springer-Verlag, 1960.

[25] Kuhn P.: *Stresses in aircraft and shell structures*, New York / Toronto / Londyn, McGraw-Hill Book Company Inc., 1956.

[26] Brzoska Z.: *Statyka i stateczność konstrukcji prętowych i cienkościennych*, Warszawa, Państwowe Wydawnictwo Naukowe, 1961.

[27] Teisseyre J.: *Budowa nadwozi, Część I – obliczenia*, Warszawa, Wydawnictwa Komunikacji i Łączności, 1965.

[28] Brzoska Z.: *Statyka i stateczność konstrukcji prętowych i cienkościennych*, Wydanie drugie – zmienione, Warszawa, Państwowe Wydawnictwo Naukowe, 1965.

[29] Jachimowicz J., Wronicz W.: *Wybrane problemy modelowania nitowanych, lotniczych struktur cienkościennych*, Przegląd Mechaniczny, 2008, 5, str. 25-34.

[30] Derewońko A., Jachimowicz J., Sławiński G., Szymczyk E.: *Modele globalne i lokalne MES w analizie struktur lotniczych na przykładzie fragmentu skrzydła samolotu PZL M28 Skytruck*, Warszawa, Biuletyn WAT, 2010. Vol. LIX, 1(657).

[31] ABAQUS: *Abaqus analysis user's manual*, United States of America, ABAQUS, Inc., 2004.

[32] ANSYS Inc., ANSYS: *Documentation Manuals, ANSYS Realase 9.0.* Canonsburg: SAS IP, Inc., 2004.

[33] MSC.Software Corporation: *MSC. Nastran 2007, User's Guides.* Santa Ana, MSC.Software Corporation, 2007.

[34] Jachimowicz J., Kajka R.: *Problemy modelowania połączeń nitowych metodą elementów skończonych*, VIII Konferencja Naukowo-Techniczna Programy MES w Komputerowym Wspomaganiu Analizy, Projektowania I Wytwarzania, Rynia, Institute of Aviation, 2003, str. 12.

[35] Mańkowski J.: *Opracowanie metodyki modelowania połączeń obrotowych metodą elementów skończonych bez użycia zagadnienia kontaktu z wykorzystaniem systemu ABAQUS/Standard*, Warszawa, 2003, praca wykonana na zlecenie FAURECIA Fotele Samochodowe Sp. z O. O..

[36] Mańkowski J., Osiński J., Żabicki A., Żach P.: *Modelowanie połączeń typu sworzeń - otwór za pomocą MES bez użycia analizy kontaktowej*, Systems IX, Wrocław, Oficyna Wydawnicza Politechniki Wrocławskiej, 2004, str. 670-674.

[37] Mańkowski J., Jachimowicz J., Osiński J.: *Selected problems concerning the analysis of thin-walled structures with the use of finite element metod*, Journal Of Kones Powertrain And Transport, 2008, str. 109-118.

[38] Jachimowicz J., Mańkowski J., Osiński J.: *Wybrane problemy analizy konstrukcji cienkościennych z zastosowaniem MES*, X Jubileuszowa Konferencja Naukowo-Techniczna „Programy MES we Wspomaganiu

Analizy, Projektowania i Wytwarzania",
Kazimierz Dolny, 2007, str. 63-64.
[39] Mańkowski J., Osiński J., Żach P.: *Pole
ciągnień w cienkościennym dźwigarze
lotniczym*, XII Sympozjum Stateczności
Konstrukcji , Zakopane, 2009, str. 285-288.

Prof. Eng. **Jerzy OSIŃSKI** He currently works at the Warsaw University of Technology - Institute of Mechanical Engineering, where he is Deputy Director for Research.

For many years he deals problems with strength analysis of structures using the Finite Element Method. He has authored a lot of scientific publications, monographs and scholarly books, among which include, inter alia, university script, entitled: *"Strength calculation of machine elements using the Finite Element Method"*.
He is also the editor of the *Dynamics Problems* journal, and CEO of the Association of Automobile Recycling Forum.

PhD Eng. **Jerzy JACHIMOWICZ** The longstanding scienti-fic-research employee of Aviation Institute in Warsaw, and The Institute of Mechanical Engineering at Warsaw University of Technology.

Currently working in the Department of Mechanics and Applied Informatics, Military University of Technology in Warsaw.

Since the beginning of his career, he designed and strength analysis of aircraft structures. For many years, deals with the practical issues associated with the Finite Element Method in the analysis of shell constructions.

He has extensive experience, supported by long-standing practice at the Aviation Institute in Warsaw. He is a lot of scientific works and publications author.

PhD Eng. **Jarosław MAŃKOWSKI** - He is a scientific - educational employee at the Institute of Mechanical Engineering at The Warsaw University of Technology.

Since the beginning of his career dealing with issues related to the design, and especially the Finite Element Method in the analysis of structures, inter alia: analysis of shell structures, nonlinear problems such as buckling, contact, large deformations, elasto-plastic materials.

He is the author of over a dozen scientific works and publications.

MSc Eng. **Przemysław RUMIANEK** - PhD student at the Faculty of Automotive and Construction Machinery Engineering at The Warsaw University of Technology - Institute of Mechanical Engineering. His main interests are related to the strength of materials and structural strength analysis using the Finite Element Method

.

NON-DESTRUCTIVE DIAGNOSTICS OF CONCRETE CANTILEVER BEAM AND SLAB BY IMPACT ECHO METHOD

Magdalena RUCKA[1], Krzysztof WILDE[1,2]

[1] Department of Structural Mechanics and Bridge Structures, Faculty of Civil and Environmental Engineering,
Gdansk University of Technology
ul. Narutowicza 11/12, 80-233 Gdańsk, Poland, tel. 058 347 24 97, e-mail: mrucka@pg.gda.pl, wild@pg.gda.pl
[2] Kujawy and Pomorze University in Bydgoszcz, Faculty of Engineering,
ul. M. Piotrowskiego 12-14, 85-098 Bydgoszcz. Poland

Summary

This paper focuses on the application of the impact-echo method for the full scale tests conducted on concrete bridge cantilever beams and a floor slab. The method uses the phenomenon of propagating waves induced by an impact and registered by one or two accelerometers. Experimental studies proved the applicability of the impact-echo method for damage detection in the considered concrete structural elements.

Keywords: ultrasonic testing, impact echo, concrete structures.

NIENISZCZĄCA DIAGNOSTYKA KONSTRUKCJI BETONOWYCH BELEK WSPORNIKOWYCH
I PŁYTY STROPOWEJ ZA POMOCĄ METODY IMPACT ECHO

Streszczenie

Praca poświęcona jest zastosowaniu fal sprężystych na przykładzie w metody impact-echo. Metoda ta wykorzystuje zjawisko propagacji fal wzbudzanych przez mechaniczne uderzenie i ich pomiar za pomocą jednego lub dwóch akcelerometrów. Przeprowadzone testy eksperymentalne dla betonowych wsporników oraz stropu potwierdziły skuteczność metody w wykrywaniu uszkodzeń.

Słowa kluczowe: diagnostyka ultradźwiękowa, metoda impact-echo, konstrukcje betonowe.

1. INTRODUCTION

The so called destructive methods [1] are widely used for diagnostics of concrete structures. They require to extract a concrete sample from a structure and laboratory tests to evaluate material properties. They are considered to be very reliable. The non-destructive diagnostic methods, like ultrasonic techniques, can be performed on the structure under operation, providing quick estimation of concrete quality [2], [3], [4].

The impact-echo technique was developed in the 1980s. This method belongs to sonic/ultrasonic methods. The method is performed by impacting a structural element by a special hammer to generate elastic waves. Acceleration signals are recorded in the selected points on the element. Then the spectral analysis of the registered time-domain waveforms is carried out. The technique enables to determine the presence of the damage, its localization or it can be used for measurement of the element thickness.

In this paper, two applications of the impact-echo method are presented. In situ experimental studies were carried out on cantilever beams of a bridge and a concrete floor slab of the petrochemical machinery supporting structure.

2. PRINCIPLE OF IMPACT ECHO METHOD

Impact-echo is a method for non-destructive testing of concrete structures based on stress waves propagating through the structure and reflecting by potential flaws or structural boundaries. The stress wave is generated by a mechanical impact. Free concrete surface is stroke by a steel ball and the time signals (acceleration signals in this study) are registered at selected points.
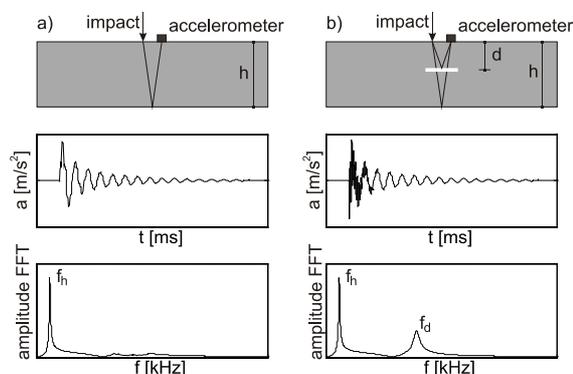

Fig. 1. Sketch showing principle of the impact echo method: a) intact structure; b) damaged structure

The principle of the impact-echo method is presented in Fig. 1. Due to the impact, a longitudinal wave (P-wave) and transverse wave (S-wave) propagate into the interior of the structure and a surface wave (R-wave) propagates along the surface. Damage detection procedure is based on the spectral analysis of registered time-domain waveforms. If an intact structure is considered (Fig. 1a), the waveform is dominated by sine wave of frequency f_h, called the thickness frequency:

$$f_h = \beta c_P / (2h), \qquad (1)$$

where c_P is a P-wave speed, h is a plate thickness and β is a correction coefficient equals 0.96 for plates [1]. Considering the plate with an internal flaw (Fig. 1b), the low-amplitude, high-frequency oscillations appears in the time signal. In this case, the spectrum exhibits two amplitude peaks of thickness frequency f_h and frequency f_d connected with the reflection from damage:

$$f_d = \beta c_P / (2d), \qquad (2)$$

where d is a defect depth.

3. DIAGNOSTICS ON CONCRETE CANTILEVER BEAMS OF THE BRIDGE

3.1. Research object and motivation

The object of the study is the road bridge (Fig. 2) in Nowy Dwór Gdański over the road no. 7 Gdańsk-Warsaw. During construction process the cantilevers of transverse beams were prestressed according to the plan (this state is referred here as 'state 0'). After prestressing process, cracks and cavities appeared on the cantilever surfaces (Fig. 3). Therefore repair operation was undertaken in the form of additional reinforcement and new gunite parts, but the cracks were not injected before gunite process. The aim of performed diagnostics was assessment of technical condition of cantilevers after repair (this state is referred here as 'state 1'). The impact-echo method was applied to non-destructive testing of the considered structure.

3.2. Field tests and results

The photo of data acquisition setup is presented in Fig. 4. The elastic waves were induced by a mechanical impactor in the form of a steel ball with a handle. The diameter of the impactor was 5 mm, what enables excitation of waves of frequency up to 58.2 kHz. The propagating signal was registered by two accelerometers (a_1 and a_2 in Fig. 4b) connected to the oscilloscope.

a)

b)
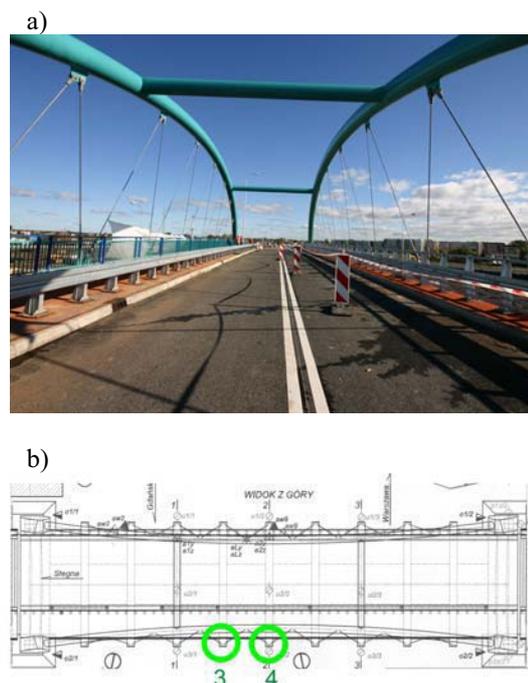
Fig. 2. The road bridge in Nowy Dwór Gdański: a) the photo ; b) top view

Fig. 3. Damaged cantilever no. 4 after prestresing

a)

b)
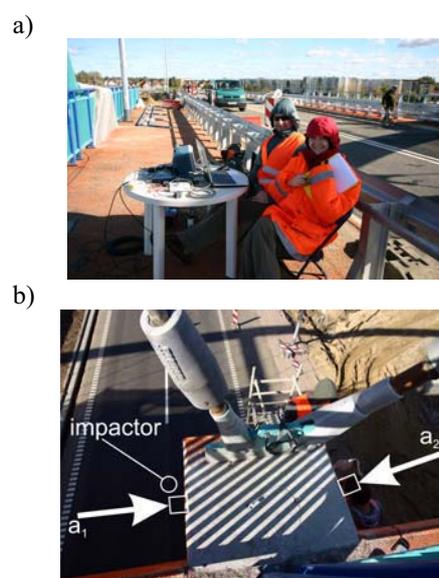
Fig. 4. Field tests: a) instrumentation setup; b) cantilever under examination

Measurements have been made on two cantilevers, no. 3 and no. 4, as indicated in Fig. 2b. Waves were generated on the left side of the cantilever, while the accelerations were measured on the left side as well as the right side (Fig. 4b). Measurements were performed at selected 59 points distributed on the cantilever surfaces. Location of measurement point is illustrated in Fig. 5. The distance of the wave travelling was constant for each point and equal to 0.986 m.
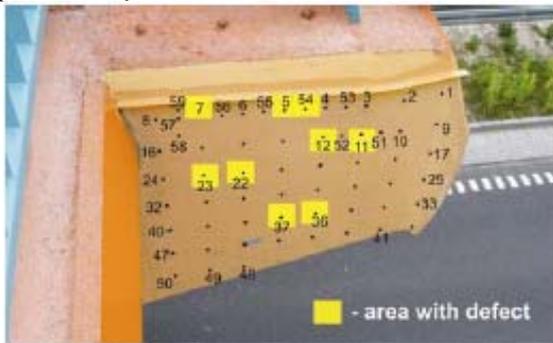

Fig. 5. Measurement points for cantilever no. 4 with marked damaged areas

To damage assessment of considered structure, velocities of propagating waves were applied. This can be done, because a wave in homogeneous material propagates faster and any flaws inside causes reduction in the wave speed. This approach was chosen, because the shape of the cantilever resembles a cube, therefore in spectrum domain reflections from the element boundaries could masks reflections form defects.

Fig. 6 shows signals registered in point no. 6 for the cantilever no. 3. The a_1 signal is the acceleration measured on the left side of the cantilever, while the a_2 is the acceleration measured on the right side, after passing through the structure. The time-of-flight t_h was 217.8 μs what enabled to calculate velocity of the P-wave as 4527.09 m/s. This procedure was repeated in all selected points.
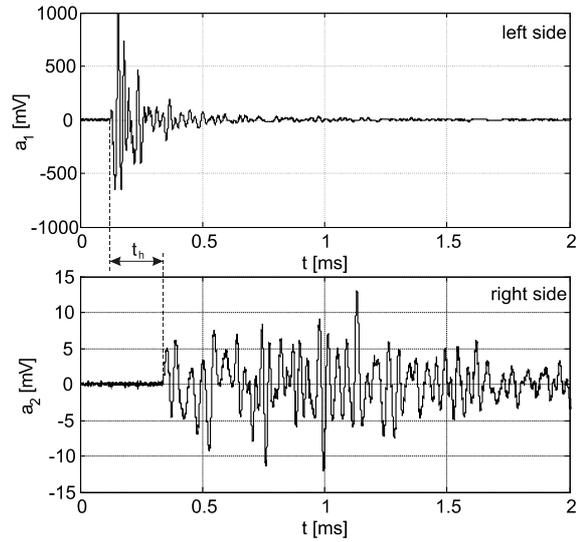

Fig. 6. Acceleration signals measured in point no. 6 for the cantilever no. 3
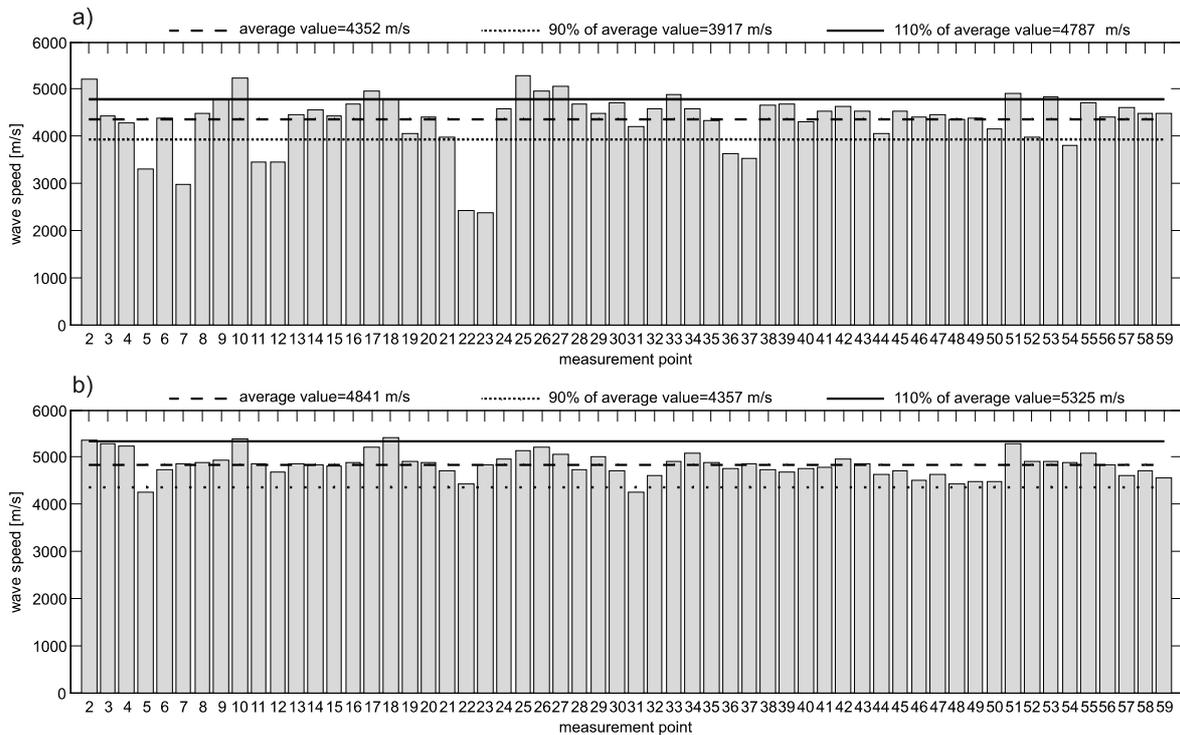
Fig. 7. Distribution of wave speeds in measurement points: a) cantilever at 'state 1'; b) cantilever after injection ('state 2')

As results, a map of distribution of wave speeds in 59 measurement points was plotted in Fig. 7a for the cantilever no. 4 at 'state 1'. The average value of P-wave speed in cantilever no. 4 was 4352 m/s. There are several points in which wave speeds are significantly smaller than average value. Points in which wave speed was smaller than 90% of average values were indicated as damaged areas (points 5, 7, 11, 12, 22, 23, 36, 37, 54). They are marked in Fig. 5 and they cover with localization of cracks observed at 'state 0' (c.f. Fig. 3).

In order to improve reliability and safety of the bridge, the injection of the epoxy resin was preformed. Both cantilevers were injected with about 5 liters of epoxy resin, and then ultrasonic testing was repeated. After injection the values of wave speeds considerably increased and the distribution of wave speeds became regular (Fig. 7b). In the cantilever no. 4 wave speeds hold in the range of 88% to 110% of the average values.

4. APPLICATION EXAMPLE ON CONCRETE FLOOR SLAB

4.1. Research object and motivation

The object of the research was the concrete floor stab (Fig. 8). Due to disturbances in concrete delivery during the slab casting, the homogeneity of the concrete became in question. The non-destructive test was performed with the use of the impact-echo method to determine presence of discontinuities.

4.2. Field tests and results

The geometry of the slab is shown in Fig. 8a. The number of measurement points was 105. They were distributed along the line of potential discontinuity, depicted as thick solid line in Fig. 8a. The hardware equipment was the same, as in the case of bridge measurements (c.f. Section 3.2). In this experiment, one-side measurement was performed, i.e. both mechanical impact and acceleration measurements were realized on the upper side of the slab only. The slab height, varied from 17 to 19 cm, was calculated in the measurement points based in known slab slopes.

Data analysis was carried out in frequency domain by interpretation of spectra obtained from time domain signals. Fig. 9 shows example of signal registered in point no. 98. In the frequency domain, one distinct peak dominates of frequency 9.77 kHz, what is equivalent of the thickness frequency f_h. By knowing frequency and the slab height P-wave speed can be determined from Eq. (1). Distribution of wave speeds were relatively regular with all measured point and the average value was 4100 m/s.
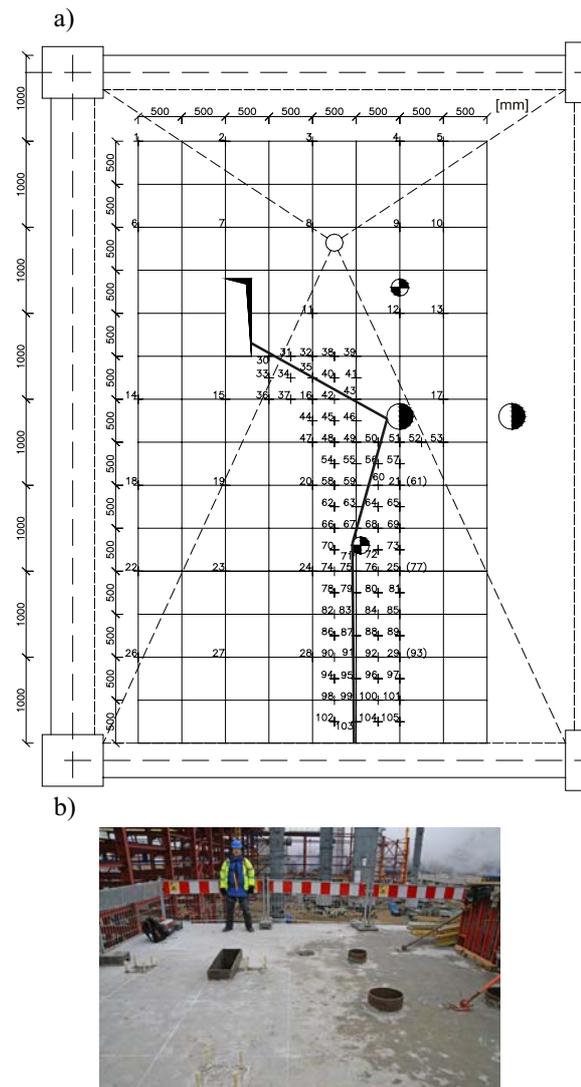

Fig. 8. Concrete floor slab: a) geometry and measurement points; b) the photo
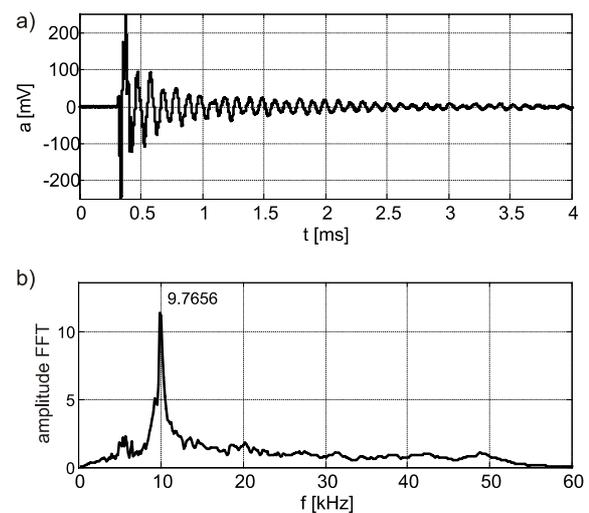
Fig. 9. Acceleration signals measured in point 98: a) in time domain; b) in frequency domain

a)

b)

c)

d)

e)

f)
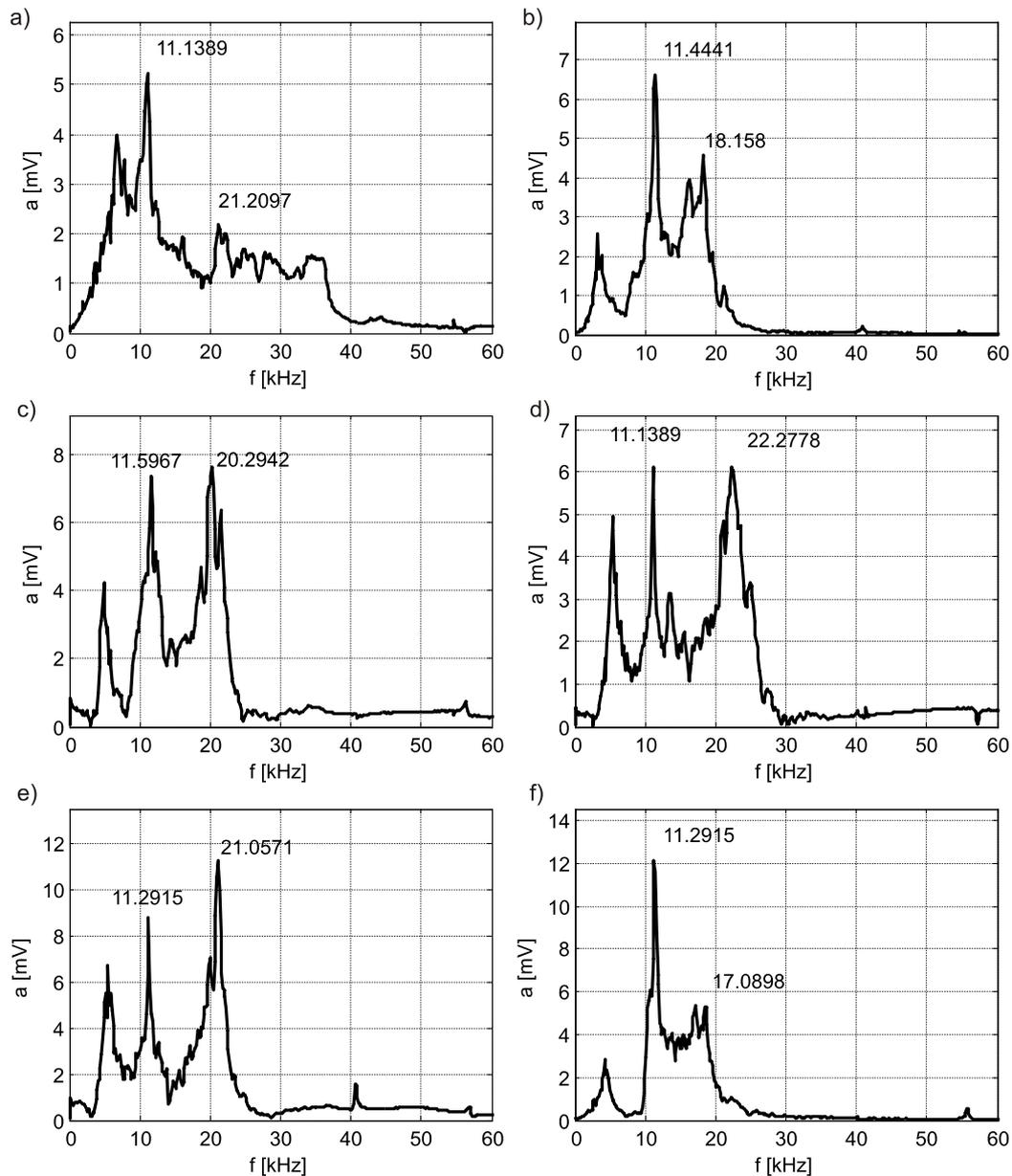
Fig. 10. Spectrums of signals measured at selected points: a) point 30; b) point 31; c) point 32; d) point 33; e) point 34; f) point 35

Spectral responses in majority points were similar to the spectrum shown in Fig. 9b. However, in points no. 30 to 35 additional peak appeared in the signal transformed to the frequency domain. Fig. 10 shows spectra for points 30 to 35. For all these points, additional peaks appeared of frequency 17.0898 kHz to 22.2779 kHz. The presence of higher frequencies indicates reflection of wave from internal defect at depth about 10 cm (from 8.96 cm to 11.84 cm). Points 30 to 35 were situated in the neighbourhood of the line of potential discontinuity.

5. CONCLUSIONS

In this paper, the impact-echo method was presented and applied in full scale tests on concrete bridge and floor slab structures. The method uses the phenomenon of propagating waves induced by a mechanical impact and spectral analysis of the recorded acceleration signals.

In this study, the impact-echo method was used in two different tests. In the first one, the measurements were made on both sides on the concrete cantilever element, and damage detection procedure was based on the analysis of P-wave speeds. This approach enabled identification of damage in the form of large internal flaws, in which substantial amount of epoxy resin was injected. The repeated ultrasonic tests on the injected structure revealed effectiveness of the applied repair method as well as the performance of the non-destructive testing.

In the second test, one-side measurements were conducted and for damage assessment of the slab floor structure. The data analysis was carried out in frequency domain by interpretation of spectra obtained from time domain signals. In the analyzed slab floor the defects were detected as additional peaks in spectral responses.

6. BIBLIOGRAPHY

[1] Sansalone M. J., Street W.B.: *Impact Echo. Nondestructive Evaluation of Concrete and Masory*. Bullbrier Press, Ithaca, N.Y., 1997.

[2] Kumar A., Raj B, Kalyanasundaram P., Jayakumar T., Thavasimuthu M.: *Structural integrity assessment of the containment structure of a pressuried heavy water nuclear reactor using impact echo technique*. NDT&E International, 2002, 35:213-220.

[3] Chaix J-F., Garnier V., Corneloup G.: *Concrete damage evaluation analysis by backscatter ultrasonic waves.* NDT&E International, 2003, 36:461-469.

[4] Hsiao C., Cheng C-C., Liou T., Juang Y.: Detecting flaws in concrete blocks using the impact-echo method. *NDT&E International,* 2008, 41:98-107.

ACKNOWLEDGEMENTS

Magdalena RUCKA, Ph.D. is an assistant professor at the Department of Structural Mechanics and Bridge Structures of Gdansk University of Technology. Her scientific interests are focused on dynamic of structures, wave propagation and development of new techniques for damage detection and structural health monitoring.

Krzysztof WILDE, Prof, Ph.D., D.Sc. is employed as associated professor at the Department of Structural Mechanics and Bridge Structures of Gdansk University of Technology. His research interests revolve around structural dynamics, damage diagnostics and structural health monitoring in civil engineering structures.

MOŻLIWOŚCI ZASTOSOWAŃ METODY TRIZ W DIAGNOSTYCE MASZYN

Artur SKORYNA, Czesław CEMPEL

Politechnika Poznańska, Instytut Mechaniki Stosowanej Politechniki Poznańskiej
a.skoryna@gmail.com

Streszczenie

W pracy zaprezentowano algorytmiczną, innowacyjną metodę TRIZ (*Teoria Rozwiązywania Innowacyjnych Zadań*) jako nowe możliwe podejście do diagnostyki. W diagnostyce nowych obiektów tradycyjne rozpoczynamy od analizy i syntezy przestrzeni uszkodzeń obiektu i możliwej przestrzeni obserwacji. Wydaje się, że metodologia TRIZ może być droga do szybkich i skutecznych metod rozwiązywania złożonych problemów diagnostycznych. Generalnie metoda ta stosowana jest w celu uniknięcia długiego procesu metody prób i błędów, jak również ograniczenia ilości prób do minimum. TRIZ jest holistycznym podejściem do problemu. Prowadzi do rozwiązań skutecznych i tanich, dzięki czemu oszczędza się czas, pieniądze i ogranicza ryzyko. Podejście to może być wykorzystane do określenia w sposób przeciwny niż w przypadku tradycyjnych metod. Obecny obszar zastosowań metody rozciąga się od zagadnień typowo inżynierskich każdej dziedziny techniki aż do inżynierii oprogramowania, finansowej i kształcenia wszystkich szczebli. Na początku definiowane jest rozwiązanie idealne, które jest wyjściem do dalszych rozważań. A potem jest czas na cały bagaż algorytmicznych narzędzi metody; 40 zasad, 76 innowacyjnych rozwiązań i 39 typowych inżynierskich parametrów opisu problemu, łącznie z macierzą sprzeczności (*contradiction matrix*).

Słowa kluczowe: diagnostyka, innowacje, TRIZ.

POSSIBILITY OF APPLICATION OF TRIZ METHODS IN MACHINE CONDITION MONITORING

Summary

The paper was presented algorithmic intensive method TRIZ (Theory of Innovative Solution Task) as a possible new approach to diagnosis. In diagnosis of new plants, the traditional start from the analysis and synthesis of space and the possible damage to the object space observation. It seems that the TRIZ methodology can be the path to rapid and effective methods for solving complex diagnostic problems. Generally, this method is used to avoid the long process of trial and error, as well as reduce the amount of testing to a minimum. TRIZ is a holistic approach to the problem. It leads to effective and affordable solutions so that saves time, money and reduces risk. This approach can be used to identify the potential causes of damage in the opposite way than traditional methods. At the beginning of the ideal solution is defined, which is the output for further deliberations. And then it is time for all baggage algorithmic tools, 40 rules, 76 and 39 innovative solutions to engineering problems, including a matrix of contradictions.

Keywords: diagnostics, innovations, TRIZ.

1. WSTĘP

Istnieje powszechne przekonanie, że **kreatywnym** trzeba się po prostu urodzić, jest to, bowiem cecha charakteru, fantazji i temperamentu. Jednakże współczesny stan wiedzy i techniki nauczania stawiają sprawę inaczej, kreatywności można się nauczyć, co najwyżej niektórzy mają do tego lepsze predyspozycje [11]. Ponad 70 lat intensywnego rozwoju inwentyki, nauki o poszukiwaniu twórczych rozwiązań, w Polsce niestety mało znanej, doprowadziły do wypracowania metod działania, w ogromnym stopniu podnoszących efektywność pracy twórczej i koncepcyjnej, pozwalającej wprowadzić innowacyjne rozwiązania lub nawet wynalazki jednocześnie do różnych dziedzin techniki. Przeciętny inżynier stając przed problemem, najczęściej wpada w pułapkę metody **prób i błędów**. Zadaje sobie pytanie: może by tak? A może nie tak, tylko tak? itd. itp. Jest to niestety metoda najpowszechniej stosowana, wykorzystywana i nieefektywna. Inwentyka rozumiana jako metodyka poszukiwania twórczych rozwiązań rozpatruje wielopłaszczyznowo potencjalne podejście do pozyskania najefektywniejszych metod. Przykładem może być wprowadzanie umysłu w tzw. **stan α**, w którym sprawność twórcza jest najwyższa. Człowiek Zachodu z dominującą lewą półkulą mózgowa ma skłonność do metod uporządkowanych, zmatematyzowanych, gdzie w sposób ustalony dąży do ustalonego celu. Tak

działają niektóre z metod analityczno-logicznych inwentyki, przykładowo: skrzynka morfologiczna, metoda delficka czy mapy myśli (*patrz np.* [12]). Dlaczego zapoznanie się z metodami uczącymi innowacyjnymi jest potrzebne? Otóż pozwalają zdobyć umiejętność twórczego, innowacyjnego rozwiązywania problemów technicznych i menedżerskich. Zmieniają masz sposób myślenia i patrzenia na świat, poszerzają horyzonty myślowe. Żyjąc w dobie globalizacji gospodarki światowej innowacyjne myślenie jest pożądane w każdej dziedzinie, dlatego właśnie warto zainteresować się metodą TRIZ. Patrząc na obecny szeroki obszar zastosowań TRIZ (*patrz dodatek*) nie zauważamy tam ani diagnostyki ani wibroakustyki maszyn, wydaje się więc że czas już wypełnić tą lukę uzyskując nowe narzędzie i nowe spojrzenie na problematykę badań i zastosowań w tych dziedzinach.

2. TRIZ JAKO METODA INNOWACYJNYCH ROZWIĄZAŃ

TRIZ, czyli Teoria Rozwiązywania Innowacyjnych Zagadnień (*w oryg. Теория Решения Изобретательских Задач*) - 40-letnie dzieło życia i pracy Henryka Sauliowicza Altszuller'a. **Altszuller** (pisownia spolszczona, w angielskim i niemieckim używa się pisowni Altshuller) w pewnym okresie życia był pracownikiem inspekcji ds. wynalazczości w dowództwie floty kaspijskiej. Praca jego polegała na przyjmowaniu i weryfikowaniu wniosków wynalazczych przed skierowaniem ich do Biura Patentowego. Mając w na swym koncie patenty i analizując tysiące opisów patentowych – Altszuller wpadł na pomysł, by sformułować ogólne prawa tworzenia wynalazków (*patrz rys. 1*). Po wielu latach pracy, odbyciu 4 letniej kary łagru i sformułowaniu zespołu przedstawił zręby algorytmicznej metody poszukiwania innowacji [13], później nazwanej TRIZ, którą można zdefiniować jako: zespół metod i narzędzi algorytmicznego pokonywania trudności w kreowaniu zagadnień wynalazczych.

Pierwszym spostrzeżeniem był fakt istnienia logiki w rozwoju systemów technicznych. Altszuller wyprowadził z tego wniosek, że skoro systemy techniczne rozwijają się według określonych zasad, to znając te zasady, można przewidywać ich dalszy rozwój i wykorzystać do rozwiązywania nowych problemów. Jednym z głównych ustaleń Altszullera było spostrzeżenie, że wynalazek niemal zawsze polega na **usunięciu sprzeczności** (*administratywnych, fizycznych, technicznych*) tkwiących w problemie, pojawiającej się na drodze do ulepszenia jakiegokolwiek produktu, technologii czy metody zarządzania. Był to ogromny materiał prowokujący do analizy i próby znalezienia odpowiedzi na pytania:

- jak powstaje wynalazek?
- jakie są prawa rozwoju systemów technicznych?
- czy można się nauczyć wynalazczości?

Całokształt spostrzeżeń i zależności doprowadziły Altszullera do opracowania metody TRIZ. W wielkim skrócie istota metody polega na zdefiniowaniu **IWK** (*idealny wynik końcowy*) i rozwiązywaniu sprzeczności fizycznych, technicznych i organizacyjnych, które znajdujemy w każdym problemie wynalazczym, czy organizacyjnym. Pomagają w tym 40 zasad usuwania sprzeczności, 76 sposobów optymalizacji rozwiązania, a także 7 zasobów transformacji do **IWK.** Metoda znalazła szerokie zastosowania także w rozwiązywaniu szeroko rozumianych problemów inżynierskich, naukowych i organizacyjnych. TRIZ jest połączeniem metod o charakterze intuicyjnym oraz algorytmicznych wywodzących się z badań operacyjnych. Jest nie tylko metodą i narzędziem, ale także filozofią (*rys.2*). Całą teoria zaczęła się rozwijać od roku 1946, przez wszystkie kolejne lata jest w ciągłym udoskonalaniu i przystosowywana do najróżniejszych dziedzin naukowych i społecznych. Na szczególną uwagę zasługuje przykładowo Japonia, która organizuje już 6-tą konferencję na ten temat.
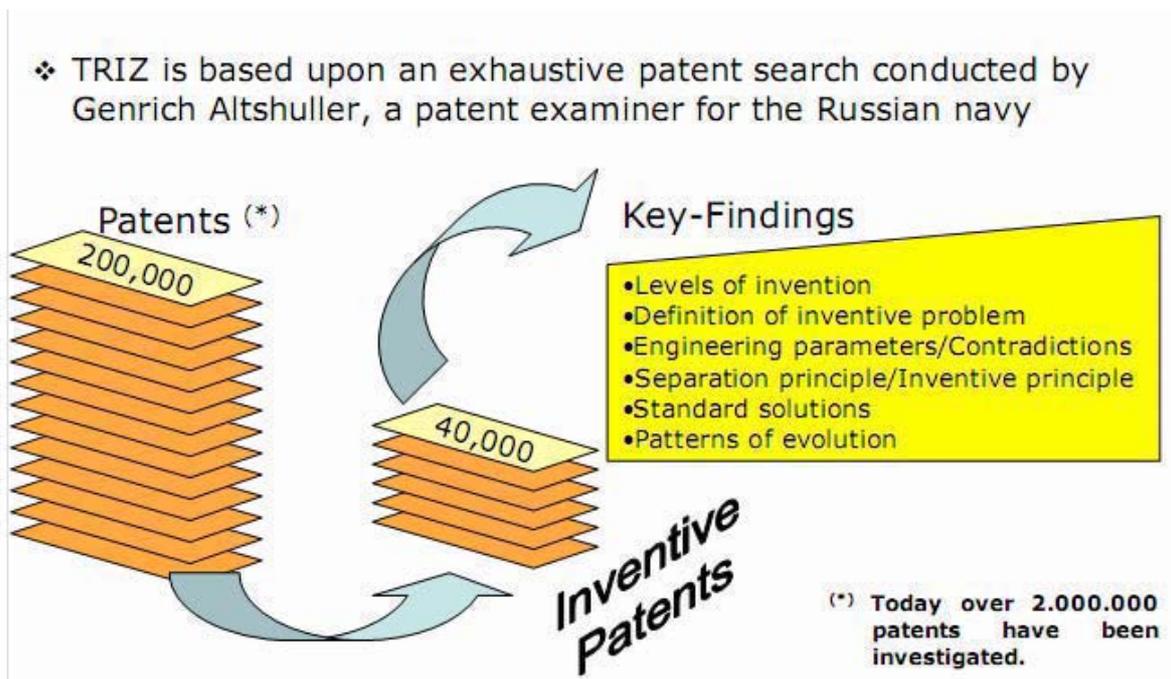
Rys. 1. Droga pozyskania wiedzy Altszullera [1]
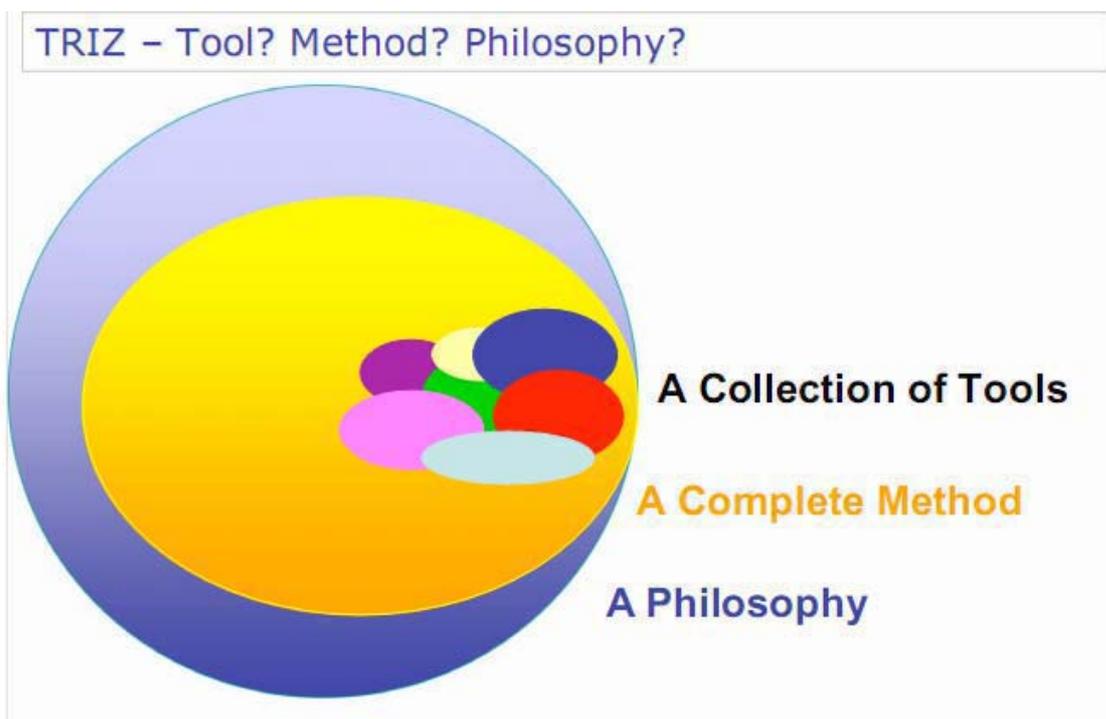
Rys. 2. Zakres metodologii TRIZ [1]

Oprócz typowo technicznych zastosowań, TRIZ trafił do innych dziedzin. Stało się tak za sprawą drobiazgowej analizy i dokładnego trzymania się zaleceń algorytmu. Stąd powstały odmiany: TRIZ-Menedżer, TRIZ-Science w zastosowaniach naukowych: w fizyce, chemii, biologii itd., a także TRIZ-Pedagogika [9] zajmujący się kształtowaniem analitycznego sposobu myślenia dzieci i młodzieży na wszystkich poziomach kształcenia, począwszy od przedszkoli. Pojawia się również TRIZ-Design do zadań kształtowania form przemysłowych, wzornictwa użytkowego.

3. GŁÓWNE POSTULATY TRIZ

Najważniejsze elementy algorytmicznej i zbieżnej metody TRIZ to:

- Zdefiniowanie idealnego wyniku końcowego *(IWK)*, niezależnego od sposobu realizacji. Formułowany za pomocą specjalnej metodyki pozwalającej zbudować model rozwiązania wolny od wpływu tzw. **wektora inercji**. Rozwiązania należy szukać w zupełnie innym kierunku niż wąskie zagadnienia problemu *(patrz rys. 2)*.
- Zdefiniowanie pięciu poziomów złożoności rozwiązań innowacyjnych, od zwykłych ulepszeń *(45%)* aż po odkrycia naukowe *(1%)*.
- Sformułowanie praw innowacyjności, np. ewolucja innowacji zgodna z krzywą logistyczną *(S)* stwarza możliwość oceny potencji i prognozy rozwoju *(lub braku)* danej innowacji [8].
- **Zasady** *(chwyty)* **wynalazcze** - Altszuller doszedł do wniosku po swojej długoletniej pracy, że niemal wszystkie wynalazki powstały metodą usuwania **sprzeczności technicznych** przy pomocy tylko ok. 40 zasad elementarnych *(chwytów)* wynalazczych. Tabela tych chwytów i metoda ich wykorzystywania to ARIZ-85.
- Standardowe rozwiązywania macierzy sprzeczności w liczbie 76 standardów daje innowatorowi silne narzędzia twórczego rozwiązania praktycznych produkcyjnych zadań. Służą do usuwania technicznych i fizycznych sprzeczności.
- Analiza substancja-pole z angielskiego **Su-Field** lub spolszczone **wepole**, dające możliwość ostatecznego rozwiązania wektora inercji. Analizę wepolową rozwiązuje się za pomocą specjalnych reguł używając symboli i znaków.

Pozwalają one zapisać to, co jest dane *(tj. model zadania)* i to, co otrzymano w rezultacie rozwiązania problemu.

- Zdefiniowanie zasobów *(substancja, pole, przestrzeń, czas, funkcja, małe ludziki)*, użycie których pozwala zbliżyć się do **zdefiniowanego** rozwiązania idealnego.
- Teoria rozwoju osobowości twórczej – TROT, program prowadzący do rozbudzenia potencjalnych możliwości umysłu człowieka w celu rozwoju twórczości, kreatywności [5].

Ostateczna wersja zalecanego sposobu postępowania to **ARIZ-85** – Algorytm Rozwiązywania Innowacyjnych Zadań. Zgodnie z definicją ARIZ-85 to bezpośrednie narzędzie prowadzące do celu, bez możliwości zbaczania na niepotrzebną ścieżkę metody prób i błędów.

Innowacyjne rozwiązanie ma wykazywać wyższy stopień idealności, niż rozwiązanie aktualne; stopień idealności określony jest formułą [6]:

I *(ideał)*= Σ **Korzyści/(Σ Kosztów+ Σ Strat)**   (1).

Natomiast metoda TRIZ redukuje znacznie stopień trudności **D** *(Difficulty)* zdefiniowany jako iloraz liczby możliwych wariantów *(V)*, do liczby kroków, które wiodą do właściwego rozwiązania *(S)*.

$$D = V/S \qquad (2).$$

Przy metodzie prób i błędów liczba wariantów niezbędnych do przeanalizowania V rośnie niewspółmiernie, a teoretyczne najmniejszy stopień trudności to D=1, z ta sama liczba wariantów i kroków, *(najlepiej 1)*.

a)   b)
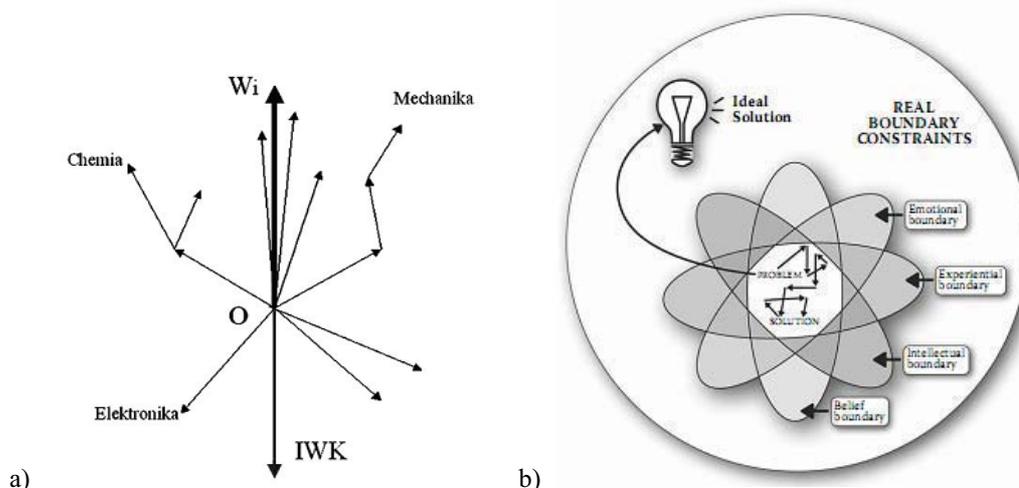
Rys. 3a, 3b. Ilustracja działania wektora inercji –jako rozbieżne poszukiwanie nowego rozwiązania w znanych obszarach techniki i efekt ograniczeń psychologicznych i poznawczych innowatora [3][4]

4. KORZYŚCI Z TRIZ

Podstawowe korzyści z zastosowania TRIZ to przede wszystkim:
- rozwiązywanie powtarzalnych problemów w oparciu o algorytm;
- redukcja błędnych rozwiązań (*oszczędność czasu, pieniędzy, minimalizacja ryzyka*);
- **więcej** innowacyjnych rozwiązań;
- pozwala znaleźć najlepsze rozwiązanie.

Podstawą metody TRIZ jest zastosowanie **algorytmu**. Dzięki niemu badania, czy analizy nie są rozbieżne, chaotyczne tak jak np. w burzy mózgów, ale nabierają uporządkowanego charakteru prowadzącego bezpośrednio do ustalonego celu *(IWK)*. Ustalone działanie prowadzi znalezienia większej ilości innowacji oraz do zmniejszenia ilości błędnych rozwiązań, a to z kolei oszczędza czas i pieniądze.

Firmy stosujące TRIZ to m.in. BMW, Boeing, LG, NASA, Hitachi, Intel, jak widać są to przodujące firmy sfery kosmicznej i gospodarczej [4 s28]. Warto dodać, że omawiana metoda jest nie tylko wykorzystywana w firmach, ale w różnych dziedzinach inżynierii m.in. w służbie zdrowia, architekturze, projektowaniu ekologicznym i wielu innych[10].

Dla potwierdzenia wartości opisanej metody został przeprowadzony test wśród dwóch grup *(doświadczonych inżynierów)*. Został im przedstawiony ten sam problem, ale jedna grupa rozwiązywała go za pomocą TRIZ. Poniższy wykres przestawia wyniki tego eksperymentu. Nie ma wątpliwości, że TRIZ nie przypadkowo pomógł rozwiązać zagadnienie inżynierskie.

5. TRIZ W PRAKTYCE

Altszuller założył tezę, że konstruowanie urządzeń zmierza do określonego ideału, według pewnej linii rozwoju. Wizja idealnej maszyny w początkowej fazie wynalazczości tworzy właściwy kierunek poszukiwań, zawęża kąt poszukiwań oraz wyklucza rozwiązania chaotyczne i przypadkowe. Planowe poszukiwanie ukierunkowuje proces myślenia i czyni go bardziej efektywnym, powodując zwiększenie prawdopodobieństwa znalezienia rozwiązania, którego efektem będzie wynalazek. Idealny obieg techniczny nazywany jest w tej teorii **Idealnym Wynikiem Końcowym (*IWK*)** [3 s37], lub **IFR** z angielskiego. Jego najważniejsze zadania to:
- wskazywać kierunek poszukiwań,
- eliminować niedostatki rozwiązania aktualnego,
- zachowywać zalety rozwiązania aktualnego,
- nie powiększać komplikacji w porównaniu z rozwiązaniem aktualnym,
- nie wprowadzać nowych wad.
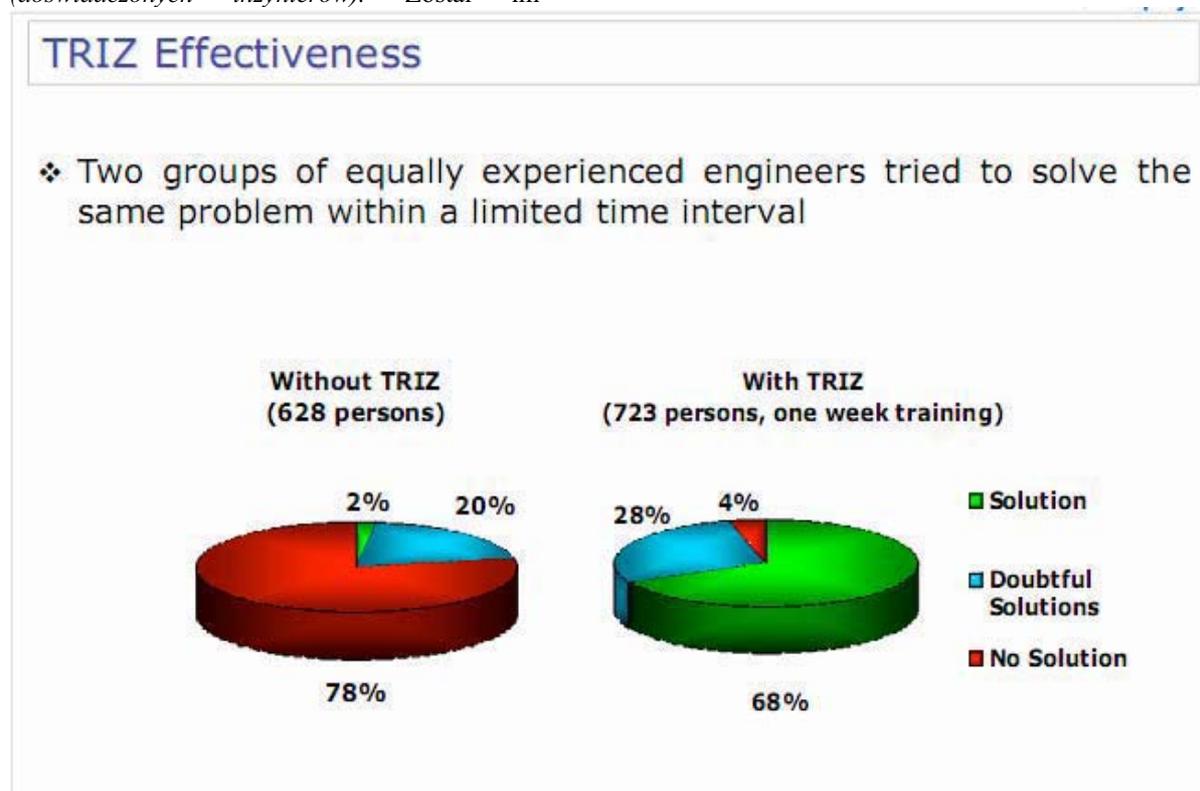
Rys. 4. Efektywność szkolenia w TRIZ [1]

-

Podejście takie poszerza horyzonty myślowe, ponieważ pobudza wyobraźnię, a nie tylko przetwarza zdobytą wiedzę. W celu sprecyzowania reguł formułowania IWK należy kierować się następującymi regułami:

Reguła 1. Nie wolno zawczasu myśleć o tym, czy możliwe lub niemożliwe jest uzyskanie wyniku idealnego.

Reguła 2. Nie wolno zawczasu myśleć o tym, jaką drogą można osiągnąć wynik idealny.

Reguła 3. Sformułowanie IWK nie powinno być wyrażone językiem fachowym; należy użyć słów potocznych, prostych, ogólnie znanych.

Reguła 4. IWK należy formułować posługując się minimalną, konieczną ilością słów [7 s26].

Po zastanowieniu się można sformułować **IWK** dla potrzeb diagnostyki maszyn; **maszyna mówi sama kiedy i co należy wymienić.** A będzie to możliwe jeśli subsystem diagnostyczny będzie zintegrowany z maszyną i będzie miał odpowiednie oprogramowanie.

Wszystkie zadania wynalazcze Altszuller poklasyfikował na 5 poziomów innowacyjności:

1. Poziom: Obiekt znany, oczywisty, wykorzystuje konwencjonalne rozwiązanie *(trywialne, niewynalazcze).*
2. Poziom: Obiekt znany, nieznacznie poprawiony *(zwykła inwencja).*
3. Poziom: Znany obiekt zostaje zmieniony w środku paradygmatu.
4. Poziom: Znany obiekt zostaje zmieniony na zewnątrz paradygmatu.
5. Poziom: Odkrycie, powstaje nowa gałąź nauki [1].

Kolejnym etapem TRIZ jest dojście do tzw. **sprzeczności technologicznej** [2]. Wcześniejszy tok rozumowania, analizowania i abstrahowanie od konkretnych warunków powinny doprowadzić do znalezienia **sprzeczności**, która jest właściwym sformułowaniem problemu. Znalezienie sprzeczności pozwala zastosować kolejne narzędzia TRIZ, przy pomocy, których opracowuje się propozycje rozwiązań. Obiekty techniczne można charakteryzować przy pomocy kilku podstawowych wzajemnie zależnych od siebie parametrów, które określają stopień ich doskonałości: wielkość, moc, niezawodność i inne.

Zmiana na korzyść jednego z parametrów często może prowadzić do pogorszenia drugiego, np. zwiększenie mocy i zmniejszenie gabarytów. Udoskonalenie pewnych właściwości obiektu wchodzi w konflikt z inną jej właściwością. W trakcie konstruowania należy poszukiwać optymalnego połączenia tych cech. Twórczość wynalazcza wymaga znalezienia takiego rozwiązania, w którym zyski są maksymalne, a straty parametrów minimalne. Z tej perspektywy, wynalazek można określić jako: wyeliminowanie sprzeczności technicznej. Po znalezieniu w zadaniu sprzeczności, stosujemy instrument wynalazcy tzw. 40 zasad rozwiązywania problemów technicznych zwanych przez Altshullera zasadami lub chwytami. Zasady te, wykorzystywane w **ARIZ** *(Algorytm Rozwiązywania Innowacyjnych Zadań)*, to operatory przekształcania wyjściowego systemu technicznego lub procesu technologicznego [2]. Poszczególne zasady dzielą się na powiązane instrukcje, w którym każda następna rozwija poprzednią.

Wykaz typowych zasad (chwytów) usuwania sprzeczności technicznych:

1. Segmentacja; 2. Wydzielenie; 3. Lokalna jakość; 4. Asymetria; 5. Łączenie; 6. Uniwersalność; 7. "Matrioszka"; 8. Przeciwciężar; 9. Przeciwdziałanie zapobiegawcze; 10. Zapobieganie; 11. Wcześniejsze wytłumienie; 12. Ekwipotencjalność; 13. Wykonanie w "na odwrót"; 14. Sferoidalność; 15. Dynamika; 16. Częściowe lub nadmierne działanie; 17. Inny wymiar; 18. Wibracje/drgania; 19. Działanie impulsowe; 20. Ciągłość; 21. Przeskok; 22. Straty na korzyści; 23. Sprzężenie zwrotne; 24.Pośrednik; 25. Samoobsługa; 26. Kopiowanie; 27. Tania nietrwałość; 28. Zastąpienie mechaniki; 29.Pneumatyka i Hydraulika; 30. Elastyczne powłoki i błony; 31. Materiały porowate; 32. Zmiana kolorów; 33. Homogeniczność; 34. Odrzucenie i regeneracja; 35. Zmiana parametrów; 36. Fazy przejściowe; 37. Rozszerzanie cieplne; 38. Utleniacze; 39. Neutralne środowisko; 40. Materiały kompozytowe[2].

Poniżej przedstawiono zestawienie parametrów systemu, inaczej problemów inżynierskich, które przy dalszym ich rozwoju na tej samej drodze ulegną pogorszeniu/ polepszeniu i stanowią podstawę do budowy macierzy sprzeczności. Do pewnych celów można zdefiniować dalsze problemy jak np.: ***40. Strata zakłóceń*** *natury (elektro, magneto, mechano, akusto)*, gdzie np. można rozpatrywać innowacyjne zagadnienia drgań i hałasu.

Tab. 1. Wykaz parametrów technicznych opisu problemu [3], jako podstawa macierzy sprzeczności

01. Ciężar obiektu ruchomego	21. Moc
02. Ciężar obiektu nieruchomego	22. Straty energii
03. Długość obiektu ruchomego	23. Straty substancji
04. Długość obiektu nieruchomego	24. Straty informacji
05. Powierzchnia obiektu ruchomego	25. Straty czasu
06. Powierzchnia obiektu nieruchomego	26. Ilość substancji
07. Objętość obiektu ruchomego	27. Niezawodność
08. Objętość obiektu nieruchomego	28. Dokładność pomiaru
09. Prędkość	29. Dokładność wytwarzania
10. Siła	30. Szkodliwe czynniki, działające na obiekt
11. Napięcie, ciśnienie	31. Szkodliwe czynniki samego obiektu
12. Kształt	32. Łatwość wytwarzania
13. Stabilność struktury obiektu	33. Łatwość eksploatacji
14. Wytrzymałość	34. Łatwość naprawy
15. Czas działania ruchomego obiektu	35. Łatwość adaptacji, uniwersalność
16. Czas działania nieruchomego obiektu	36. Złożoność ustroju
17. Temperatura	37. Złożoność kontroli i pomiaru
18. Jasność (promieniowanie)	38. Stopień automatyzacji
19. Nakłady energii na ruch obiektu	39. Wydajność
20. Nakłady energii przy nieruchomym obiekcie	

W Algorytmie Rozwiązywania Problemów Wynalazczych *(ARIZ)* wykorzystuje się drogę abstrahowania rozwiązywanego problemu do pewnego problemu uogólnionego (*znanego z badań patentowych*), a następnie eliminację sprzeczności na podstawie matryc analogii. (*rys. 3*). Tysiące rozwiązanych zagadnie pokazują, że ARIZ jest elastycznym algorytmem do opracowywania zadania wynalazczego lub innowacyjnego.
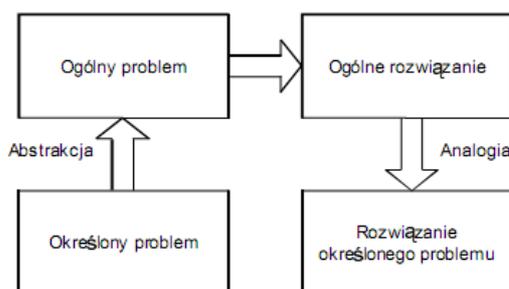
Rys. 3. Ogólny schemat działania algorytmu ARIZ [3].

6. PODSUMOWANIE

TRIZ jest metodą algorytmiczną poszukiwania rozwiązań innowacyjnych, do tego bardzo rozbudowaną. Dzięki wnikliwej pracy Altszullera możemy korzystać z syntezy wiedzy zdobytej przez kilkadziesiąt lat. Metoda TRIZ jest całkowicie nowym podejściem do rozwiązywania problemów. Pozwala spojrzeć na zagadnienie z punktu widzenia ostatecznego celu lub etapu poszukiwań rozwiązania. W nowoczesnej diagnostyce maszyn wg. TRIZ to maszyna nam „powie" kiedy należy zużyte elementy naprawić lub wymienić. Możliwość rozwiązywania problemów w oparciu o stały algorytm umożliwia błyskawiczne rozwiązywanie powtarzalnych problemów, a jej uniwersalność i połączenie wiedzy z różnych dziedzin gwarantuje jej skuteczność, co w konsekwencji prognozuje w niedalekiej przyszłości szersze jej zastosowanie. Całokształt interdyscyplinarnego podejścia daje wyższość na innymi metodami.

7. LITERATURA

[1] Rossi B., Muzi V., *An introduction to TRIZ*, Ciaotech-WUT, Internet, http://www.ciaotech.it, 2007, p46.

[2] Jadkowski K., Andrzejewski G., *TRIZ– metoda interdyscyplinarna*, II Konferencja Naukowa KNWS, Złotniki Lubańskie, czerwiec 2005.

[3] Boratyński J. , Majchrzak Z., *TRIZ Teoria Rozwiązywania Innowacyjnych Zadań*. Promado s.c., Kielce 2009, s 261.

[4] Silverstein D. DeCarlo N., Slocum M., *Insourcing Innovation How to Achieve Competitive Excellence Using TRIZ*, Auerbach Publ. Taylor & Francis Group, New York 2007, s 280.

[5] TQMsoft *Rozwiązania dla jakości i produktywności, Inwentyka? TRIZ? Co to takiego?*

[6] Internet: http://www.tqmsoft.net.pl/node/216, luty 2010.

[7] Domb E., Dettmer H. W., *Breakthrough innovation in conflict resolution*, The TRIZ Journal, maj *1999*, www.triz-journal.com.

[8] Boratyński J., *Co to jest TRIZ ?* – Internet, www.triz-innowacje.pl, s 252.

[9] Orloff M. A., *Inventive Thinking through TRIZ, a practical guide*, II.ed., Springer Verlag, Berlin, 2006,s 351.

[10] TRIZ-Pedagogika, Internet, http://triz-pedagogika.pl, 2010.

[11] TRIZ,Internet:http://www.triz-journal.com/404.asp?404;http://www.triz-journal.com:80/archives/contradiction_matrix/, czerwiec 2010.

[12] Alder H., *Inteligencja Kreatywna*, Amber, Warszawa 2003, s223.

[13] Cempel C., *Teoria i Inżynieria Systemów*, wyd.2, ITE Radom 2008, s291.

[14] Altshuller H., *Algorytm Wynalazku*, Wiedza Powszechna, Warszawa 1975, s280.

DODATEK
D1. Dziedzinowe warianty zastosowania metodologii TRIZ[1]

(*idealny wynik końcowy, macierz sprzeczności, 40 zasad wynalazczych, 7 zasad ewolucji systemów,…*)

1. Technical Examples: The TRIZ Journal[2], July 1997
2. Business Examples: The TRIZ Journal, September 1999
3. Social Examples: The TRIZ Journal, June 2001
4. Architecture Examples: The TRIZ Journal, July 2001
5. Food Technology Examples: The TRIZ Journal, October 2001
6. Software Development Examples: The TRIZ Journal, September and November 2001
7. Microelectronics Examples: The TRIZ Journal, August 2002
8. Quality Management Examples: The TRIZ Journal, March 2003
9. Public Health (*fighting SARS*): The TRIZ Journal, June 2003
10. Applying the TRIZ Methodology to Machine Maintenance, TRIZ Journal, August 2003.
11. Chemistry Examples: The TRIZ Journal, July 2003
12. Ecological Design Examples: The TRIZ Journal, August 2003
13. Service Examples: The TRIZ Journal, December 2003
14. Education, The TRIZ Journal, April 2004
15. Finance, The TRIZ Journal, October 2004
16. TRIZ for Software Engineers, Mann D. L., IFR Press October 2004
17. Marketing, Sales and Advertising, The TRIZ Journal, April 2005
18. Examples for Chemical Engineering, The TRIZ Journal, June 2005
19. Examples in Construction Engineering. The TRIZ Journal, March 2005
20. Examples in Customer Satisfaction enhancement, The TRIZ Journal, January 2007
21. Examples in Latin Phrases, The TRIZ Journal, January 2008
22. Business Process Reengineering, The TRIZ Journal, October 2009
23. Examples in Aviation Safety, The TRIZ Journal November 2009
24. Human Factors & Ergonomics, The TRIZ Journal February 2010
25. Condition Monitoring of Machines, *no reference*.
26. Noise Control and Vibroacoustic of Machines, *no reference*.

Artur **SKORYNA** - Doktorant w Instytucie Mechaniki Stosowanej PP

D2. Struktura teorii rozwiązywania innowacyjnych zadań

Mapka myśli TRIZ
wersja 06, cc 25.06.10 r.
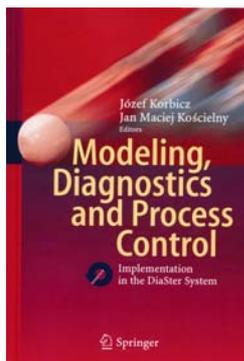
**Korbicz J.,
Kościelny J. M. (Red.)**
Modeling, Diagnostics
and Process Control:
Implementation in the
DiaSter System

Wyd. Springer

**Korbicz J.,
Kościelny J. M. (Red.)**
Modelowanie, diagnostyka
 i sterowanie nadrzędne
procesami Implementacja
w systemie DiaSter

WNT Warszawa

Modern control systems are complex in the sense of implementing numerous functions, such as process variable processing, digital control, process monitoring and alarm indication, graphic visualization of process running, or data exchange with other systems or databases.

This book conveys a description of the developed *DiaSter* system as well as characteristics of advanced original methods of modeling, knowledge discovery, simulator construction, process diagnosis, as well as predictive and supervision control applied in the system. The system allows early recognition of abnormal states of industrial processes along with faults or malfunctions of actuators as well as technological and measuring units. The universality of solutions implemented in *DiaSter* facilitates its broad application, for example, in the power, chemical, pharmaceutical, metallurgical and food industries. The system is a world-scale unique solution, and due to its open architecture it can be connected practically with any other control systems.

The monograph presents theoretical and practical results of research into fault diagnosis and control conducted over many years within the cooperation of Polish research teams from the Warsaw University of Technology, the University of Zielona Góra, the Silesian University of Technology in Gliwice, and the Technical University of Rzeszów.

The book will be of great interest to researchers and advanced students in automatic control, technical diagnostics and computer engineering, and to engineers tasked with the development of advanced control systems of complex industrial processes.

W książce przedstawiono zaawansowane metody i algorytmy modelowania procesów dynamicznych, odkrywania wiedzy w bazach danych, budowy symulatorów, diagnostyki procesów i systemów oraz nadrzędnego sterowania, samostrojenia i adaptacji nastaw pętli regulacyjnych.

Opisane metody zostały zaimpletowane w oryginalnym w skali światowej systemie automatyki i diagnostyki- DiaSter. Uniwersalność przyjętych rozwiązań w systemie daje możliwość jego szerokiego zastosowania między innymi w przemyśle energetycznym, chemicznym, farmaceutycznym czy spożywczym. Ze względu na otwartą architekturę możliwe jest połączenie systemy DiaSter praktycznie z dowolnymi systemami automatyki.

Książka skierowana jest do studentów i doktorantów uczelni technicznych, zespołów badawczych zajmujących się kompleksową automatyzacją złożonych procesów przemysłowych. Ze względu na interdyscyplinarny charakter tematyki może zainteresować i zainspirować zarówno automatyków i informatyków, jak i projektantów technologii przemysłowych i specjalistów z zakresu inżynierii produkcji.

Diagnostyka

Obszar zainteresowania czasopisma to:
– ogólna teoria diagnostyki technicznej
– eksperymentalne badania diagnostyczne procesów i obiektów technicznych;
– modele analityczne, symptomowe, symulacyjne obiektów technicznych;
– algorytmy, metody i urządzenia diagnozowania, prognozowania i genezowania stanów obiektów technicznych;
– metody detekcji, lokalizacji i identyfikacji uszkodzeń obiektów technicznych;
– sztuczna inteligencja w diagnostyce: sieci neuronowe, systemy rozmyte, algorytmy genetyczne, systemy ekspertowe;
– diagnostyka energetyczna systemów technicznych;
– diagnostyka systemów mechatronicznych i antropotechnicznych;
– diagnostyka procesów przemysłowych;
– diagnostyczne systemy utrzymania ruchu maszyn;
– ekonomiczne aspekty zastosowania diagnostyki technicznej;
– analiza i przetwarzanie sygnałów.

Topics discussed in the journal:
– General theory of the technical diagnostics,
– Experimental diagnostic research of processes, objects and systems,
– Analytical, symptom and simulation models of technical objects,
– Algorithms, methods and devices for diagnosing, prognosis and genesis of condition of technical objects,
– Methods for detection, localization and identification of damages of technical objects,
– Artificial intelligence in diagnostics, neural nets, fuzzy systems, genetic algorithms, expert systems,
– Power energy diagnostics of technical systems,
– Diagnostics of mechatronic and antropotechnic systems,
– Diagnostics of industrial processes,
– Diagnostic systems of machine maintenance,
– Economic aspects of technical diagnostics,
– Analysis and signal processing.

Wszystkie opublikowane artykuły uzyskały pozytywne recenzje wykonane przez niezależnych recenzentów.

All the published papers were reviewed positively by the independent reviewers.

International Conference on Quality, Reliability, Risk, Maintenance, and Safety Engineering (ICQR²MSE 2011)

Welcome Information

The objective of ICQR²MSE 2011 is to bring together leading academics, industry practitioners, and research scientists from around the world to advance the body of knowledge in quality, reliability, maintenance, and safety of engineering systems, to establish and strengthen the link between academia and industry, to promote applications of research results in practice, and to showcase state of the art industrial technologies.

At ICQR²MSE 2011, recognised academics and leading researchers will present their new findings and achievements, manufacturing industries and service providers will showcase applications and state of the art technologies, and distinguished keynote speakers will present the latest developments in relevant fields. In addition, ICQR²MSE 2011 will host special sessions, panel discussions, and workshops, as well as offer opportunities for networking among attendees.

We cordially invite you to participate in ICQR²MSE 2011 by submitting papers, giving presentations, showcasing your products, learning from leading experts, and/or visiting the world-renowned historic and cultural city of XiˇŻan, China.

June 17-19, 2011, XiˇŻan, China

www.icqrms.uestc.edu.cn